

**LATENT VARIABLE METHODS
IN PROTEIN DELIVERY APPLICATIONS**

LATENT VARIABLE METHODS IN PROTEIN DELIVERY APPLICATIONS

By VIDA RAHMANI, B.Sc., M.Sc.

A Thesis Submitted to the School of Graduate Studies in Partial Fulfilment of the
Requirements for the Degree Doctor of Philosophy

Doctor of Philosophy (2017)

McMaster University

Chemical Engineering

Hamilton, Ontario

TITLE: Latent Variable Methods in Protein Delivery Applications

AUTHOR: Vida Rahmani, B.Sc. (Sharif University of Technology), M.Sc. (Isfahan University of Technology)

SUPERVISOR: Professor Heather Sheardown

NUMBER OF PAGES: xx, 178

Lay Abstract

While there has been explosive growth in the development of protein therapeutics, effective protein delivery still remains a challenge. The objective of this thesis is quantifying the controlling factors in protein release from polymeric particle delivery systems using statistical analysis methods.

In this project, alginate, which is a natural and non-toxic polymer, was used in preparation of particle systems for protein delivery applications. The interactions of model proteins with the alginate, either in the form of protein-alginate complexes or as in calcium-alginate microparticles with encapsulated proteins, were investigated and the physical properties and/or protein release kinetics were modelled with multivariate statistical analysis methods.

Multivariate analysis methods simplify the understanding of the underlying factors which affect the process. These methods are not only a powerful tool for understanding the trends and predicting future patterns, but they also save time as well as resources in process optimizations compared to traditional trial-and-error methods.

Abstract

While there has been explosive growth in the development of protein therapeutics, the many challenges associated with the delivery of proteins need to be overcome for achieving desired results. Among the various particle synthesis and encapsulation methods, ionic gelation has gained significant attention due to simplicity and the mild conditions of the process.

Electrostatic interactions can not only drive the ionic gelation process with polysaccharide based systems, they also control the system dynamics due to complex formations between the polysaccharides and proteins. In this work, it was hypothesized that the electrostatic interactions between the charged polysaccharide network and the protein can be used as a means of controlling protein entrapment and release. This hypothesis was studied and further investigated using multivariate statistical analysis which offers a mathematical description of the correlations and therefore, provides a useful tool for optimizing delivery systems.

Statistical analysis of a lysozyme/crosslinker-alginate complex system quantified the effects of the initial concentration of the compounds on complex composition and the influence of the crosslinker nature on complex degradation rates; the mathematical relationships developed were subsequently used for predicting complex properties (Chapter 2). The potential use of the complex systems as protein delivery systems, which would release the protein in response to changes in environmental conditions, was studied (Chapter 3). The statistical model showed high fitting capability (R^2 values between 0.834

and 0.906) for the complex properties and also quantified the dependence of the release kinetics (kt^n) on the ionic strength and pH of the release media. In addition to protein release from disintegration-controlled complex systems, the factors affecting diffusion-controlled protein release from calcium-alginate microparticles were investigated (Chapter 4). Multivariate analysis showed that while the parameter k was mainly influenced by protein properties (net charge and molecular weight), the parameter n was mostly affected by polymer and buffer properties. Overall, the multivariate statistical method provides a great platform for understanding the trends and predicting future patterns. By understanding the effect of different factors on the release, protein delivery systems from polysaccharide based systems have a great deal of potential to lead to effective protein therapeutics.

Acknowledgements

As I write this acknowledgement and look back over my PhD journey, so many names and faces come to my mind belonging to people whom without their support, encouragement, and advice this thesis would have not been possible.

Most importantly, I would like to express my deepest appreciation to my supervisor, Dr. Heather Sheardown. Heather, I am extremely grateful not only for your academic support, but also the emotional support I required at times. Thank you for believing in me, providing me with invaluable guidance and at the same time with the freedom to grow as an independent researcher. Thank you for encouraging me throughout this whole journey, which was full of ups and downs, from stressful moments all the way to excitements over pictures of “cute” microparticles. I could not imagine going through it all without such an understanding supervisor.

I would like to deeply thank my supervisory committee members, Dr. Harald Stöver and Dr. Todd Hoare, for their thoughtful comments and insights which provided me with different perspectives to ponder upon and helped me in shaping the research. I would also like to express my sincere gratitude to Dr. Rand Elshereef for his help, guidance, and insightful feedback. Many thanks to Dr. Dan Chen, for his invaluable advice and always positive attitude in helping me.

Special thanks to my volunteers, Salwa Farooqi and Karishma Manji, due to their tireless work in preparing the zillion milligrams of microparticles! Many thanks to Fei Xu for performing SEM imaging, Dr. Megan Dodd for her assistance in cytotoxicity tests, and Ashutosh Kulkarni for the ProMV and MATLAB discussions. Special thanks to Lina Liu, for her patience in helping me, and sharing her knowledge and experience with me.

I wish to thank the entire staff of the Department of Chemical Engineering, especially Ms. Kristina Trollip and Ms. Michelle Whalen for their administrative assistance always accompanied with a smile. The friendly nature of the department made my stay here an enjoyable experience. I specifically would like to thank Dr. Roozbeh Mafi, Dr. Jianfeng Zhang, Dr. Ali Mohammad Rabea, Sahar Mokhtari, and Amir Kazemi for all our discussions and for all their help and support.

Many thanks to all the members of the Sheardown lab, whom working by their side has made for many cheerful memories (even including the annual ski trip ritual discussions!) in the past couple of years. I consider myself lucky to be part of a group that not only helped me in improving my research through our discussions, but also consisted of people whom I could count on as friends. Fran, thank you for being my go-to person for all my “life in Canada” questions since the first day that I joined the lab! Myrto, our office/lab/bus/coffee chats are something that I will forever appreciate and also thank you

for sharing as little as your “baby magnetic stir bars” all the way to your desk with me! Ivana, Marion, Cheryl, and Alysha, I cherish all our conversations so much and thank you for being my buffer during hard times.

A heartfelt thank you to my parents, who have been constant sources of love, strength, and wisdom. Mum, dad, words are incapable of expressing how grateful I am for all the sacrifices you have made for me to reach this point of my life and for giving me the opportunities and experiences that have made me who I am. The love, support, and guidance you have given me throughout my entire life carry me through, always. Thanks to my brothers, Navid and Vahid, who have both kept things light and had me smiling with their sense of humor for as long as I can remember. My love for you all is infinite.

Last, but certainly not least, tremendous thanks to my husband, Hojat, whom through his unconditional love, patience, and support, I have been able to complete this long dissertation journey. I love you and thank you with all my heart and soul.

Table of Contents

Chapter 1: Introduction and Literature Review.....	1
1.1. Introduction.....	1
1.2. Protein Drug Delivery.....	2
1.2.1. Protein Structure.....	2
1.2.2. Proteins as Therapeutics.....	3
1.2.3. Protein Delivery Challenges.....	5
1.2.4. Protein Delivery Approaches.....	7
1.3. Particle Delivery Systems.....	9
1.3.1. Microparticles and Nanoparticles.....	9
1.3.2. Particle Synthesis Methods.....	9
1.3.3. Polymers for Protein Delivery.....	12
1.4. Alginate.....	14
1.4.1. Alginate Structure.....	14
1.4.2. Alginate Gelation.....	15
1.4.3. Alginate for Protein Delivery.....	17
1.5. Proteins and Polysaccharides in Solution.....	19
1.5.1. Protein-Polysaccharide Interactions.....	19
1.5.2. Protein-Polysaccharide Complexes and Coacervates.....	21
1.6. Multivariate Statistical Analysis.....	24
1.6.1. Latent Variable Methods.....	24

1.6.2. Theory of Projection to Latent Structures (PLS) Models	24
1.6.3. PLS Model Evaluation	28
1.7. Thesis Outline	29
1.7.1. Chapter 2: Property Modelling of Lysozyme/Crosslinker-Alginate Complexes Using Latent Variable Methods	29
1.7.2. Chapter 3: Protein-Alginate Complexes as pH-/Ion-Sensitive Carriers of Proteins	30
1.7.3. Chapter 4: Optimizing Electrostatic Interactions for Controlling the Release of Proteins from Anionic and Cationically Modified Alginate	31
References	32
Chapter 2: Property Modelling of Lysozyme/Crosslinker-Alginate Complexes Using Latent Variable Methods	41
Abstract	42
2.1. Introduction	43
2.2. Materials and Methods	46
2.2.1. Materials	46
2.2.2. Preparation of Fluorescently-Labeled BSA	46
2.2.3. Preparation of Complexes	47
2.2.4. Complex Composition Analysis	49
2.2.5. Physical Characterization	51
2.2.6. Protein Release	52
2.2.7. Statistical Analysis	53

2.2.8. Multivariate Statistical Analysis	54
2.3. Results and Discussion.....	56
2.3.1. Complex Composition Analysis	56
2.3.2. Physical Characterization.....	60
2.3.3. Protein Release.....	63
2.3.4. Multivariate Statistical Analysis	65
2.3.5. Model Verification	75
2.4. Conclusion	77
2.5. Acknowledgements.....	78
References.....	78
Supplementary Material for Chapter 2.....	82
Chapter 3: Protein-Alginate Complexes as pH-/Ion-Sensitive Carriers of Proteins .88	
Abstract	89
3.1. Introduction.....	90
3.2. Materials and Methods.....	93
3.2.1. Materials	93
3.2.2. Preparation of Protein-Alginate Complexes	93
3.2.3. Complex Composition Analysis	94
3.2.4. Physical Characterization.....	95
3.2.5. Protein Release.....	96
3.2.6. Multivariate Statistical Analysis	97
3.3. Results and Discussion.....	98

3.3.1. Complex Composition Analysis	98
3.3.2. Physical Characterization.....	99
3.3.3. Protein Release.....	101
3.3.4. Multivariate Statistical Analysis	104
3.4. Conclusion	116
3.5. Acknowledgements.....	116
References.....	116
Supplementary Material for Chapter 3.....	120
Chapter 4: Optimizing Electrostatic Interactions for Controlling the Release of Proteins from Anionic and Cationically Modified Alginate	121
Abstract.....	122
4.1. Introduction.....	122
4.2. Materials and Methods.....	125
4.2.1. Materials	125
4.2.2. Alginate Modification.....	126
4.2.3. Characterization of the Modified Alginates.....	127
4.2.4. Synthesis of Microparticles.....	128
4.2.5. Particle Characterization.....	129
4.2.6. Protein Quantification.....	129
4.2.7. Protein Loading.....	129
4.2.8. Protein Release.....	130
4.2.9. Protein Release Kinetics	131

4.2.10. Statistical Analysis.....	131
4.2.11. Multivariate Statistical Analysis.....	132
4.3. Results and Discussion.....	134
4.3.1. Characterization of the Modified Alginates.....	134
4.3.2. Particle Characterization.....	137
4.3.3. Protein Loading.....	140
4.3.4. Protein Release.....	142
4.3.5. Multivariate Statistical Analysis.....	145
4.4. Conclusion.....	151
4.5. Acknowledgements.....	152
References.....	152
Supplementary Material for Chapter 4.....	156
Chapter 5: Summary and Conclusions.....	169
Appendix A – Bradford Assay.....	174
Appendix B - Potentiometric-Conductometric Titration.....	175
Appendix C – PLS Cross-Validation.....	177

List of Figures

Figure 1.1. Chemical structure of alginate.....	15
Figure 1.2. Schematic representation of the “egg box model”, showing interactions between calcium ions and sodium alginate in the gelation process.....	16
Figure 1.3. Schematic representation of various interactions between proteins and polysaccharides.	20
Figure 1.4. Schematic representation of matrices and algorithm steps in PLS model.....	26
Figure 2.1. (a) Precipitation of alginate and lysozyme at various pH values; (b) n^+/n^- ratio in complex.....	57
Figure 2.2. (a) Precipitation of alginate, lysozyme, and calcium at pH=7.4 and $[n^+]/[n^-]=1$; (b) n^+/n^- ratio in complex.	58
Figure 2.3. (a) Precipitation of alginate, lysozyme, and calcium at constant lysozyme and varying calcium concentration; (b) n^+/n^- ratio in complex at constant lysozyme and varying calcium concentration; (c) Precipitation of alginate, lysozyme, and calcium at constant calcium and varying lysozyme concentration; (d) n^+/n^- ratio in complex at constant calcium and varying lysozyme concentration.	60
Figure 2.4. Release of proteins from protein/crosslinker-alginate complexes; (a) pH=4.5, $I=10$ mM, (b) pH=4.5, $I=150$ mM, (c) pH=7.4, $I=10$ mM, (d) pH=7.4, $I=150$ mM.	64
Figure 2.5. (a) Cumulative R^2X , R^2Y , and Q^2Y for the PLS model for physical properties; (b) R^2 and Q^2 for each of the Y variables.	66
Figure 2.6. Correlation-loading plot for contributors to Y variables.....	67
Figure 2.7. Coefficient plots showing the effect of each X parameter on complex composition and mole fractions of (a) COO^- , (b) lysozyme.	68
Figure 2.8. Coefficient plots showing the effect of each X parameter on (a) average size, (b) zeta potential.....	69
Figure 2.9. (a) Cumulative R^2X , R^2Y , and Q^2Y for the PLS model for release kinetics; (b) R^2 and Q^2 for each of the Y variables.	70
Figure 2.10. Coefficient plots showing the effect of each X parameter on release kinetic parameters; (a) $\ln(k)$, (b) n	72

Figure 2.11. Contour surface plots from the PLS model for protein release kinetics as functions of protein properties and crosslinker charge density at physiological ionic strength ($I=150$ mM); (a) $\ln(k)$, (b) n	73
Figure 2.12. Observed vs. Predicted plots for Y variables.	75
Figure 3.1. Composition of protein-alginate complexes; (a) mole compositions, (b) n^+/n^- ratio in complex. Lys=Lysozyme, Chym=Chymotrypsin, BSA=Bovine Serum Albumin.	99
Figure 3.2. Release of proteins from protein-alginate complexes; (a) 0.5:1, pH=4.5, $I=10$ mM, (b) 1:1, pH=4.5, $I=10$ mM, (c) 0.5:1, pH=4.5, $I=150$ mM, (d) 1:1, pH=4.5, $I=150$ mM, (e) 0.5:1, pH=7.4, $I=10$ mM, (f) 1:1, pH=7.4, $I=10$ mM, (g) 0.5:1, pH=7.4, $I=150$ mM, (h) 1:1, pH=7.4, $I=150$ mM.....	103
Figure 3.3. (a) Cumulative R^2X , R^2Y , and R^2Y for the PLS model; (b) R^2 and Q^2 for each of the Y variables.	105
Figure 3.4. Correlation-loading plot for contributors to Y variables.	106
Figure 3.5. Coefficient plots showing the effect of each X parameter on complex composition and mole fractions of (a) COO^- , (b) protein.	108
Figure 3.6. Coefficient plots showing the effect of each X parameter on release kinetic parameters; (a) $\ln(k)$, (b) n	109
Figure 3.7. Observed vs. Predicted plots for Y variables.	111
Figure 3.8. Squared prediction error (SPE) values for the experimental observations....	112
Figure 3.9. Contour surface plots from the PLS model as functions of the main two contributing factors and the experimental data for (a) protein (mol%) in complex, (b) average diameter (μm), (c) zeta potential (mV).....	113
Figure 3.10. Contour surface plots from the PLS model for protein release kinetics as functions of protein properties (molecular weight and net charge) at physiological ionic strength ($I=150$ mM); (a) $\ln(k)$, (b) n	115
Figure 4.1. Synthesis of amine modified alginate.....	127
Figure 4.2. FT-IR spectra of the amine modified alginates.	135
Figure 4.3. ^1H NMR spectra; (a) spectra of alginate, DMEN, and amine modified alginates in D_2O , (b) spectra of alginate and amine modified alginates in D_2O	136

Figure 4.4. SEM images of amine modified alginate assemblies; (a) Alg, (b) Am-Alg 20, (c) Am-Alg 40, (d) Am-Alg 60, (e) Am-Alg 80, (f) Am-Alg 100.....	138
Figure 4.5. Size distributions of alginate and modified alginate microparticles.....	139
Figure 4.6. Loading of proteins in microparticles of Alg, Am-Alg 20, Am-Alg 40, and Am-Alg 60 after soaking time of 2 hours.	141
Figure 4.7. Release of proteins from microparticles; (a) Alg, PBS 0.1X, (b) Alg, PBS 1X, (c) Am-Alg 20, PBS 0.1X, (d) Am-Alg 20, PBS 1X, (e) Am-Alg 40, PBS 0.1X, (f) Am-Alg 40, PBS 1X, (g) Am-Alg 60, PBS 0.1X, (h) Am-Alg 60, PBS 1X.....	143
Figure 4.8. (a) Cumulative R^2X , R^2Y , and Q^2Y for each of the latent variable components of the PLS model; (b) R^2 and Q^2 for each of the Y variables.	145
Figure 4.9. Correlation-loading plot for contributors to protein release.....	146
Figure 4.10. Coefficients plot showing the effect of each X variable on release kinetic parameters; (a) $\ln(k)$, (b) n	148
Figure 4.11. Observed vs. Predicted plots for (a) $\ln(k)$ and (b) n ; (c) squared prediction error (SPE) values for the observations.	150
Figure 4.12. Contour surface plots from the PLS model as functions of the main two contributing factors and the experimental data for (a) $\ln(k)$ and (b) n	151

List of Supplementary Information Figures

SI Figure 2.1. (a) Mole composition of lysozyme-alginate complexes at various pH values; (b) Mole composition of lysozyme/calcium-alginate complexes at pH=7.4 and $[n^+]/[n^-]=1$	82
SI Figure 2.2. Mole Composition of lysozyme/calcium-alginate complexes at pH=7.4; (a) constant lysozyme and varying calcium concentrations, (b) constant calcium and varying lysozyme concentrations.	82
SI Figure 2.3. (a) Mole composition of lysozyme/crosslinker-alginate complexes; (b) n^+/n^- ratio in complex. Ca=Calcium, Ba=Barium, Fe=Iron(III), BSA=Bovine Serum Albumin, Lys=Lysozyme.....	83
SI Figure 2.4. Lysozyme activity of the complex structures.	85
SI Figure 2.5. Correlation-loading plot for contributors to Y variables.	86
SI Figure 2.6. Squared prediction error (SPE) values for the experimental observations; (a) PLS model for physical properties, (b) PLS model for release kinetics.....	87
SI Figure 4.1. Potentiometric titration curves of the native alginate and the amine modified alginates.	156
SI Figure 4.2. SEM images of alginate microparticles prepared with varying concentrations of alginate and calcium chloride solutions; (a) Alginate 1.5% (w/v), CaCl_2 1 M, (b) Alginate 1.5% (w/v), CaCl_2 0.1 M, (c) Alginate 2.5% (w/v), CaCl_2 1 M, (d) Alginate 2.5% (w/v), CaCl_2 0.1 M.....	158
SI Figure 4.3. Size distributions of alginate microparticles prepared with varying concentrations of alginate and calcium chloride solutions.	159
SI Figure 4.4. Loading of proteins in microparticles at various soaking times; (a) Alg, (b) Am-Alg 20, (c) Am-Alg 40, (d) Am-Alg 60.	160
SI Figure 4.5. Lysozyme activity of the release studies from Alg and Am-Alg 60 microparticles in PBS 1X.....	163
SI Figure 4.6. MTT assay results of 3T3 cells growth with varying alginate modification degrees over 48 hours.	166
SI Figure 4.7. Live/Dead assay results of 3T3 cells growth with varying alginate modification degrees over 48 hours.....	167

List of Tables

Table 1.1. Summary of recent studies on proteins encapsulation in alginate beads.	17
Table 2.1. Physical characteristics of lysozyme-alginate complexes at various pH values.	61
Table 2.2. Physical characteristics of lysozyme/calcium-alginate complexes at pH=7.4 and $[n^+]/[n^-]=1$	61
Table 2.3. Physical characteristics of lysozyme/calcium-alginate complexes at varying mixing ratios.	62
Table 2.4. Selected complex compositions and their required initial mixing conditions. .	76
Table 2.5. Comparison of model predicted and measured experimental values for complex compositions and their physical properties.	77
Table 3.1. Isoelectric point, net charge at physiological pH, and molecular weight of the model proteins.	94
Table 3.2. Physical properties of protein-alginate complexes.	100
Table 4.1. Isoelectric point (pI), net charge at physiological pH, and molecular weight of the model proteins.	130
Table 4.2. Values of amine content of the amide functionalized alginates determined by ^1H NMR.	137
Table 4.3. Zeta potential measurements of alginate and modified alginate microparticles.	140

List of Supplementary Information Tables

SI Table 2.1. Physical characteristics of lysozyme/crosslinker-alginate complexes; Ca=Calcium, Ba=Barium, Fe=Iron(III), BSA=Bovine Serum Albumin, Lys=Lysozyme.	83
SI Table 2.2. Values of parameters obtained from fit into the Korsmeyer-Peppas model and the PLS model-predicted values.....	84
SI Table 3.1. Values of parameters obtained from fit into the Korsmeyer-Peppas model and the PLS model-predicted values.....	120
SI Table 4.1. Values of amine content of the amide functionalized alginates determined by titration.....	157
SI Table 4.2. Values of parameters obtained from fit into the Korsmeyer-Peppas model and the PLS model-predicted values.....	161

List of Abbreviations and Symbols

Am-Alg	Amine Modified Alginate
ANOVA	Analysis of Variance
BSA	Bovine Serum Albumin
Calcein AM	Calcein Acetoxymethyl
DMEM	Dulbecco's Modified Eagle Medium
DMEN	N,N-Dimethylethylenediamine
DMSO	Dimethyl Sulfoxide
DS	Degree of Substitution
EDC	1-(3-Dimethylaminopropyl)-3-Ethylcarbodiimide
EDTA	Ethylenediaminetetraacetic Acid
EthD-1	Ethidium Homodimer-1
FDA	Food and Drug Administration
FGF-1	Fibroblast Growth Factor-1
FT-IR	Fourier Transform Infrared Spectroscopy
GI	Gastro-Intestinal
¹H NMR	Proton Nuclear Magnetic Resonance Spectroscopy
HOBt	1-Hydroxybenzotriazole
HRP	Horseradish Peroxidase
IPN	Interpenetrating Polymer Network
LCST	Lower Critical Solution Temperature
MTT	3-[4,5-Dimethylthiazol-2-yl]-2,5-Diphenyltetrazolium Bromide
MW	Molecular Weight
MWCO	Molecular Weight Cut Off
NN Indicator	Calconcarboxylic Acid
PBS	Phosphate Buffered Saline
PCA	Principal Component Analysis
PEC	Polyelectrolyte Complex
PEG	Poly(Ethylene Glycol)
PGA	Poly(Glycolic Acid)
PLA	Poly(Lactic Acid)
PLGA	Poly(Lactic-co-Glycolic Acid)
PLS	Projection to Latent Structures (Partial Least Squares)
Poly(SA)	Poly(Sebacic Anhydride)
Poly(CPH)	Poly(1,6-bis- <i>p</i> -Carboxyphenoxy)Hexane
SEM	Scanning Electron Microscopy
SPE	Squared Prediction Error
TPP	Tripolyphosphate
UV	Ultraviolet

Declaration of Academic Achievement

In accordance with the guidelines for the preparation of a doctoral thesis set forth by the McMaster University School of Graduate Studies, this work has been prepared as a sandwich thesis. The majority of the work described in this thesis was conducted, interpreted, and written by the author of this thesis. The work was done in consultation with and under the supervision of Dr. Heather Sheardown who also revised the drafts to the final versions.

The following statements outline the contributions of the authors (not including myself and my supervisor), as well as the assistances of students who helped with the work, to each chapter:

In **Chapter 2**, Dr. Rand Elshereef revised and edited the multivariate statistical sections.

In **Chapter 4**, Dr. Rand Elshereef revised and edited the multivariate statistical sections. Salwa Farooqi and Karishma Manji assisted in preparing the microparticles. Fei Xu performed SEM imaging and Dr. Megan Dodd assisted in cytotoxicity tests.

Chapter 1: Introduction and Literature Review

1.1. Introduction

While there has been explosive growth in the development of protein therapeutics in the recent years for the treatment of a wide range of diseases, such as cancer, metabolic disorders and autoimmune diseases, the delivery of the proteins still remains a significant challenge¹. Different strategies, such as design of carrier systems and chemical modifications, have been evaluated for overcoming the protein delivery obstacles² and for achieving the goals of enhancing protein delivery, maintaining the protein concentration within the effective therapeutic window over the desired period of time, and reducing the need for frequent drug administration³.

Encapsulation methods, using for example hydrogels and particle delivery systems, are the primary method adopted in design of carrier systems for the delivery of proteins². Among the various particle synthesis methods, ionic gelation, in which particles are formed through electrostatic interactions between crosslinker and polymer, has attracted significant interest in the recent years due to method simplicity as well as the mild conditions of the process which is very favorable for retaining protein bioactivity⁴. Clinically safe calcium-crosslinked alginate hydrogels are an example of hydrogels synthesized through the ionic gelation method which are widely used as carriers in enzyme, protein and drug delivery applications⁴⁻⁶.

Since alginate is an anionic polymer⁵ and proteins are also charged⁷, it is hypothesized that a promising technique for achieving effective protein delivery would take advantage of the molecular interactions, specifically electrostatic interactions, between the protein and the polysaccharide hydrogel network for optimizing the protein entrapment and release. Furthermore, statistical analysis methods can offer further understanding of the interactions between proteins and polysaccharides by mathematically describing the correlations and trends. The statistical approach has the potential to be a useful tool for optimizing the design of delivery systems in order to achieve the desired protein release kinetics.

1.2. Protein Drug Delivery

1.2.1. Protein Structure

Proteins carry out many functional and vital biochemical roles in living organisms. These macromolecules perform a wide variety of physiological and biological processes such as enzymes in biotransformation reactions, ligands in signaling, receptors in pharmacological response elucidation, antibodies in immune system interactions, transcription, and translation⁸ to ensure proper development and functioning of entire organs of the body.

Although all proteins are built from the same 20 amino acids⁹ linked through peptide bonds¹⁰ (covalent amide bond between α -carboxyl and α -amino groups of adjacent amino acid residues¹¹), they are the most functionally diverse of all biological substances¹². Peptides which contain eight or more amino acid residues are called

polypeptides, while polypeptides with approximately 50 amino acid residues to as many as 2500 residues are referred to as proteins¹⁰.

Since proteins are constructed of amino acids, which contain the ionizable amine and carboxyl groups, a protein molecule can also carry a charge depending on the pH of the solution. The pH value where the protein possesses equal amounts of negative carboxyl charges and positive amine charges or the protein has a net zero charge is known as the isoelectric point (pI)⁷. At pH values below the pI, a high degree of protonation of the amine groups and a low degree of dissociation of the carboxyl groups lead to a net positively charged protein. At pH values higher than the pI, the high degree of dissociation of the carboxyl groups and the low degree of protonation of the amine groups make a predominantly negatively charged protein¹³. However, because proteins are large molecules, there may be regions of positive charge in a negatively charged protein and vice versa.

1.2.2. Proteins as Therapeutics

The first use of therapeutic proteins can be traced back to 1922 when purified insulin from bovine pancreas was introduced as a life-saving daily injection for type 1 diabetes treatment^{1,14}. However, the first US Food and Drug Administration (FDA) approval of protein therapeutics occurred only about 30 years ago when human insulin was introduced as the first recombinant protein drug. Since then, the number and frequency of usage of proteins as therapeutics has significantly increased to currently more than 130 approved products with many more in clinical development³. This

increasing share of the global pharmaceutical market is due to the development of genomic information with the results proving that more than half of our 30,000 genes encode proteins¹⁵. This, represents a significant potential in regards to the use of protein therapeutics in disease treatments¹⁶.

Protein therapeutics have several advantages compared to small-molecule drugs. First, the specific and complex functionality of proteins often cannot be mimicked by simple chemical compounds. Second, it is expected that proteins will interfere less with the routine biological processes and cause fewer side effects due to their specific functionality. Third, protein therapeutics have the potential to offer effective replacement treatment for gene therapy in disorders with deleted or mutated genes and in cases where gene therapy is not available. Finally, the clinical development and FDA approval time of protein therapeutics may be shorter compared to development and approval time period of small-molecule drugs. The last advantage highlights the financial promise of proteins compared to small-molecule drugs¹⁶.

Protein and peptide drugs can be categorized based on their function and application as follows¹⁶:

- Proteins with enzymatic or regulatory activity: replacing a deficient or abnormal protein, augmenting an existing pathway, providing a novel functionality
- Proteins with special targeting activity: interfering with a molecule or organism, delivering other compounds or proteins
- Protein vaccines: protecting against a harmful foreign agent, treating an autoimmune disease, treating cancer

- Protein diagnostics: affecting clinical decision making

1.2.3. Protein Delivery Challenges

Due to the relatively specific functionality of proteins, theoretically only low doses of proteins and peptide drugs are required to be delivered¹⁵. However, their direct delivery is hampered by various challenges such as *in vitro* and *in vivo* instability, immunogenicity, and a relatively short half-life within the body¹. Protein structure is extremely sensitive and protein physical and chemical ability can be compromised by environmental conditions such as pH, temperature, surface interactions, and contaminants for excipients².

While parenteral delivery of proteins remains the most common route of protein delivery^{3,8}, non-injectable methods such as oral¹⁷, pulmonary¹⁸, ocular¹⁹, and transdermal²⁰ routes have also drawn extensive attention in the recent years. Parenteral injections of liquid formulations containing proteins offer the fastest and usually the least expensive route to commercialization of protein therapeutics²¹. However, due to the hepatic first-pass effect, the fast renal clearance, and consequently the short half-life of many proteins, this traditional method requires multiple daily injections for achieving therapeutic effectiveness which results in patient discomfort and inconvenience^{3,22}.

Oral administration is the most preferred route of drug delivery in regards to patient comfort and compliance². The main drawback of this route for protein delivery is protein degradation and loss of protein biological activity due to the harsh conditions of the gastro-intestinal (GI) tract such as high proteolytic activity and low pH of the

stomach³. In addition, the large molecular size of proteins and their hydrophilicity is a limiting factor in their permeability and absorption through biological membranes^{2,3}.

Considerable emphasis has gone into exploring pulmonary routes of protein delivery due to the large surface area of the lungs, the high permeability and slow mucociliary clearance of lung tissues, and absence of first-pass hepatic metabolism^{18,23}. However, this route is also associated with challenges such as dose reproducibility. The drug dose absorbed is usually less than the dose present in the device and this loss is a function of airway geometry and humidity, respiratory capacity (such as breathing frequency), and patient inhalation technique²⁴.

Although a few macromolecular therapeutics are already used in the treatment of some ocular diseases and many more are currently under development, ophthalmic delivery of proteins is challenging and associated with obstacles. The large size of proteins restricts their diffusion which makes their topical administration (such as eye drops) highly inefficient if not impossible. Their systemic delivery is also limited by barriers such as the blood retinal barrier which restrict the diffusion of the macromolecules across the tissue¹⁹.

In transdermal protein delivery, the stratum corneum, the outermost layer of skin, acts as the limiting barrier. The stratum corneum is a lipophilic layer which only allows small and moderately lipophilic molecules to diffuse across and reach the deeper layers of skin and the systemic circulation. Therefore, the partition of proteins, which are large hydrophilic molecules, through this layer is very limited²⁰.

1.2.4. Protein Delivery Approaches

In order to overcome the various barriers and challenges in protein delivery, different techniques and strategies have been investigated such as chemical modification and design of carrier systems². Generally, all approaches aim for achieving the following goals: (a) maintaining target tissue protein concentration within the effective therapeutic window over the desired period of time, (b) protecting the protein from degradation, (c) enhancing drug delivery while reducing side effects, (d) lowering drug dosage and need for frequent administration³.

While chemical modifications of proteins can be carried out for optimizing the pharmacokinetic properties of the protein, consideration must be taken into account to ensure protein biological efficacy is not compromised². Conjugation of proteins with poly(ethylene glycol) (PEG) is an example of chemical modification strategies for extending protein circulation times and masking protein immunogenicity³. The grafting of PEG, which is a non-toxic and hydrophilic polymer, results in a steric barrier at the hydrophobic surface and therefore decreases the adsorption of proteins to surfaces⁸. Also, PEGylation hinders plasma clearance of the protein from the systemic circulation by reducing metabolic degradation and receptor-mediated uptake of proteins².

Encapsulation and entrapment are the primary methods adopted for protein delivery and design of carrier systems. Lipid-based delivery systems such as liposomes, hydrogels, nanocapsules and microparticles, are examples of such polymeric protein-delivery systems².

Liposomes, first designed in the late 1960s, are microscopic vesicles of discrete aqueous compartments surrounded by lipid membranes¹⁵. The incorporation and release of proteins from these systems can be manipulated by modifying the physico-chemical properties of the protein, such as tailoring the hydrophobic surface area of the protein by acylation. Triggered degradation of lipid bilayers by enzymes, such as secretory phospholipase A2 which exist in inflammatory and certain cancerous tissues, can also control protein release from these vehicles².

Hydrogels, first designed in early 1950s, are three-dimensional, crosslinked networks of hydrophilic polymers which have the ability to uptake large amounts of water (up to >99% of their weight²⁵) while maintaining their structure³. Hydrogels can be designed to respond to certain environmental stimuli, including pH²⁶, temperature²⁷, ionic strength²⁸, or enzymatic activity²⁵, for triggering protein release. Desired protein release kinetics can also be achieved by tailoring the degradation rates of the hydrogels². The high water content, similar in structure to natural extracellular matrices, minimizes tissue irritation. As well, the often mild preparation conditions used for hydrogels has led to increasing interest in using hydrogels as protein delivery carriers³. Hydrogels can be formulated in various physical forms such as microparticles, nanoparticles, coatings, slabs, or *in situ* forming delivery systems²⁹.

1.3. Particle Delivery Systems

1.3.1. Microparticles and Nanoparticles

Depending on the discipline, there are discussions about sizes of particles to be classified as microparticles or nanoparticles. For example, in colloid chemistry, only particles with diameters below 100 nm, and sometimes even below 20 nm, are referred to as nanoparticles. However, in pharmaceutical sciences and in general, nanoparticles are defined as particles with diameters in the range of 1 nm to 1000 nm, and microparticles are referred to particles with sizes ranging between 1 μm and 1000 μm ³⁰. Microparticle and nanoparticle drug delivery systems are among the several kinds of sustained release devices which offer controlled release of therapeutics with high target specificity as well as minimizing drug degradation, preventing harmful side effects, and enhancing drug permeation^{31,32}.

1.3.2. Particle Synthesis Methods

Depending on the hydrophilicity/hydrophobicity of the polymers used for protein encapsulation, various particle synthesis techniques have been utilized. Techniques such as emulsion crosslinking³³, emulsification-solvent removal³⁴, spray-drying^{35,36}, coacervation/precipitation^{37,38}, template-assembly method³⁹, and ionic gelation^{40,41} have been used for particle preparation using both hydrophilic and hydrophobic polymers. Regardless of the technique used, maintaining the unique folded three-dimensional conformation of the proteins is the main concern and challenge in the encapsulation process⁴.

In the emulsion crosslinking method, protein is dispersed in the hydrophilic polymer-containing aqueous phase (W), which is then emulsified into oil phase (O) by mechanical stirring or ultrasonication to form a W/O emulsion. Finally, crosslinker is added to the system to solidify the emulsion into microspheres³³. In the case of hydrophobic polymers, emulsification-solvent removal technique has been widely investigated. A primary W/O emulsion is formed by dispersing the aqueous protein solution in a polymer-dissolved organic phase. This primary emulsion is then further dispersed into a large volume of emulsifier-containing aqueous phase to form a W/O/W double emulsion. Hardened microparticles are formed by extracting the organic solvent from the system³⁴. Although proteins can be successfully encapsulated using emulsification methods, some drawbacks exist. Protein activity reduction due to aggregation at the interface between the water and oil phases, protein denaturation due to the intense shearing strength of the sonication process, and removal of excess crosslinking agent are among the challenges associated with the emulsion crosslinking technique⁴.

Spray drying involves atomization of a liquid suspension into droplets by spraying them along with hot gas into a drying chamber³⁵. Hydrophilic polymers and proteins are dissolved and dispersed in an aqueous phase which is then atomized in a flow of drying air at a hot temperature. The solvent is instantaneously evaporated and small particles are formed. When hydrophobic polymers are used, a W/O emulsion (aqueous protein solution emulsified in organic polymer-containing phase) is atomized in a stream of hot air and particles are formed with the evaporation of the organic phase⁴. While spray drying is

known to be a rapid and easy to scale-up method, the application of high temperature imposes potential thermal stress to the protein. Also, spray drying and the removal of water molecules can alter the secondary structure of protein (α -helix, β -sheet, and random coil) due to the destabilization of the hydrogen bonds which could result in protein deactivation⁴².

The coacervation/precipitation method consists of dispersing the protein in an aqueous polymer solution (in case of hydrophilic polymers) and decreasing polymer solubility by adding a third component to the system⁴. For hydrophobic polymers, the aqueous protein solution is added to the polymer dissolved in an organic phase to form a W/O emulsion. This is followed by addition of an organic non-solvent which gradually extracts the polymer solvent⁴³. At the phase separation point, the system splits into two different phases: the coacervate phase rich in polymer and the supernatant phase poor in polymer. The coacervate phase consists of polymeric coacervate droplets encapsulating the protein which are then solidified and collected^{4,43}. The challenges associated with this method include agglomeration of particles due to absence of stabilizers and difficulty removing residual solvents from the final particle products⁴.

The template-assembly method is a recent addition to the suite of microencapsulation techniques³⁹. In this method, proteins are adsorbed onto the surface of a sacrificial template, followed by adsorption of oppositely charged polyelectrolytes by layer-by-layer technology for construction of composite multilayers. Finally, the template is removed to form a hollow capsule entrapping protein⁴. A common example of the sacrificial template includes calcium carbonate (CaCO_3) particles which are inexpensive,

are easy to produce, have high porosity which offers potential for large adsorption amounts, and easily decompose upon exposure to hydrochloric acid (HCl)³⁹.

The ionic gelation method has gained significant attention in recent years due to the simple and mild conditions of the process which is very beneficial for retaining protein bioactivity. In this technique, the aqueous hydrophilic polymer solution is added to a solution of ionic crosslinkers where particles are formed through electrostatic interactions between crosslinker and polymer molecules⁴.

1.3.3. Polymers for Protein Delivery

In the past three decades, biodegradable polymers, mostly poly(glycolic acid) (PGA), poly(lactic acid) (PLA), and poly(lactic-co-glycolic acid) (PLGA), have been extensively used for delivery and microencapsulation of proteins with the hypothesis that the release kinetics of the encapsulated protein can be controlled by tailoring the degradation rate of the polymers²². In fact, PLGA is the most widely polymer explored in protein encapsulation and delivery applications^{4,22} due such advantages as having non-toxic degradation products, and importantly, adaptability^{4,44}. Controlled degradation of PLGA can be achieved by changing the lactide/glycolide ratio as well as the polymer molecular weight⁴⁴. However, a drawback of PLGA for protein delivery is that the acidic microenvironment (pH 2-3) caused by its degradation products could result in protein denaturation or aggregation⁴. Another concern with PLGA is that as it goes through degradation and bulk-erosion in an aqueous environment, the encapsulated protein is exposed to elevated levels of moisture which may cause protein aggregation^{4,45}.

Polyanhydrides are another class of hydrophobic and biodegradable polymers which have been investigated for protein delivery applications. Where polyesters, such as PLGA, exhibit bulk erosion; polyanhydrides degrade through surface-erosion which limits the protein exposure to moisture and therefore, minimizes protein aggregation. Also, the pH of polyanhydride degradation products is not as low as the pH observed with PLGA degradation. Thus, polyanhydrides potentially offer a more suitable microenvironment for encapsulated and released protein molecules compared to polyesters. Examples of polyanhydrides used for protein encapsulation include poly(sebacic anhydride) (poly(SA)) and poly(1,6-bis-*p*-carboxyphenoxy)hexane (poly(CPH)) which have degradation rates on time scales of weeks and years, respectively⁴⁵.

Hydrophilic polymers such as alginate⁴⁶, chitosan⁴⁷, hyaluronic acid⁴⁸, and dextran⁴⁹ have also been widely used in preparation of hydrogels for protein encapsulation and delivery applications. These polymers offer advantages such as low toxicity and also their hydrophilicity facilitates water uptake and continuous protein release which is necessary for maintaining stable protein concentrations in plasma^{4,50}. Protein release from hydrogels is mainly governed by diffusion⁵¹ and is also controlled by mechanisms such as swelling, erosion/degradation, or combinations of these procedures³.

The hydrogel network from hydrophilic polymers can be prepared by physical and/or chemical crosslinking methods⁴⁹. Physical crosslinking can be accomplished through non-covalent interactions such as electrostatic interactions, hydrophobic interactions, hydrogen bonding, or combinations of these. Chemical crosslinking can be

achieved by techniques such as photopolymerization or coupling reactions such as click chemistry³. The degradation time of chemically crosslinked gels can be tailored by controlling the nature of the chemical bonds in the building blocks as well as in the crosslinks. However, chemical crosslinking methods have the potential to affect protein activity. Additionally, crosslinking agents are mostly toxic and need to be totally removed before *in vivo* application. Therefore, interest in physical crosslinking for hydrogel preparations has significantly increased recently⁴⁹.

Alginate-calcium hydrogels, prepared through extrusion of sodium alginate solution into a calcium containing crosslinking solution, and also chitosan-tripolyphosphate (TPP) hydrogels, made from dropwise addition of chitosan solution into a TPP solution, are examples of physically crosslinked hydrogels synthesized through the ionic gelation method⁴.

1.4. Alginate

1.4.1. Alginate Structure

Alginate, with the chemical structure shown in Figure 1.1⁵², is a high molecular weight unbranched polysaccharide mainly extracted from brown algae⁵. The anionic polysaccharide⁵, which is composed of mannuronic (M) and guluronic (G) acid residues⁵², was first discovered by Edward Stanford in 1883 and its commercial production was initiated in 1927⁵.

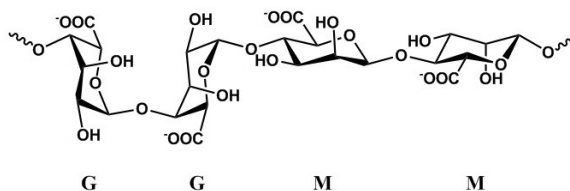


Figure 1.1. Chemical structure of alginate⁵².

The G and M blocks can form homopolymeric GG and MM blocks as well as heteropolymeric MG blocks. M and G blocks have conformational and structural differences. While the G section is buckled (due to its axial glycosidic bonds) the M blocks are flat (due to their equatorial binding). Therefore, a change in the relative content of these blocks in the copolymer results in different properties in the alginate. For instance, alginates which have a high content of mannuronic acid are more flexible compared to high guluronic acid content alginates which have stiffer polymer chains. The source of the seaweed, the harvest season, and the part of the algae from which the alginate is extracted, are among the factors influencing the ratios of the M and G blocks in the alginate chain⁵.

1.4.2. Alginate Gelation

Alginate is a non-toxic, relatively inexpensive, and degradable polymer⁵ which has been widely investigated in microparticle preparations⁵³. In the presence of multivalent cations, such as Ca^{2+} , Sr^{2+} , Ba^{2+} , Fe^{3+} , and Al^{3+} , alginate ionically crosslinks to form a gel at room temperature and under mild conditions, a process free from the use of organic and toxic solvents^{5,53}. The spontaneous gel formation is a result of the crosslinking of adjacent alginate chains by ionic bonds via the cations⁵⁴.

Among the different cation-alginate gels, calcium-alginate hydrogels are the most widely used carriers in enzyme, protein and drug delivery applications and are considered to be clinically safe^{5,6}. The mild processing conditions and low cost make this encapsulation method very attractive⁶. Extrusion of alginate solution through needles into a calcium chloride solution is the most common method used for producing Ca-alginate beads^{5,55}.

As illustrated in Figure 1.2, the location of Ca^{2+} ions in electronegative cavities between homopolymeric G blocks simulates the position of eggs in an egg box and has led to the use of the term “egg-box model” for the cation-alginate gels^{5,6}.

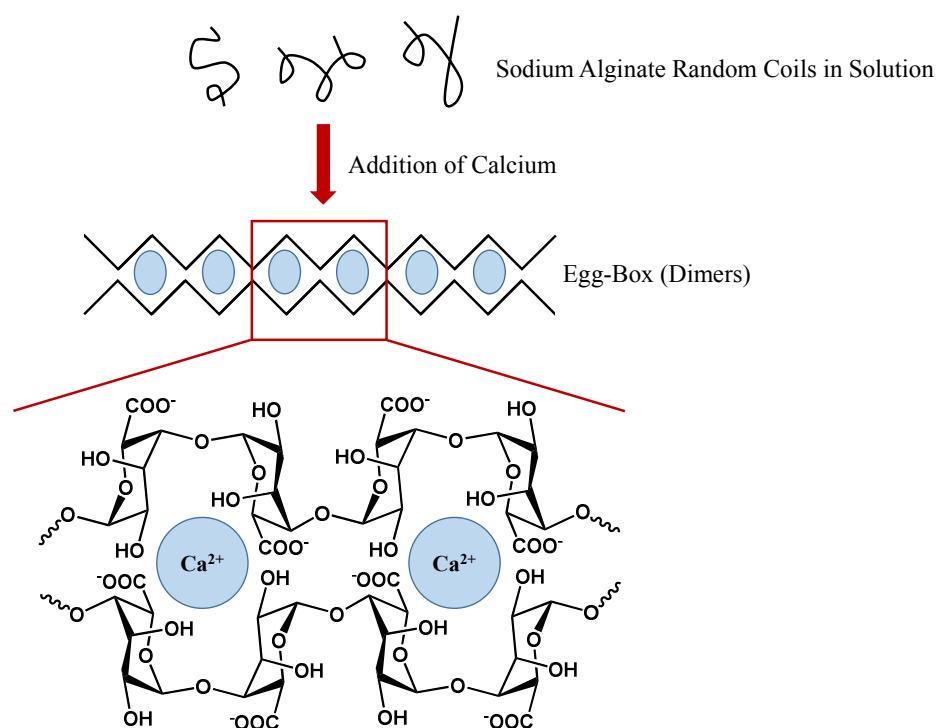


Figure 1.2. Schematic representation of the “egg box model”, showing interactions between calcium ions and sodium alginate in the gelation process⁵.

While alginate is considered non-biodegradable in mammals due to the lack of an alginase enzyme which can cleave the polymer, alginate gels ionically crosslinked with multivalent cations are degraded through ion exchange with monovalent cations such as sodium ions in the surrounding media⁵⁶.

1.4.3. Alginate for Protein Delivery

Numerous studies have been done on protein encapsulation and release from alginate hydrogels. An overview of some of the investigations carried out in the recent decade is summarized in Table 1.1.

Table 1.1. Summary of recent studies on proteins encapsulation in alginate beads.

Protein	Notes
Bovine Serum Albumin (BSA)	<i>Hydrophobic modification of sodium alginate was done by coupling the polysaccharide with polybutyl methacrylate in order to control protein release through hydrophobic interactions between the polymer matrix and the protein⁵⁷.</i>
	<i>Protein release was optimized and gel dissolution was hindered by including guar gum along with glutaraldehyde as its crosslinking agent in the calcium-alginate matrix⁵⁸.</i>
Chymotrypsin	<i>Protein loading was increased by opening the pore structure of the hydrogel through partial degradation and by soaking alginate microparticles in protein-containing sodium chloride solution⁵⁹.</i>
Fibrinogen	<i>Calcium-alginate beads were coated with calcium poly(L-glutamate) as a gel disintegration barrier and to modulate an onset release time of model proteins including fibrinogen⁶⁰.</i>
Fibroblast Growth Factor-1 (FGF-1)	<i>Multilayered alginate microcapsules with poly-L-ornithine coating and an outer alginate layer were shown to retain protein activity and provide sustained release⁶¹.</i>

Immunoglobulin G (IgG)	<i>A microfluidic approach was taken for obtaining homogeneous alginate-based particles with unique biconcave shape resembling mammalian red blood cells⁶².</i>
Insulin	<i>Calcium-alginate microparticles with narrow size distribution were prepared by membrane emulsification and chitosan solidification⁶³. Insulin protection from degradation in the gastric environment was improved by reinforcing the calcium-alginate matrix with chitosan and/or dextran sulphate⁶⁴.</i>
Lysozyme	<i>Alginate matrix crosslinked with Fe^{3+} cations was electrochemically generated and used to encapsulate lysozyme. Protein release was triggered by applying an electrochemical signal which converted the iron cations to the Fe^{2+} state and therefore weakened the hydrogel structure⁶⁵.</i>
Myoglobin	<i>An injectable semi-Interpenetrating Polymer Network (semi-IPN) system was developed by dispersion of dextran-methacrylated derivative (Dex-MA) chains into protein-containing-alginate solution which was followed by alginate crosslinking with calcium. The semi-IPN was then cured using a UV source to obtain an IPN with drug delivery potential⁶⁶.</i>
Horseradish Peroxidase (HRP)	<i>Thermosensitive properties were introduced to calcium-alginate microspheres by soaking them in a solution of poly-[(3-acrylamidopropyl)-trimethylammonium chloride-b-N-isopropylacrylamide] which has a lower critical solution temperature (LCST) of 41 °C and was grafted on the microspheres through polyion interactions. The proposed system showed retained protein activity and showed potential for drug depot applications⁶⁷.</i>

As seen in Table 1.1, various methods including chemical⁵⁷ and physical⁶⁷ modifications, reinforcing^{58,63,64,66}, coated⁶⁰ and multilayered⁶¹ assemblies have been applied for overcoming the rapid release of the loaded molecules⁶⁴ from the alginate matrix and obtaining the desired protein encapsulation and release kinetics. Since protein release from hydrogels is mostly diffusion-controlled through aqueous channels of the

hydrogel^{51,68}, another promising approach for effective protein delivery would be taking advantage of the molecular interactions between the protein and the polysaccharide hydrogel network for optimizing the protein entrapments and release⁶⁸.

1.5. Proteins and Polysaccharides in Solution

1.5.1. Protein-Polysaccharide Interactions

Electrostatic interactions, steric exclusion, hydrophobic interactions, and hydrogen bonding are the major non-covalent interactions between proteins and polysaccharides. Electrostatic interactions are considerable when the protein and polymer have electrical charges at the pH and ionic strength of the solution in which they are dispersed. Depending on whether their charge groups have similar or opposite signs, the electrostatic forces will be of repulsive or attractive nature, respectively. The relatively large volume occupied by proteins and polysaccharides in solutions results in steric exclusion effects due to the less available volume for the molecules to occupy. Hydrophobic interactions are the tendency for non-polar groups of molecules to associate with each other in aqueous solutions. Hydrogen bonding occurs through segments of molecules which can form relatively strong hydrogen bonds through helical or sheet-like structures with groups on other molecules. The relative significance of each of these interactions is dependent on the properties of proteins and polymers involved (molecular weight, charge density vs. pH profile, flexibility, hydrophobicity), the solution composition (pH and ionic strength), and the environmental conditions (temperature, shearing). These parameters can be modulated for controlling the interactions⁶⁹.

Figure 1.3 shows the possible different scenarios when protein and polysaccharide solutions are mixed. Depending on the nature of the biopolymers, the solution and environmental conditions, single-phase or two-phase systems are formed as proteins and polysaccharides are mixed. In single-phase systems, the protein and polysaccharide can exist either as soluble complexes or as individual molecules which are evenly distributed throughout the entire system⁶⁹. In two-phase systems, phase separation occurs as a result of either associative or segregative interactions between the two biopolymers due to the attraction and repulsion forces, respectively^{69,70}.

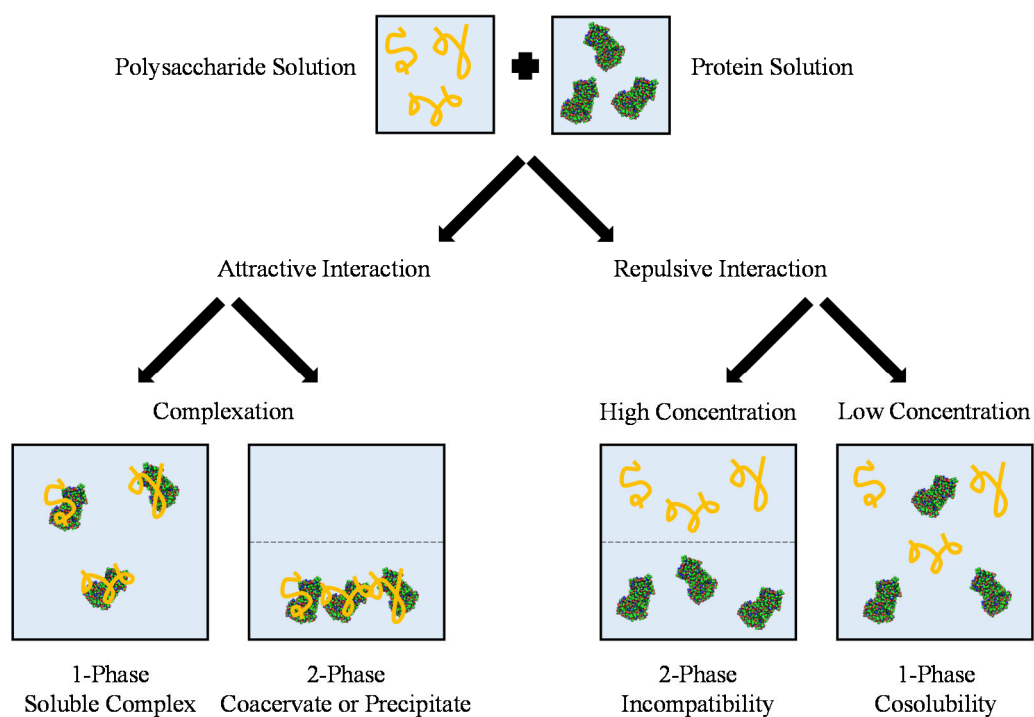


Figure 1.3. Schematic representation of various interactions between proteins and polysaccharides⁶⁹.

Generally, when the electrostatic attractions are inhibited (repulsive forces are present), the biopolymers maintain cosolubility in a dilute solution. As the concentrations increase and exceed a specific critical value, the biopolymers lose their cosolubility due to the large sizes and rigidity of the macromolecules. In the case of the presence of attractive forces between the biopolymers, either soluble or insoluble complexes are formed⁷¹. Strong attractive electrostatic interactions result in the biopolymers associating with each other to form insoluble complexes. This results in phase separation in which the resulting two-phase system consists of one phase rich in both biopolymers and the other phase is depleted in both biopolymers⁶⁹. Soluble complexes are normally formed when one of the biopolymers is present in excess⁷¹.

1.5.2. Protein-Polysaccharide Complexes and Coacervates

Since the pioneering work of Bungenberg *et al.*⁷² on gum arabic-gelatin system in 1929, protein-polysaccharide complexes have gained significant interest in the past years due to their high availability as natural resources⁷³, their simultaneous uses as functional ingredients in food and pharmaceutical industries^{74,75}, and also their great potential for biomedical applications⁷⁶. These self-assembled structures, also referred to as “polyelectrolyte complexes (PEC)s”⁷⁴, are formed upon spontaneous association of oppositely charged polyelectrolytes and/or macromolecules in solution due to strong attractive electrostatic interactions⁷⁵. These systems offer advantages such as formation in the absence of toxic covalent crosslinkers⁷⁷ and in aqueous solution under ambient conditions favorable for proteins⁷⁸.

The theoretical physicochemical aspects of protein-polysaccharide complex systems have not only gained attention due to their wide applicability in a variety of fields such as food, pharmaceuticals, medicine, biotechnology, and cosmetics, but also because of their significant role in biological systems⁷⁴. Proteins and polysaccharides play key roles in cell structure, energy production/storage, and enzymatic transformations in many living organisms⁷⁶. In many of these functions, known as cognate systems, polysaccharide and protein interact specifically when present in the same physiological environment, such as lysozyme and proteoglycans in mammalian cartilage causing possible induction of cartilage calcification^{75,76}. On the other hand, non-cognate systems include protein-polysaccharide pairs that do not necessarily interact specifically⁷⁶.

Complex coacervation occurs between oppositely charged macromolecules at low ionic strengths (less than 300 mM⁷⁹) and low total biopolymer concentrations⁸⁰. The complex formation and stability of these systems is mainly dependent on parameters such as protein/polymer ratio, pH, and ionic strength. The electrostatic complexation is a reversible process and changes in pH or ionic strength will result in complex dissociation⁸¹. For instance, while complexation between anionic polysaccharides and proteins occurs at pH values below the protein isoelectric point (pI), where the protein carries a net positive charge¹³, the complex will dissociate at pH values above the pI due to the repulsion forces between the now similarly charged protein and anionic polysaccharide⁸¹. Electrostatic complexes also dissociate at high ionic strengths (above 200-300 mM)^{79,81} due to charge screening effects of the microions present in the solution

which reduce the range of the associative interactions between the protein and the polysaccharide⁸².

As a result of the responsive behavior of protein-polymer complexes to environmental conditions, these complex systems offer potential to be used as pH-/ion-sensitive drug or protein delivery vehicles. Complex nanoparticles of insulin and amino poly(glycerol methacrylate)s are an example of these responsive delivery vehicles which have been shown to act as a carrier for insulin⁸³. Poly(methacrylic acid)/gelatin, poly(acrylic acid)/gelatin, and heparin/gelatin are also examples of pH- sensitive complexes which have been studied for controlled release of model proteins (myoglobin, cytochrome c, and pepsin)⁸⁴.

Protein-polysaccharide complex systems with pharmaceutical focus have been documented as early as the 1960s, where interactions between serum albumin and hyaluronic acid were investigated^{76,85}. Complexes of alginate with proteins such as lysozyme⁷⁴, β -Lactoglobulin⁸⁶, and bovine serum albumin⁸⁷ have been studied in the recent years for evaluating their potential as delivery systems. Further understanding of the self-assembly process between proteins and polysaccharides and their intermolecular interactions, such as electrostatic interactions, offers possibilities in the design of carriers with enhanced encapsulation and optimized release kinetics.

1.6. Multivariate Statistical Analysis

1.6.1. Latent Variable Methods

Latent variable methods offer a valuable platform for property prediction and optimization by providing insight into existing correlations and building upon the available data⁸⁸. Latent variable methods have revolutionized process control⁸⁹ and have been used for various applications including design of polymers⁸⁸, gene expression data prediction⁹⁰, predicting protein binding affinity⁹¹, and prediction of red wine total antioxidant capacity⁹².

Statistical methods such as Principal Component Analysis (PCA) and Projection to Latent Structures (PLS), also known as Partial Least Squares, offer unique advantages over classical statistical regressions in developing and optimizing processes and products. These methods are able to handle highly correlated, noisy, and missing data, which is often the nature of many process datasets. These methods derive a set of uncorrelated variables called latent variable or principal components from the original variables which summarize all of the factors affecting the process. The latent variables are mathematically described as linear combinations of the original variables and normally the number of such significant latent variables that are truly driving the process behavior is small compared to the number of the process variables measured during the experiment⁹³.

1.6.2. Theory of Projection to Latent Structures (PLS) Models

In a dataset $\mathbf{x} = [x_1, x_2, \dots, x_k]$, where k is the number of measured variables, latent variable models describe the driving behavior of the process by a set of $a \ll k$

latent components. The latent variable space can be represented by an orthogonal set of vectors $\mathbf{t} = [t_1, t_2, \dots, t_a]^{94}$.

For data from two spaces consisting of an \mathbf{X} ($n \times k$) matrix of (n observations of k measured variables) process variables and a response \mathbf{Y} ($n \times m$) matrix (n measurements of m properties), latent variable multivariate regression model is given by Equation 1.1 and Equation 1.2. In the model, \mathbf{T} ($n \times a$) and \mathbf{U} ($n \times a$) are the score matrices (latent variable matrices), \mathbf{P} ($k \times a$) and \mathbf{Q} ($m \times a$) are the loading matrices which show how the latent variables are related to the original \mathbf{X} and \mathbf{Y} variables, superscript T stands for transposed, and \mathbf{E} and \mathbf{F} are residual matrices (random error)^{89,95}.

$$\mathbf{X} = \mathbf{TP}^T + \mathbf{E} \quad \text{Equation 1.1}$$

$$\mathbf{Y} = \mathbf{UQ}^T + \mathbf{F} \quad \text{Equation 1.2}$$

In order to determine the latent variables, two sets of weights denoted as \mathbf{w} and \mathbf{c} are found to create linear combinations of \mathbf{X} and \mathbf{Y} , respectively (Equation 1.3 and Equation 1.4), in such a way that these two linear combinations have maximum covariance⁹⁶.

$$\mathbf{t} = \mathbf{Xw} \quad \text{Equation 1.3}$$

$$\mathbf{u} = \mathbf{Yc} \quad \text{Equation 1.4}$$

The Projection to Latent Structures (PLS) algorithm is a multi-step iteration process where both data matrices \mathbf{X} and \mathbf{Y} are scaled to zero-mean and unit-variance

followed by initializing the vector \mathbf{u} with random values. The algorithm then performs and repeats the following steps until convergence is reached⁹⁶:

Step 1. Estimating X weights: $\mathbf{w} = \mathbf{X}^T \mathbf{u}$

Step 2. Estimating X scores: $\mathbf{t} = \mathbf{X} \mathbf{w}$

Step 3. Estimating Y weights: $\mathbf{c} = \mathbf{Y}^T \mathbf{t}$

Step 4. Estimating Y scores: $\mathbf{u} = \mathbf{Y} \mathbf{c}$

A schematic visualization of the X and Y matrices along with the latent space matrices including the algorithm steps for generating the latent variables is shown in Figure 1.4^{95,97}.

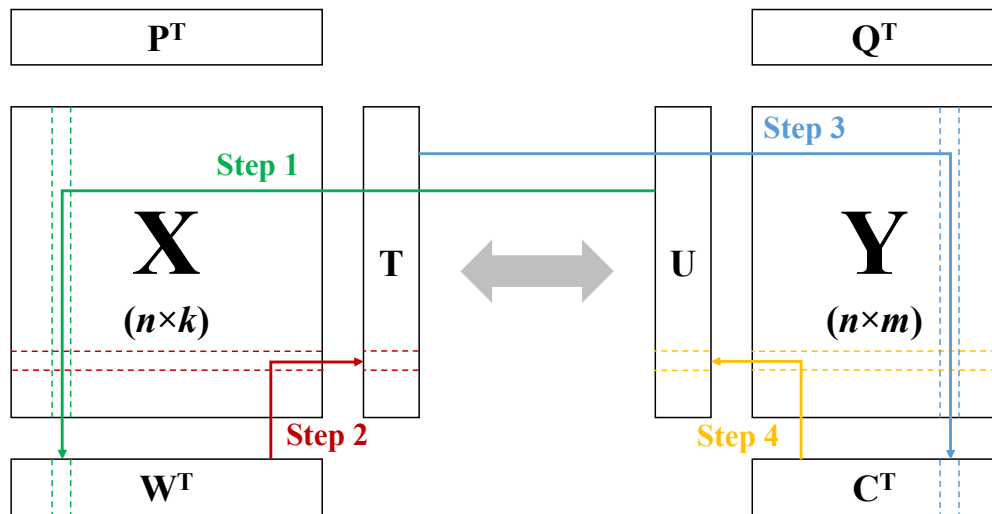


Figure 1.4. Schematic representation of matrices and algorithm steps in PLS model^{95,97}.

The \mathbf{T} and \mathbf{U} matrices are calculated to be maximally correlated⁹⁸ where the residual difference matrix is defined as \mathbf{H} (Equation 1.5)⁹⁹.

$$\mathbf{U} = \mathbf{T} + \mathbf{H} \quad \text{Equation 1.5}$$

When building the initial model, the \mathbf{T} and \mathbf{U} matrices can both be calculated since the \mathbf{X} and \mathbf{Y} data are available. However, when using the built model for future predictions of \mathbf{Y} where the \mathbf{Y} data are unavailable, the \mathbf{U} matrix cannot be calculated. Due to maximal correlation between \mathbf{T} and \mathbf{U} , in a plot of \mathbf{t} versus \mathbf{u} for each component, the observations should fall on the $y=x$ line. Therefore, Equation 1.2 can be rewritten as shown in Equation 1.6 which then can be used for \mathbf{Y} predictions⁹⁸.

$$\mathbf{Y} = \mathbf{T}\mathbf{Q}^T + \mathbf{F} \quad \text{Equation 1.6}$$

Each column in the \mathbf{T} matrix represents a latent variable and often the first few of these latent components are sufficient for explaining a large portion (70-90%) of the total data variance¹⁰⁰.

Latent variable models project the high-dimensional \mathbf{X} and \mathbf{Y} spaces onto the low-dimensional latent variable space \mathbf{T} and therefore, reduce the dimensions of the problem which greatly simplifies the process analysis. Principal component analysis (PCA) defines the latent variables which represent the maximum variance in only a single space (\mathbf{X} or \mathbf{Y}). Projection to Latent Structures or Partial Least Squares (PLS) not only describes the variance in each of the \mathbf{X} and \mathbf{Y} spaces, but also explains the correlation between \mathbf{X} and \mathbf{Y} and therefore maximizes the covariance of \mathbf{X} and \mathbf{Y} ⁸⁹.

1.6.3. PLS Model Evaluation

A variety of parameters are looked at for evaluating the accuracy and the reliability of a PLS model.

Among the common validation criterion are the R^2 and Q^2 parameters which show how well the model fits and predicts data, respectively. R^2X and R^2Y are the fraction of the sum of squares of all the X and Y variables, respectively, explained by the model¹⁰¹. R^2X and R^2Y are similar to R^2 in linear regression and represent how much of the variance in X and Y is explained by the latent components. Q^2 represents the predictive power of the PLS model¹⁰². In other words, R^2 represents the “goodness of fit” while Q^2 is an indicator of the “goodness of prediction” of the model¹⁰³. Although achieving values close to 1 for these parameters is difficult, examining the values before using the models is very important¹⁰⁴.

Plots of the PLS model (correlation-loading plots, score plots) are considered as main validation approaches¹⁰³. In these plots, correlated data are localized in the same regions and form clusters¹⁰⁴. Correlation-loading plots and/or score plots can be used for detection and correction of data outliers or data points with extreme positions¹⁰³. Furthermore, the Squared Prediction Error (SPE) plot, which represents the distance of observations from the model plane, can also be used for detection of data outliers¹⁰⁴.

The observed versus predicted (Obs vs. Pred) plot is a powerful tool for the examination of the model. When comparing the observed values with their model predicted values, a linear relationship is an indication of a “good” prediction¹⁰⁴.

1.7. Thesis Outline

Various strategies have been approached for overcoming the challenging obstacles in protein delivery. The focus of this research is to investigate particle-based delivery systems and specifically, taking advantage of the protein-polymer interactions for designing protein carriers with desirable properties and controlled release kinetics. For further understanding of the molecular interactions and the controlling factors, Projection to Latent Structures (PLS) method was applied as a modelling approach.

Alginate was used as the polysaccharide in preparation of various particles throughout the entire thesis. The interactions of model proteins with the alginate, either in the form of protein-alginate complexes or as in calcium-alginate microparticles with encapsulated proteins, were studied and the physical properties and/or protein release kinetics were modelled and further investigated with multivariate statistical analysis methods.

This thesis is structured in five chapters, with the first chapter covering the introduction and objectives, and chapter 5 concluding the research highlights. Chapter 2, 3, and 4 report the carried out experimental work.

1.7.1. Chapter 2: Property Modelling of Lysozyme/Crosslinker-Alginate Complexes

Using Latent Variable Methods

In this chapter, complexes of alginate and lysozyme (a net positively charged protein at physiological pH) were prepared in the absence and presence of cationic crosslinkers calcium, barium, iron(III), and bovine serum albumin (at pH=4.5), which

would compete with the positively charged lysozyme for crosslinking the alginate chains. Complex properties such as composition, average diameter, and zeta potential were measured in response to different preparation conditions such as initial concentration and pH. Furthermore, the effect of crosslinker charge density on protein release kinetics from the alginate-based complex was evaluated at varying pH and ionic strength conditions. Multivariate statistical analysis was applied for understanding the correlations between the preparation conditions and the final complex properties as well as quantifying the influence of the crosslinker nature on complex degradation and protein release rates. It is believed that the statistical model can be used as a tool in prediction of the complex properties and the ability of the model in predicting initial conditions for obtaining complexes with desired properties was evaluated.

1.7.2. Chapter 3: Protein-Alginate Complexes as pH-/Ion-Sensitive Carriers of Proteins

The study of protein-alginate complexes was further followed in this chapter where lysozyme, chymotrypsin, and bovine serum albumin were used as model proteins for preparing complexes. Physical properties of the complexes including composition, zeta potential, and average diameter were measured and their correlation to the preparation conditions such as the initial protein concentrations were explored using multivariate statistical analysis. In addition, the release of the proteins from the complexes in response to changes in media pH and ionic strength and the potential use of these complexes in ion-/pH-sensitive protein delivery systems were studied. Multivariate statistical analysis was applied for obtaining further insight into the release kinetics which

provided mathematical descriptions of the correlations and a reliable model for prediction of future release patterns of proteins from the protein-alginate complex systems.

1.7.3. Chapter 4: Optimizing Electrostatic Interactions for Controlling the Release of Proteins from Anionic and Cationically Modified Alginate

This focus of this chapter, in line with chapter 2 and 3, is gaining in depth insight into the polymer and protein interactions, specifically electrostatic interactions. While in chapter 2 and 3, self-assembled complexes were prepared by mixing alginate and protein solutions, in this chapter, alginate microparticles were prepared in the absence of protein and through crosslinking with calcium. Model proteins (insulin, bovine serum albumin, lysozyme, chymotrypsin, myoglobin, and horseradish peroxidase), which cover a variety of net charges and a range of molecular weights, were then loaded into the calcium-alginate microparticles.

Furthermore, anionic alginate was cationically modified and was used for evaluating the release of the model proteins from the positively charged calcium-alginate microparticles. The hypothesis of controlling the release of proteins mainly through modifying the absolute charge of the hydrogel network and using electrostatic interactions as a means of manipulating the protein release was further explored using multivariate statistical analysis. Projection to Latent Structures (PLS) not only offered insight into understanding the ongoing trends, but also provided a reliable model as a tool for predicting future release patterns and optimizing delivery systems.

References

1. Lu, Y., Sun, W. & Gu, Z. Stimuli-responsive nanomaterials for therapeutic protein delivery. *J. Control. Release* **194**, 1–19 (2014).
2. Frokjaer, S. & Otzen, D. E. Protein drug stability: a formulation challenge. *Nat. Rev. Drug Discov.* **4**, 298–306 (2005).
3. Vermonden, T., Censi, R. & Hennink, W. E. Hydrogels for Protein Delivery. *Chem. Rev.* **112**, 2853–2888 (2012).
4. Wang, L. *et al.* Microspheres and Microcapsules for Protein Delivery: Strategies of Drug Activity Retention. *Curr. Pharm. Des.* **19**, 6340–6352 (2013).
5. Shilpa, A., Agrawal, S. S. & Ray, A. R. Controlled Delivery of Drugs from Alginate Matrix. *J. Macromol. Sci. Part C Polym. Rev.* **43**, 187–221 (2003).
6. Fundueanu, G., Nastruzzi, C., Carpov, A., Desbrieres, J. & Rinaudo, M. Physico-chemical characterization of Ca-alginate microparticles produced with different methods. *Biomaterials* **20**, 1427–1435 (1999).
7. Fortis, F. *et al.* A pI-based protein fractionation method using solid-state buffers. *J. Proteomics* **71**, 379–389 (2008).
8. Sinha, V. R. & Trehan, A. Biodegradable microspheres for protein delivery. *J. Control. Release* **90**, 261–280 (2003).
9. Weber, A. L. & Miller, S. L. Reasons for the occurrence of the twenty coded protein amino acids. *J. Mol. Evol.* **17**, 273–284 (1981).
10. Zhou, X. H. & Li Wan Po, A. Peptide and protein drugs: I. Therapeutic applications, absorption and parenteral administration. *Int. J. Pharm.* **75**, 97–115 (1991).
11. Pandey, R. B. & Farmer, B. L. Residue energy and mobility in sequence to global structure and dynamics of a HIV-1 protease (1DIFA) by a coarse-grained Monte Carlo simulation. *J. Chem. Phys.* **130**, 44906 (2009).
12. Sutherland, B. W., Toews, J. & Kast, J. Utility of formaldehyde cross-linking and mass spectrometry in the study of protein–protein interactions. *J. Mass Spectrom.* **43**, 699–715 (2008).
13. Siddiqui, O., Sun, Y., Liu, J.-C. & Chien, Y. W. Facilitated Transdermal Transport of Insulin. *J. Pharm. Sci.* **76**, 341–345 (1987).
14. Banting, F. G., Best, C. H., Collip, J. B., Campbell, W. R. & Fletcher, A. A.

- Pancreatic Extracts in the Treatment of Diabetes Mellitus. *Can. Med. Assoc. J.* **12**, 141–146 (1922).
15. Tan, M. L., Choong, P. F. M. & Dass, C. R. Recent developments in liposomes, microparticles and nanoparticles for protein and peptide drug delivery. *Peptides* **31**, 184–193 (2010).
 16. Leader, B., Baca, Q. J. & Golan, D. E. Protein therapeutics: a summary and pharmacological classification. *Nat. Rev. Drug Discov.* **7**, 21–39 (2008).
 17. Yun, Y., Cho, Y. W. & Park, K. Nanoparticles for oral delivery: Targeted nanoparticles with peptidic ligands for oral protein delivery. *Adv. Drug Deliv. Rev.* **65**, 822–832 (2013).
 18. Al-Qadi, S., Grenha, A., Carrión-Recio, D., Seijo, B. & Remuñán-López, C. Microencapsulated chitosan nanoparticles for pulmonary protein delivery: In vivo evaluation of insulin-loaded formulations. *J. Control. Release* **157**, 383–390 (2012).
 19. Kim, Y. C., Chiang, B., Wu, X. & Prausnitz, M. R. Ocular delivery of macromolecules. *J. Control. Release* **190**, 172–181 (2014).
 20. Kalluri, H. & Banga, A. K. Transdermal Delivery of Proteins. *AAPS PharmSciTech* **12**, 431–441 (2011).
 21. Cleland, J. L., Daugherty, A. & Msrny, R. Emerging protein delivery methods. *Curr. Opin. Biotechnol.* **12**, 212–219 (2001).
 22. Ye, M., Kim, S. & Park, K. Issues in long-term protein delivery using biodegradable microparticles. *J. Control. Release* **146**, 241–260 (2010).
 23. Lee, J., Oh, Y. J., Lee, S. K. & Lee, K. Y. Facile control of porous structures of polymer microspheres using an osmotic agent for pulmonary delivery. *J. Control. Release* **146**, 61–67 (2010).
 24. Andrade, F., Videira, M., Ferreira, D. & Sarmiento, B. Nanocarriers for pulmonary administration of peptides and therapeutic proteins. *Nanomedicine* **6**, 123–141 (2011).
 25. Aimetti, A. A., Machen, A. J. & Anseth, K. S. Poly(ethylene glycol) hydrogels formed by thiol-ene photopolymerization for enzyme-responsive protein delivery. *Biomaterials* **30**, 6048–6054 (2009).
 26. Yang, J., Chen, J., Pan, D., Wan, Y. & Wang, Z. pH-sensitive interpenetrating network hydrogels based on chitosan derivatives and alginate for oral drug delivery. *Carbohydr. Polym.* **92**, 719–725 (2013).

27. Sim, H. J., Thambi, T. & Lee, D. S. Heparin-based temperature-sensitive injectable hydrogels for protein delivery. *J. Mater. Chem. B* **3**, 8892–8901 (2015).
28. Rasool, N., Yasin, T., Heng, J. Y. Y. & Akhter, Z. Synthesis and characterization of novel pH-, ionic strength and temperature- sensitive hydrogel for insulin delivery. *Polymer (Guildf)*. **51**, 1687–1693 (2010).
29. Hoare, T. R. & Kohane, D. S. Hydrogels in drug delivery: Progress and challenges. *Polymer (Guildf)*. **49**, 1993–2007 (2008).
30. Junghanns, J.-U. A. H. & Müller, R. H. Nanocrystal technology, drug delivery and clinical applications. *Int. J. Nanomedicine* **3**, 295–309 (2008).
31. Shah, S. S. *et al.* Drug delivery to the posterior segment of the eye for pharmacologic therapy. *Expert Rev. Ophthalmol.* **5**, 75–93 (2010).
32. Paolicelli, P., de la Fuente, M., Sánchez, A., Seijo, B. & Alonso, M. J. Chitosan nanoparticles for drug delivery to the eye. *Expert Opin. Drug Deliv.* **6**, 239–253 (2009).
33. Wang, L.-Y., Gu, Y.-H., Su, Z.-G. & Ma, G.-H. Preparation and improvement of release behavior of chitosan microspheres containing insulin. *Int. J. Pharm.* **311**, 187–195 (2006).
34. Geng, Y. *et al.* Formulating erythropoietin-loaded sustained-release PLGA microspheres without protein aggregation. *J. Control. Release* **130**, 259–265 (2008).
35. Bowey, K., Swift, B. E., Flynn, L. E. & Neufeld, R. J. Characterization of biologically active insulin-loaded alginate microparticles prepared by spray drying. *Drug Dev. Ind. Pharm.* **39**, 457–465 (2013).
36. Mok, H. & Park, T. Water-free microencapsulation of proteins within PLGA microparticles by spray drying using PEG-assisted protein solubilization technique in organic solvent. *Eur. J. Pharm. Biopharm.* **70**, 137–144 (2008).
37. Özbaş-Turan, S., Akbuğa, J. & Aral, C. Controlled Release of Interleukin-2 from Chitosan Microspheres. *J. Pharm. Sci.* **91**, 1245–1251 (2002).
38. Thomasin, C., Merkle, H. P. & Gander, B. A. Physico-chemical parameters governing protein microencapsulation into biodegradable polyesters by coacervation. *Int. J. Pharm.* **147**, 173–186 (1997).
39. Shenoy, D. B. & Sukhorukov, G. B. Microgel-Based Engineered Nanostructures and Their Applicability with Template-Directed Layer-by-Layer Polyelectrolyte Assembly in Protein Encapsulation. *Macromol. Biosci.* **5**, 451–458 (2005).

40. Avadi, M. R. *et al.* Preparation and characterization of insulin nanoparticles using chitosan and Arabic gum with ionic gelation method. *Nanomedicine Nanotechnology, Biol. Med.* **6**, 58–63 (2010).
41. Lee, M. *et al.* Biomimetic apatite-coated alginate/chitosan microparticles as osteogenic protein carriers. *Biomaterials* **30**, 6094–6101 (2009).
42. Ameri, M. & Maa, Y.-F. Spray Drying of Biopharmaceuticals: Stability and Process Considerations. *Dry. Technol.* **24**, 763–768 (2006).
43. Jain, R. A. The manufacturing techniques of various drug loaded biodegradable poly(lactide-co-glycolide) (PLGA) devices. *Biomaterials* **21**, 2475–2490 (2000).
44. Frangione-Beebe, M., Rose, R. T., Kaumaya, P. T. P. & Schwendeman, S. P. Microencapsulation of a synthetic peptide epitope for HTLV-1 in biodegradable poly(D,L-lactide-co-glycolide) microspheres using a novel encapsulation technique. *J. Microencapsul.* **18**, 663–677 (2001).
45. Determan, A. S., Trewyn, B. G., Lin, V. S.-Y., Nilsen-Hamilton, M. & Narasimhan, B. Encapsulation, stabilization, and release of BSA-FITC from polyanhydride microspheres. *J. Control. Release* **100**, 97–109 (2004).
46. Gombotz, W. R. & Wee, S. F. Protein release from alginate matrices. *Adv. Drug Deliv. Rev.* **31**, 267–285 (1998).
47. Amidi, M., Mastrobattista, E., Jiskoot, W. & Hennink, W. E. Chitosan-based delivery systems for protein therapeutics and antigens. *Adv. Drug Deliv. Rev.* **62**, 59–82 (2010).
48. Oh, E. J. *et al.* Target specific and long-acting delivery of protein, peptide, and nucleotide therapeutics using hyaluronic acid derivatives. *J. Control. Release* **141**, 2–12 (2010).
49. Van Tomme, S. R. & Hennink, W. E. Biodegradable dextran hydrogels for protein delivery applications. *Expert Rev. Med. Devices* **4**, 147–164 (2007).
50. Bilati, U., Allémann, E. & Doelker, E. Strategic approaches for overcoming peptide and protein instability within biodegradable nano- and microparticles. *Eur. J. Pharm. Biopharm.* **59**, 375–388 (2005).
51. Lee, K. Y. & Yuk, S. H. Polymeric protein delivery systems. *Prog. Polym. Sci.* **32**, 669–697 (2007).
52. Leng, B., Jiang, F., Lu, K., Ming, W. & Shao, Z. Growth of calcium carbonate mediated by slowly released alginate. *CrystEngComm* **12**, 730–736 (2010).

53. Joshi, A., Keerthiprasad, R., Jayant, R. D. & Srivastava, R. Nano-in-micro alginate based hybrid particles. *Carbohydr. Polym.* **81**, 790–798 (2010).
54. Zarate, J. *et al.* Design and characterization of calcium alginate microparticles coated with polycations as protein delivery system. *J. Microencapsul.* **28**, 614–620 (2011).
55. Fundueanu, G. *et al.* Preparation and characterization of Ca-alginate microspheres by a new emulsification method. *Int. J. Pharm.* **170**, 11–21 (1998).
56. Lee, K. Y. & Mooney, D. J. Alginate: Properties and biomedical applications. *Prog. Polym. Sci.* **37**, 106–126 (2012).
57. Yao, B., Ni, C., Xiong, C., Zhu, C. & Huang, B. Hydrophobic modification of sodium alginate and its application in drug controlled release. *Bioprocess Biosyst. Eng.* **33**, 457–463 (2010).
58. George, M. & Abraham, T. E. pH sensitive alginate–guar gum hydrogel for the controlled delivery of protein drugs. *Int. J. Pharm.* **335**, 123–129 (2007).
59. Wells, L. A. & Sheardown, H. Extended release of high pI proteins from alginate microspheres via a novel encapsulation technique. *Eur. J. Pharm. Biopharm.* **65**, 329–335 (2007).
60. Suzuki, S., Asoh, T.-A. & Kikuchi, A. Design of core-shell gel beads for time-programmed protein release. *J. Biomed. Mater. Res. Part A* **101A**, 1345–1352 (2013).
61. Khanna, O., Moya, M. L., Opara, E. C. & Brey, E. M. Synthesis of multilayered alginate microcapsules for the sustained release of fibroblast growth factor-1. *J. Biomed. Mater. Res. Part A* **95A**, 632–640 (2010).
62. Mazutis, L., Vasiliasuskas, R. & Weitz, D. A. Microfluidic Production of Alginate Hydrogel Particles for Antibody Encapsulation and Release. *Macromol. Biosci.* **15**, 1641–1646 (2015).
63. Zhang, Y., Wei, W., Lv, P., Wang, L. & Ma, G. Preparation and evaluation of alginate–chitosan microspheres for oral delivery of insulin. *Eur. J. Pharm. Biopharm.* **77**, 11–19 (2011).
64. Martins, S., Sarmiento, B., Souto, E. B. & Ferreira, D. C. Insulin-loaded alginate microspheres for oral delivery – Effect of polysaccharide reinforcement on physicochemical properties and release profile. *Carbohydr. Polym.* **69**, 725–731 (2007).
65. Jin, Z. *et al.* Electrochemically stimulated release of lysozyme from an alginate

- matrix cross-linked with iron cations. *J. Mater. Chem.* **22**, 19523–19528 (2012).
66. Matricardi, P., Pontoriero, M., Coviello, T., Casadei, M. A. & Alhaique, F. In Situ Cross-Linkable Novel Alginate-Dextran Methacrylate IPN Hydrogels for Biomedical Applications: Mechanical Characterization and Drug Delivery Properties. *Biomacromolecules* **9**, 2014–2020 (2008).
 67. Oddo, L. *et al.* Novel thermosensitive calcium alginate microspheres: Physico-chemical characterization and delivery properties. *Acta Biomater.* **6**, 3657–3664 (2010).
 68. Tabata, Y. & Ikada, Y. Protein release from gelatin matrices. *Adv. Drug Deliv. Rev.* **31**, 287–301 (1998).
 69. McClements, D. J. Non-covalent interactions between proteins and polysaccharides. *Biotechnol. Adv.* **24**, 621–625 (2006).
 70. de Kruif, C. G. & Tuinier, R. Polysaccharide protein interactions. *Food Hydrocoll.* **15**, 555–563 (2001).
 71. Tolstoguzov, V. Some thermodynamic considerations in food formulation. *Food Hydrocoll.* **17**, 1–23 (2003).
 72. Bungenberg de Jong, H. G. & Kruyt, H. R. Coacervation (Partial Miscibility in Colloid Systems). *Proc. K. Ned. Akad. van Wet.* **32**, 849–856 (1929).
 73. Fioramonti, S. A., Perez, A. A., Aringoli, E. E., Rubiolo, A. C. & Santiago, L. G. Design and characterization of soluble biopolymer complexes produced by electrostatic self-assembly of a whey protein isolate and sodium alginate. *Food Hydrocoll.* **35**, 129–136 (2014).
 74. Fuenzalida, J. P. *et al.* On the role of alginate structure in complexing with lysozyme and application for enzyme delivery. *Food Hydrocoll.* **53**, 239–248 (2016).
 75. Schmitt, C. & Turgeon, S. L. Protein/polysaccharide complexes and coacervates in food systems. *Adv. Colloid Interface Sci.* **167**, 63–70 (2011).
 76. Fuenzalida, J. & Goycoolea, F. Polysaccharide-Protein Nanoassemblies: Novel Soft Materials for Biomedical and Biotechnological Applications. *Curr. Protein Pept. Sci.* **16**, 89–99 (2015).
 77. Mizrahy, S. & Peer, D. Polysaccharides as building blocks for nanotherapeutics. *Chem. Soc. Rev.* **41**, 2623–2640 (2012).
 78. van Rijn, P. Polymer Directed Protein Assemblies. *Polymers (Basel)*. **5**, 576–599

(2013).

79. Ye, A. Complexation between milk proteins and polysaccharides via electrostatic interaction: principles and applications – a review. *Int. J. Food Sci. Technol.* **43**, 406–415 (2008).
80. Wang, L. *et al.* Hydrogen bonding enhances the electrostatic complex coacervation between κ -carrageenan and gelatin. *Colloids Surfaces A Physicochem. Eng. Asp.* **482**, 604–610 (2015).
81. Benichou, A., Aserin, A. & Garti, N. Double emulsions stabilized with hybrids of natural polymers for entrapment and slow release of active matters. *Adv. Colloid Interface Sci.* **108–109**, 29–41 (2004).
82. Weinbreck, F., de Vries, R., Schrooyen, P. & de Kruif, C. G. Complex Coacervation of Whey Proteins and Gum Arabic. *Biomacromolecules* **4**, 293–303 (2003).
83. Lu, X. *et al.* Polyelectrolyte complex nanoparticles of amino poly(glycerol methacrylate)s and insulin. *Int. J. Pharm.* **423**, 195–201 (2012).
84. Jiang, H. L. & Zhu, K. J. Polyanion/gelatin complexes as pH-sensitive gels for controlled protein release. *J. Appl. Polym. Sci.* **80**, 1416–1425 (2001).
85. Pigman, W., Gramling, E. & Holley, H. L. Interactions of hyaluronic acid with serum albumin. *Biochim. Biophys. Acta* **46**, 100–107 (1961).
86. Hosseini, S. M. H. *et al.* β -Lactoglobulin–sodium alginate interaction as affected by polysaccharide depolymerization using high intensity ultrasound. *Food Hydrocoll.* **32**, 235–244 (2013).
87. Zhao, Y., Li, F., Carvajal, M. T. & Harris, M. T. Interactions between bovine serum albumin and alginate: An evaluation of alginate as protein carrier. *J. Colloid Interface Sci.* **332**, 345–353 (2009).
88. Tzoc Torres, J. M. G., Nichols, E., MacGregor, J. F. & Hoare, T. Designing multi-responsive polymers using latent variable methods. *Polymer (Guildf)*. **55**, 505–516 (2014).
89. Kourti, T. Application of latent variable methods to process control and multivariate statistical process control in industry. *Int. J. Adapt. Control Signal Process.* **19**, 213–246 (2005).
90. Nguyen, D. V & Roche, D. M. Partial least squares proportional hazard regression for application to DNA microarray survival data. *Bioinformatics* **18**, 1625–1632 (2002).

91. Catana, C. & Stouten, P. F. W. Novel, Customizable Scoring Functions, Parameterized Using N-PLS, for Structure-Based Drug Discovery. *J. Chem. Inf. Model.* **47**, 85–91 (2007).
92. Versari, A., Parpinello, G. P., Scazzina, F. & Rio, D. Del. Prediction of total antioxidant capacity of red wine by Fourier transform infrared spectroscopy. *Food Control* **21**, 786–789 (2010).
93. MacGregor, J. F., Bruwer, M. J., Miletic, I., Cardin, M. & Liu, Z. Latent Variable Models and Big Data in the Process Industries. *IFAC-PapersOnLine* **48**, 520–524 (2015).
94. MacGregor, J. F., Yu, H., García Muñoz, S. & Flores-Cerrillo, J. Data-based latent variable methods for process analysis, monitoring and control. *Comput. Chem. Eng.* **29**, 1217–1223 (2005).
95. Galindo-Prieto, B., Eriksson, L. & Trygg, J. Variable influence on projection (VIP) for OPLS models and its applicability in multivariate time series analysis. *Chemom. Intell. Lab. Syst.* **146**, 297–304 (2015).
96. Abdi, H. Partial least squares regression and projection on latent structure regression (PLS Regression). *Wiley Interdiscip. Rev. Comput. Stat.* **2**, 97–106 (2010).
97. Dunn, K. *Process Improvement Using Data*. (2016).
98. ProSensus Inc. *ProSensus Multivariate Help 16.02 Documentation*. (2016).
99. Wold, S. Nonlinear partial least squares modelling II. Spline inner relation. *Chemom. Intell. Lab. Syst.* **14**, 71–84 (1992).
100. Guha, R., Stanton, D. T. & Jurs, P. C. Interpreting Computational Neural Network Quantitative Structure–Activity Relationship Models: A Detailed Interpretation of the Weights and Biases. *J. Chem. Inf. Model.* **45**, 1109–1121 (2005).
101. Jenssen, H. *et al.* Evaluating Different Descriptors for Model Design of Antimicrobial Peptides with Enhanced Activity Toward *P. aeruginosa*. *Chem. Biol. Drug Des.* **70**, 134–142 (2007).
102. Sobek, S., Tranvik, L. J., Prairie, Y. T., Kortelainen, P. & Cole, J. J. Patterns and regulation of dissolved organic carbon: An analysis of 7,500 widely distributed lakes. *Limnol. Oceanogr.* **52**, 1208–1219 (2007).
103. Henningsson, M., Sundbom, E., Armelius, B.-A. & Erdberg, P. PLS model building: A multivariate approach to personality test data. *Scand. J. Psychol.* **42**, 399–409 (2001).

104. Tzoc Torres, J. M. G. Designing Dual Thermoresponsive & Photoresponsive Materials for Biomedical Applications. (McMaster University, 2011).

Chapter 2: Property Modelling of Lysozyme/Crosslinker-Alginate Complexes

Using Latent Variable Methods

Vida Rahmani¹, Rand Elshereef², Heather Sheardown^{1,3*}

¹ Department of Chemical Engineering, McMaster University, 1280 Main Street West, Hamilton ON L8S 4L7, Canada

² ProSensus Inc., 303-1425 Cormorant Road, Ancaster ON L9G 4V5, Canada

³ School of Biomedical Engineering, McMaster University, 1280 Main Street West, Hamilton ON L8S 4L7, Canada

* Corresponding author: sheadow@mcmaster.ca

Objectives:

Applying multivariate statistical analysis for providing insight into complex systems composed of lysozyme/crosslinker and alginate, for quantifying the factors which influence complex properties and protein release rates, and for building a model which would offer a platform for prediction of property and degradation kinetic of complexes.

Main Scientific Contributions:

- Preparation of lysozyme/crosslinker and alginate complexes at various pH and ionic composition of the mixing solutions.
- Property measurements of the complexes.
- Investigating protein release from the complexes prepared in presence of different crosslinkers in response to changes in pH and ionic strength of the release media.
- Applying multivariate statistical analysis for quantitatively describing the correlations between the initial conditions and the final properties as well as release kinetics.
- Using the model provided by the multivariate statistical approach for prediction of properties and design of desired complexes.

Author Contribution:

Vida was responsible for the experimental work (synthesis and characterization of the complexes, property measurements, protein release experiments, applying multivariate analysis) and paper write-up.

Dr. Rand Elshereef revised and edited the multivariate statistical sections.

The work was done in consultation with and under the supervision of Dr. Heather Sheardown. Dr. Heather Sheardown revised the draft to the final version.

Abstract

The purpose of this study was to provide insight into the complex system composed of lysozyme/crosslinker and alginate and to quantify the effects of various parameters on complex properties by means of statistical methods. Changes in the properties of the lysozyme-alginate complexes such as composition, average diameter, and zeta potential, prepared in the presence and absence of calcium due to changes in pH and ionic composition of the mixing solutions were studied. Furthermore, crosslinkers calcium, barium, iron(III), and bovine serum albumin (BSA), were used alongside lysozyme for forming complexes with alginate in order to investigate the effect of crosslinker charge density on protein release kinetics (kt^n) from the alginate-based complex. Multivariate statistical analysis assisted in quantifying the influence of the crosslinker nature on protein release rates and showed the high dependency of the release kinetic parameters on the ionic strength of the release media. It was revealed that next to ionic strength, parameter k was most dependent on protein properties while parameter n , which is indicative of the release mechanism, had a slight dependency on the charge density of the crosslinker. It was concluded that the influence of the nature of the crosslinker on release rates at typical *in vivo* conditions is minimal due to the high ion-sensitivity of these complex systems and their disintegration-based release mechanisms rather than diffusion-governed kinetics. In addition to understanding the trends, the multivariate statistical approach provided a reliable model that has the potential to be used for optimization of the complexes and prediction of their physical properties as well as their degradation rates.

Keywords: Alginate; Lysozyme; Protein-Polysaccharide interactions; Polyelectrolyte complex; Protein release; Multivariate statistical analysis

2.1. Introduction

Since the work of Bungenberg *et al.*¹ in 1929, polysaccharide-protein electrostatic complexes have been extensively studied due to their high availability², their potential for use as functional ingredients in both the food and pharmaceutical industries^{3,4}, and their potential for use in biomedical applications⁵. The polyelectrolyte complexes (PECs) formed upon spontaneous association of oppositely charged polyelectrolytes in solution as a result of strong electrostatic interactions⁴, also offer the advantages of formation in aqueous solution under ambient conditions favorable for proteins⁶ and in the absence of toxic covalent crosslinkers⁷.

The theoretical physicochemical aspects of these self-assembled systems have gained significant attention due to their numerous potential applications in various fields, particularly in biological systems³. Proteins and polysaccharides play key roles in cell structure, energy production and storage, and enzymatic transformation in many living organisms⁵. In many of these instances, proteins and polysaccharides interact specifically when present in the same physiological environment. For example, interaction of lysozyme and proteoglycans in mammalian cartilage has been suggested to play a role in the induction of cartilage calcification^{4,5}.

Lysozyme is an enzymatic protein with a molecular weight of 14,300 Da and an isoelectric point (pI) of 11.4⁵. Lysozyme has been widely used as a food preservative due

to its antimicrobial properties which includes hydrolysis of the β -(1 \rightarrow 4) glycosidic linkages between N-acetylmuramic acid and N-acetylglucosamine of the peptidoglycan bacterial cell wall⁸. The high pI of lysozyme results in a net positive charge for the protein over a wide range of pH, giving it the ability to bind electrostatically to many anionic polysaccharides⁵ including alginate³, hyaluronic acid⁹, and pectin⁸.

Of particular interest, alginate is an anionic polysaccharide composed of mannuronic (M) and guluronic (G) acid residues⁷ with pKa values of 3.38 and 3.65³, respectively. In the presence of multivalent cations such as calcium, alginate is crosslinked ionically to form gels under ambient conditions and without the need for toxic organic solvents^{10,11}. Furthermore, as a result of its low toxicity and highly mucoadhesive nature⁷, alginate has been broadly investigated for use in biomedical applications such as drug delivery, cell encapsulation, and wound healing¹². Alginate is also widely used as stabilizer, and thickening and gelling agent in the food industry¹³.

Lysozyme-alginate complexes have been mostly explored from the perspective of lysozyme enzymatic activity¹⁴ or more recently, as carriers in enzyme delivery applications³. It has also been shown that ionic crosslinking, using for example calcium as a crosslinking agent, can strengthen the polysaccharide-protein interactions^{3,7}. This study focuses on preparation of lysozyme-alginate complexes, in the presence and absence of cationic crosslinkers, and establishing relationships between the preparation conditions and the final properties of the complex. Complexes were prepared at various initial conditions (pH, charge ratios) and the final properties such as complex composition, average diameter, and zeta potential were measured. A variety of crosslinkers with

different charge densities were incorporated into the complex system and the effect of their presence on the degradation behavior of the complexes was studied.

Despite numerous studies on protein-polysaccharide complexes, the related literature does not provide a comprehensive understanding of the relationships and correlations. Due to the sensitivity of these systems to changes in environmental conditions including pH, ionic composition, and temperature¹³, the influence of each of these factors should be carefully taken into consideration for the preparation of complexes with desired properties. In addition, with the high dispersity and heterogeneous molecular composition of polysaccharides associated with their biological source and extraction methods, establishing structure-function relationships is a major challenge; understanding these relationships would provide a tool for control and optimization of polyelectrolyte complex systems³.

The Projection to Latent Structures (PLS) method was used for multivariate statistical analysis and model generation. The method operates in a reduced dimensional space by summarizing all of the variables into a lower number of independent latent variables. These latent variables are described mathematically as linear combinations of the original variables and therefore can describe how combinations of variables affect each of the response factors. This regression method simultaneously models the relationships among all X and among all Y variables as well as the correlation between X and Y variables¹⁵. It is hypothesized that this unique regression method can provide better insight into the existing correlations and can be used as a beneficial tool for optimized design of complexes and prediction of properties. To the best of our knowledge, this is

the first study using such statistical method for design optimizations and property prediction of a protein-polysaccharide complex system. The goal of this study was therefore to investigate lysozyme/crosslinker-alginate complexes as an example of protein-polysaccharide systems and to develop relationships between the preparation conditions and the properties of the resulting complexes.

2.2. Materials and Methods

2.2.1. Materials

Sodium alginate from brown algae (65% guluronic acid and 35% mannuronic acid residues) was purchased from Sigma-Aldrich (Oakville, ON). The molecular weight of this alginate was in the range of 100,000-200,000 g/mol. Lysozyme (from chicken egg white), bovine serum albumin (BSA), and all other reagents were also obtained from Sigma-Aldrich (Oakville, ON).

2.2.2. Preparation of Fluorescently-Labeled BSA

A stock solution of rhodamine B isothiocyanate (RITC) at a concentration of 1 mg/mL was prepared in sodium carbonate buffer (pH=9.2, I=100 mM). The RITC solution was added to a solution of BSA (5 mg/mL), which had also been prepared in sodium carbonate buffer (pH=9.2, I=100 mM), in a 0.29:1 volumetric ratio to give a final RITC:BSA molar ratio of 7:1. The mixture was stirred at room temperature overnight. The unreacted RITC was separated from the conjugation by dialysis in deionized water using a 12,000-14,000 MWCO dialysis tube. The fluorescently-labeled protein was then

lyophilized and stored in dark and sealed containers at 4°C until further use. The conjugation reaction was confirmed using a Fluoroskan Ascent™ Microplate Fluorometer (Thermo Fisher Scientific, Waltham, Massachusetts, USA) at 544 nm excitation/590 nm emission.

2.2.3. Preparation of Complexes

Complexes were prepared by mixing solutions of alginate and lysozyme with and without crosslinker in buffers at room temperature. The concentration of the solutions was set to achieve different molar charge mixing ratios. The concentration of anionic charges on alginate was fixed in all solutions to 1 mM. Lysozyme/crosslinker-alginate complexes were formed under these conditions using the method described by Fuenzalida *et al.*³ with the addition of 1.2 mL of alginate solution to 1.8 mL lysozyme/crosslinker solution under constant stirring.

2.2.3.a. Effect of pH (Effect of Protein Net Charge)

At pH=7.4 the total concentration of cationic charges on lysozyme was set to equal the total concentration of anionic charges on the alginate ($[n^+] = [n^-] = 1$ mM). At this equivalent mixing ratio, the charges are equal and opposite. In order to investigate the effect of protein charge distribution on the properties of the complexes formed, the same lysozyme concentration used at pH=7.4 was used for preparing particles at pH values of 4.5 and 10. The concentration of positive charges were calculated to be 1.22 mM at

pH=4.5 and 0.44 mM at pH=10, considering that lysozyme carries a net positive charge of +11, +9, and +4 per mole at pH values of 4.5, 7.4, and 10, respectively^{3,16,17}.

Sodium acetate buffer, sodium phosphate buffer, and sodium carbonate buffer were used for maintaining the pH of the solutions at 4.5, 7.4, and 10, respectively. The ionic strength of the buffers was set to approximately 10 mM.

2.2.3.b. *Effect of Calcium*

The concentration of lysozyme, calcium, and alginate in the solutions was set to achieve different molar ratios of cationic and anionic units. The following experiments were carried out:

- Varying ratios of lysozyme and calcium were used while the concentration of cationic charges on lysozyme plus cationic charges of calcium was set to equal the total concentration of anionic charges on the alginate $[n^+]/[n^-]=1$.
- Lysozyme concentration was kept constant while calcium concentration varied and *vice versa*.

The concentrations of lysozyme and calcium were calculated to achieve different molar ratios of calcium and lysozyme considering that at pH=7.4, lysozyme carries a net positive charge of +9 per mole¹⁶ and each mole of calcium binds two groups of carboxylate groups³. Sodium phosphate buffer ($I=10$ mM, pH=7.4) was used in preparation of the lysozyme, calcium, and alginate solutions.

2.2.3.c. Effect of Crosslinker (Matrix Effects)

In order to investigate the effect of crosslinkers on complex properties such as degradation rates, complexes of lysozyme and alginate were prepared in the presence of calcium, barium, iron(III), and bovine serum albumin (BSA). Complexes were prepared by mixing solutions of alginate, lysozyme, and crosslinker in sodium acetate buffer (pH=4.5, $I=10$ mM) at room temperature. Since BSA has an isoelectric point of 5.4¹⁸, the pH of 4.5 ensured that BSA is carrying a net positive charge and is capable of crosslinking the anionic alginate. The concentration of crosslinkers was calculated to obtain a crosslinker to lysozyme molar charge ratio of 1:1. Furthermore, the concentration of the cationic charges on lysozyme plus the cationic charges on crosslinker was set to equal the total concentration of anionic charges on the alginate.

2.2.4. Complex Composition Analysis

Component precipitation and mole fraction in the complexes were determined indirectly by measuring the concentration of the components in the supernatant collected after centrifugation ($100 \times g$, 90 s).

Calcium concentration was measured using the ethylenediaminetetraacetic acid (EDTA) titration method¹⁹. Briefly, 1 mL of sample solution was mixed with 1 mL of 8 M potassium hydroxide solution and subsequently approximately 2 mg of calconcarboxylic acid (NN indicator) was added. The wine-red colored solution was titrated immediately with 0.001 M EDTA solution until a sky-blue color was developed. The amount of calcium in the sample was calculated using $\text{Ca}^{2+}:\text{EDTA}=1:1$ mole ratio.

Barium concentration was determined by EDTA titration method and using methylthymol blue indicator. The pH of the sample was adjusted to 12 using 0.1 M NaOH solution and approximately 2 mg of methylthymol blue was added to the solution. Titration was carried out with 0.001 M EDTA solution until the initial blue color of the solution was changed to gray. The amount of barium in the sample was calculated using $\text{Ba}^{2+}:\text{EDTA}=1:1$ mole ratio^{20,21}.

Iron(III) concentration was measured by titration with EDTA and using variamine blue indicator. The pH of the sample was adjusted to 3 using 0.1 M HCl solution followed by addition of 10 μL of variamine blue solution (10 mg in 1 mL in deionized water) to the sample. The blue colored solution was titrated with 0.001 M EDTA solution until a yellow colored solution was reached. The amount of iron in the sample was calculated using $\text{Fe}^{3+}:\text{EDTA}=1:1$ mole ratio²⁰.

Alginate content was determined using the phenol-sulfuric acid assay²². Briefly, 0.1 mL of alginate sample was mixed with an equal volume of distilled water followed by the addition of 0.2 mL of 5% (w/v) phenol and 1 mL of concentrated sulfuric acid. The mixture was incubated at room temperature for 15 min after which the sample absorbance was measured at 488 nm. Alginate concentrations were determined from comparison with known standards.

Fluorescently-labeled BSA (RITC-BSA) was measured using a Fluoroskan AscentTM Microplate Fluorometer (Thermo Fisher Scientific, Waltham, Massachusetts, USA) at 544 nm excitation/590 nm emission. The concentration of fluorescence was calculated on the basis of calibration curves.

Lysozyme content was determined using a Bradford assay. Bradford reagent was added to the lysozyme samples and the absorbance was measured at 595 nm (SpectraMax Plus 384 Microplate reader, Molecular Devices LLC, CA, USA). Lysozyme concentration was determined based on comparison with known standards. In the case of measuring lysozyme concentration in samples containing fluorescently-labeled BSA, due to both proteins reacting with the Bradford reagent resulting in measurement of total protein concentration, samples were blanked with fluorescently-labeled BSA solutions of the same concentration measured through fluorescence.

Component precipitation was calculated using Equation 2.1.

$$\text{Precipitation (\%)} = \frac{\text{moles precipitated}}{\text{moles in initial mixing solution}} \times 100\% \quad \text{Equation 2.1}$$

2.2.5. Physical Characterization

Physical characterization of complexes was carried out by investigating the zeta potential of the complexes (Zeta PALS, Brookhaven Instruments Corp., NY, USA) and measuring particle size distributions (Mastersizer 2000 equipped with Hydro 2000S, Malvern Instruments Ltd., UK). The particle size distribution was reported in volume mean diameter and also in terms of SPAN factor (Equation 2.2).

$$\text{SPAN} = \frac{d_{90} - d_{10}}{d_{50}} \quad \text{Equation 2.2}$$

In Equation 2.2, values of d_{10} , d_{50} , and d_{90} indicate the diameters below which the given percentages (10, 50, and 90) of the particles are smaller. Wide size distributions are indicated by high SPAN values²³.

2.2.6. Protein Release

Protein release studies were carried out in sodium acetate buffer and sodium phosphate buffer at pH values of 4.5 and 7.4, respectively. Furthermore, for evaluating the effect of ionic strength of the buffer and salt concentration on the release kinetics, low ionic strength ($I=10$ mM) and high ionic strength ($I=150$ mM) buffers were used as release media at each of the pH conditions. Complexes were suspended in 1.5 mL of buffer and placed in a 37°C and 100 rpm incubator. At regular intervals, release tubes were centrifuged (2000 rpm, 2 min) and 0.5 mL samples were taken and replaced with 0.5 mL of fresh buffer. Release was carried out until no more protein release was detected or the complexes were fully degraded (100% of the theoretical protein loading was released).

Equation 2.3 shows the Korsmeyer-Peppas kinetic model which is commonly used for studying the release mechanisms²⁴. In order to obtain values for parameters $\ln(k)$ and n , the first 60% of the protein release kinetic data were fitted to the logarithmic form of the Korsmeyer-Peppas kinetic model (Equation 2.4). In Equation 2.3 and Equation 2.4, M_t/M_∞ is the fraction of drug released at time t , k is the release rate constant, and n is the release exponent.

$$\frac{M_t}{M_\infty} = kt^n \quad \text{Equation 2.3}$$

$$\ln\left(\frac{M_t}{M_\infty}\right) = \ln k + n \ln t \quad \text{Equation 2.4}$$

In drug release from degradable polymers, a three-step sequence is followed: (i) water penetration into the matrix, (ii) a degradation-dependent “relaxation of the network” which creates more free volume for drug dissolution, and (iii) drug removal to the surrounding medium usually through diffusion process. The slowest step becomes the rate limiting step which ultimately controls the release rate²⁵. Equation 2.3 has distinct physical realistic meanings for drug release from spherical polymeric delivery systems in the special cases of $n=0.43$ and $n=0.85$, which indicate diffusion-controlled drug release and swelling-controlled drug release, respectively. In Fickian diffusion ($n=0.43$), the diffusion process occurs at a much slower rate than the polymer relaxation process and the system is controlled by diffusion. In Case-II transport ($n=0.83$), the rate of diffusion is much faster than the rate of relaxation and the rate controlling step is the velocity of an advancing front upon water imbibition into the system. Values of n between 0.43 and 0.85 can be considered as an indicator for the superposition of both phenomena (anomalous transport) where the diffusion and relaxation rates are comparable^{26,27}.

2.2.7. Statistical Analysis

All experiments were performed in triplicate and error bars on graphs represent standard deviations. Statistical comparisons for the release kinetics data were made using two-way repeated-measures analysis of variance (ANOVA) with $p < 0.05$ used as the level

of significance. Statistical significance for complex size and zeta potential was determined using a one-way ANOVA test ($p < 0.05$ used as the level of significance).

2.2.8. Multivariate Statistical Analysis

Multivariate analysis or latent variable modeling, is a statistical modeling approach that summarizes all of the variables affecting the process using a smaller number of latent variables that are described mathematically as linear combinations of the original variables. The number of such latent variables that are truly influencing the process is always smaller when compared to the number of original process variables measured during experiments¹⁵.

The Projection to Latent Structures (PLS) method was used to interpret the relationships in the X and Y matrices as well as the relationship between the two by projecting and distilling data into low dimensional latent variable spaces¹⁵. ProMV software (ProSensus Inc.) was used to apply multivariate methods in two separate models for quantifying and assessing the relative importance of each of the X variables on the complex properties as well as the factors affecting the protein release kinetics.

In the model for physical properties, the concentration of n^+ (lysozyme and calcium) as well as protein net charge were imported into ProMV as the X matrix. The complex composition and the physical properties of the complexes (average diameter and zeta potential) were imported into ProMV as the Y matrix.

In the model for release kinetics, protein molecular weight, electrostatic attraction, the crosslinker charge density, and the ionic strength of the release media were imported

as the X matrix. The data obtained from fitting the protein release data into the logarithmic form of the Korsmeyer-Peppas kinetic model were imported as the Y matrix.

In building this model, the following assumptions were made:

- The electrostatic contributions of the ionized groups of all the amino acids composing a protein as well as the distributions of the exposed and the buried charges are complicated to quantify²⁸ and are beyond the scope of this study. In this model, only the net charge was considered in the calculations.
- At pH=4.5, the net charge of the proteins were considered as +11 for lysozyme³ and +3 for BSA²⁹. At pH=7.4, the net charge of the proteins were considered as +9 for lysozyme¹⁶ and -16 for BSA³⁰.
- Based on Coulomb's law, the magnitude of the electrostatic forces between charged objects is directly proportional to the product of their charges³¹. In this study, the electrostatic attraction between components was calculated based on Coulomb's law as shown in Equation 2.5 where x_i and n_i represents mole fraction and net charge of component i , respectively.

$$\text{Electrostatic Attraction} = - (x_1 \cdot n_1) \times (x_2 \cdot n_2)$$

Equation 2.5

- All three components of the complexes in this study (alginate, lysozyme, crosslinker) are charged and therefore, electrostatically interact with each other. Based on the principle of linear superposition, the electrostatic force acting on the released protein

was calculated as the vector sum of all the Coulomb law forces from each of the other two charges³².

- The average charge density of the crosslinker was defined as the net charge divided by the surface area of a sphere of equivalent volume³³. The radius of calcium and barium ions was considered 1.14 Å and 1.74 Å, respectively³⁴. The radius of iron cation (Fe^{3+}) was considered to be 0.64 Å³⁵. The Stokes radius for lysozyme and BSA was considered 2 nm and 3.8 nm, respectively, at both pH values of 4.5 and 7.4³⁶.

2.3. Results and Discussion

2.3.1. Complex Composition Analysis

2.3.1.a. Effect of pH (Effect of Protein Net Charge)

Figure 2.1(a) shows the effect of pH on alginate and lysozyme precipitation amounts. A decrease in the amount precipitated for both alginate and lysozyme was observed as the pH was increased. This is due to a decrease in the net positive charge of lysozyme with pH increase¹⁷ and therefore a decrease in the attractive electrostatic interactions between alginate and lysozyme which are the main driving forces in the formation of complexes⁴.

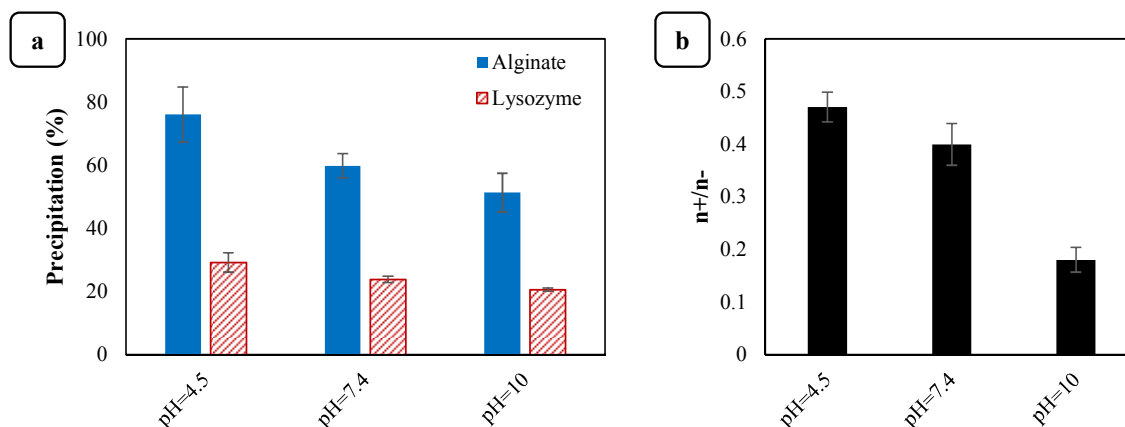


Figure 2.1. (a) Precipitation of alginate and lysozyme at various pH values; (b) n^+/n^- ratio in complex.

Although the alginate and lysozyme precipitation was decreased by increases in pH, the alginate to lysozyme ratio in the formed complexes were consistent regardless of the pH (Figure 2.1(a)). At higher pH values, larger amounts of lysozyme would be expected to interact with the alginate to compensate for the loss of positive charge. However, with the fixed concentrations of protein and polymer in the mixing solutions for all pH values and possible steric constraints, the alginate to lysozyme ratios in the complex were not significantly impacted. Also, pH changes may not affect the entire protein structure, as hidden pockets and microenvironments could preserve the charge of amino acids regardless of fluctuations in the local pH³⁷, thus altering the overall effect from what is theoretically anticipated. Lower theoretical values of n^+/n^- in the complex were observed with increases in pH (Figure 2.1(b)) as a result of the decrease in the concentration of positive charges associated with the protein.

2.3.1.b. Effect of Calcium

At pH=7.4 and $[n^+]/[n^-]=1$, the addition of calcium resulted in an increase in the sedimentation of alginate and especially lysozyme (Figure 2.2(a)). These results are consistent with reports in literature where the creation of “egg-box” structures in the alginate formed by calcium crosslinks cause reduced polymer flexibility and led to higher lysozyme complexation³. While increased calcium concentration resulted in larger precipitation percentages for lysozyme, these higher precipitation percentages did not necessarily correspond to a higher amount of precipitated lysozyme due to differences in the initial concentration. For the preparation of these samples, the initial lysozyme concentration was decreased with an increase in the initial calcium concentration in order to maintain the $[n^+]/[n^-]=1$ ratio. Therefore, although higher calcium and lysozyme precipitation was observed with increased calcium concentration, the final n^+/n^- ratio in complex did not follow a linear trend with increases in calcium concentration (Figure 2.2(b)).

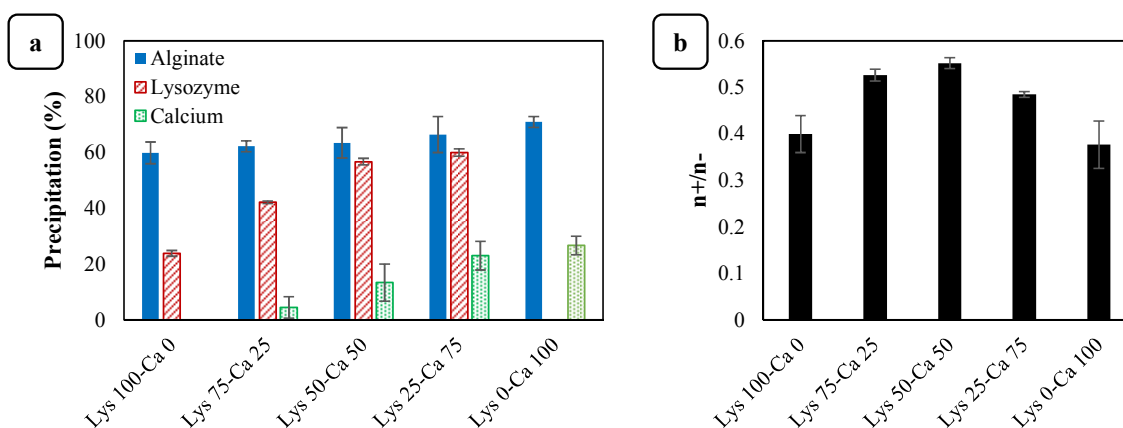


Figure 2.2. (a) Precipitation of alginate, lysozyme, and calcium at pH=7.4 and $[n^+]/[n^-]=1$; (b) n^+/n^- ratio in complex.

Figure 2.3(a) and Figure 2.3(c) show the precipitation of alginate, lysozyme, and calcium at various mixing ratios. In general, increasing the total concentration of positive charges led to the presence of higher amounts of alginate in the complexes. Figure 2.3(b) and Figure 2.3(d) show the final n^+/n^- ratio in the complex. Increase in the concentration of the positive charges in the initial mixing solutions resulted in higher n^+/n^- ratios in the complex. Also, it seems that while an increase in calcium concentration resulted in higher lysozyme precipitation, an increase in the lysozyme concentration did not have a similar impact on calcium complexation. The addition of calcium reduces alginate chain flexibility³ and increases the molecular size of alginate due to the formation of chain interconnections⁵ therefore allowing more lysozyme to be crosslinked. However, crosslinking of alginate with calcium occurs through interaction between calcium ions and guluronate rich regions on the alginate chain. Interaction between calcium ions and single guluronate units forms monocomplexes, which, with the increase in calcium concentration, are paired together to generate “egg-box” dimers. Finally, at higher calcium concentrations, the dimers associate to form multimers. Therefore, calcium binding to alginate follows a multistep mechanism which is mostly dependent on the concentration of calcium ions and the composition of alginate chains^{3,38}.

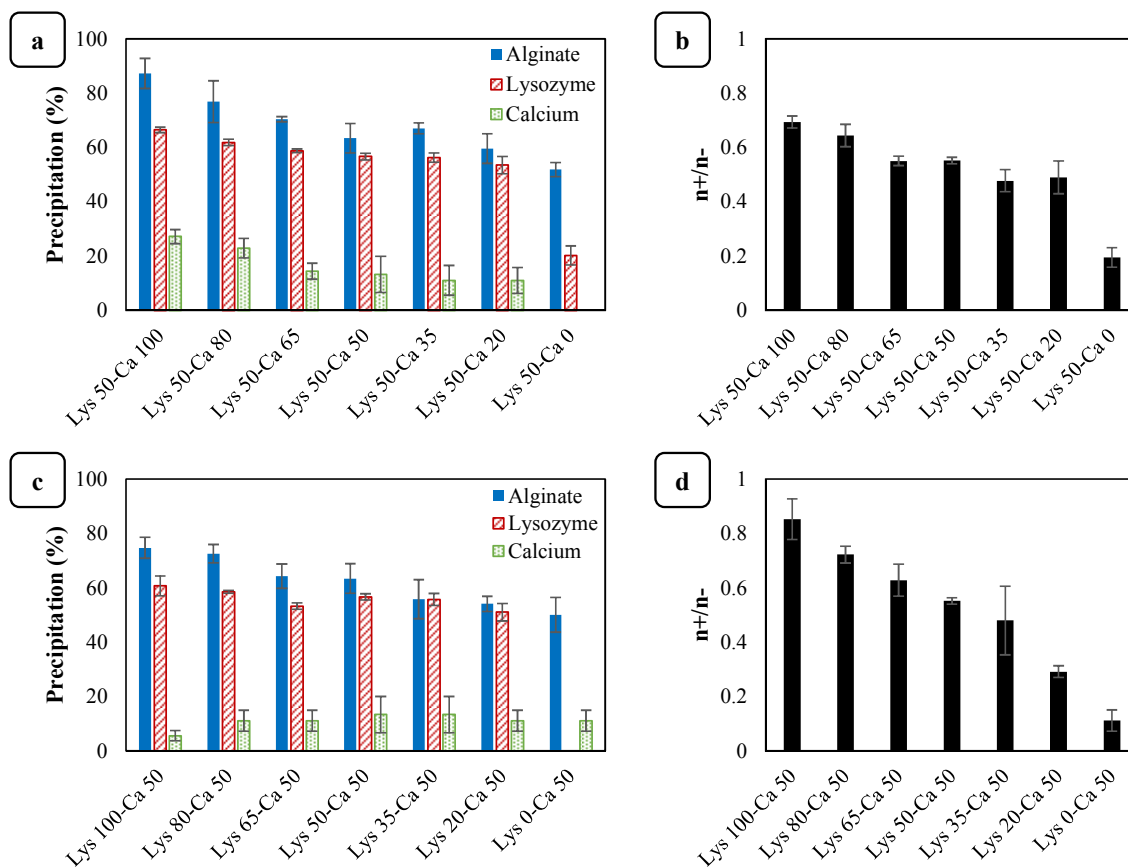


Figure 2.3. (a) Precipitation of alginate, lysozyme, and calcium at constant lysozyme and varying calcium concentration; (b) n^+/n^- ratio in complex at constant lysozyme and varying calcium concentration; (c) Precipitation of alginate, lysozyme, and calcium at constant calcium and varying lysozyme concentration; (d) n^+/n^- ratio in complex at constant calcium and varying lysozyme concentration.

2.3.2. Physical Characterization

Table 2.1 shows the results from the zeta potential and average size measurements at different pH values. An increase in pH resulted in more negative zeta potential values and smaller complexes. As the pH values were increased, the positive charge associated with lysozyme was partially lost¹⁷. This resulted in the presence of a lower amount of positive charge in the final complex (Figure 2.1(b)) and an increasingly negative zeta

potential. At higher pH values, alginate and lysozyme precipitation was decreased (Figure 2.1) which contributed to the formation of smaller complexes.

Table 2.1. Physical characteristics of lysozyme-alginate complexes at various pH values.

Complex	Zeta potential (mV)	Mean complex size	
		Volume mean diameter (μm)	SPAN
pH=4.5, Lys 100-Ca 0	-31.0 ± 2.2	3.0 ± 0.2	1.6 ± 0.1
pH=7.4, Lys 100-Ca 0	-33.0 ± 1.6	2.8 ± 0.1	1.2 ± 0.0
pH=10, Lys 100-Ca 0	-42.6 ± 1.4	2.2 ± 0.1	1.4 ± 0.0

Table 2.2 reports the physical characteristics of the samples prepared at pH=7.4 and $[n^+]/[n^-]=1$. As seen in Figure 2.2(b), the final n^+/n^- ratio in complex composition, which is determinant of the zeta potential and size characteristics, did not follow a linear trend with the addition of calcium. This non-linearity was reflected in the absence of a general decreasing or increasing trend in the complex size and zeta potential of the complexes presented in Table 2.2.

Table 2.2. Physical characteristics of lysozyme/calcium-alginate complexes at pH=7.4 and $[n^+]/[n^-]=1$.

Complex	Zeta potential (mV)	Mean complex size	
		Volume mean diameter (μm)	SPAN
Lys 100-Ca 0	-33.0 ± 1.6	2.8 ± 0.1	1.2 ± 0.0
Lys 75-Ca 25	-23.5 ± 1.9	2.8 ± 0.1	1.2 ± 0.1
Lys 50-Ca 50	-25.4 ± 1.2	2.5 ± 0.2	1.6 ± 0.1
Lys 25-Ca 75	-27.9 ± 1.3	2.3 ± 0.1	1.5 ± 0.1
Lys 0-Ca 100	-35.4 ± 1.5	2.1 ± 0.1	1.2 ± 0.1

The zeta potential and average size of the complexes prepared at pH=7.4 and with varying ratios of the initial lysozyme and calcium concentrations is reported in Table 2.3. As seen, the relative negativity of the zeta potential was decreased with an increase in the total concentration of positive charges in the mixing solution due to the complexation of higher amounts of positive charges causing greater values of n^+/n^- in the final complex (Figure 2.3(b) and Figure 2.3(d)). Alginate precipitation was also increased with an increase in the initial concentration of positive charges (Figure 2.3(a) and Figure 2.3(c)) and with more moles involved in the complexation, larger particle sizes are expected.

Table 2.3. Physical characteristics of lysozyme/calcium-alginate complexes at varying mixing ratios.

Complex	Zeta potential (mV)	Mean complex size	
		Volume mean diameter (μm)	SPAN
Lys 50-Ca 100	-20.9 ± 1.1	3.0 ± 0.1	1.4 ± 0.1
Lys 50-Ca 80	-22.9 ± 1.2	2.7 ± 0.2	1.6 ± 0.0
Lys 50-Ca 65	-23.6 ± 1.7	2.5 ± 0.1	1.4 ± 0.1
Lys 50-Ca 50	-25.4 ± 1.2	2.5 ± 0.2	1.6 ± 0.1
Lys 50-Ca 35	-28.1 ± 1.5	2.3 ± 0.1	1.4 ± 0.0
Lys 50-Ca 20	-29.5 ± 1.8	3.0 ± 0.1	1.4 ± 0.1
Lys 50-Ca 0	-43.0 ± 1.9	2.7 ± 0.1	1.4 ± 0.1
Lys 100-Ca 50	-19.5 ± 2.1	3.4 ± 0.2	1.9 ± 0.1
Lys 80-Ca 50	-24.1 ± 2.4	2.9 ± 0.2	1.6 ± 0.1
Lys 65-Ca 50	-25.4 ± 1.8	3.0 ± 0.2	1.6 ± 0.1
Lys 50-Ca 50	-25.4 ± 1.2	2.5 ± 0.2	1.6 ± 0.1
Lys 35-Ca 50	-31.7 ± 2.1	2.5 ± 0.2	1.5 ± 0.0
Lys 20-Ca 50	-37.1 ± 1.9	2.5 ± 0.1	1.3 ± 0.1
Lys 0-Ca 50	-43.9 ± 2.0	2.4 ± 0.1	1.0 ± 0.1

2.3.3. Protein Release

Complexes of lysozyme-alginate were prepared in the presence of crosslinkers (calcium, barium, iron(III), bovine serum albumin (BSA)) and their degradation rates were investigated. Figure 2.4 shows the release of lysozyme from the complexes as well as the release of BSA from the lysozyme/BSA-alginate complex at varying pH and ionic strength conditions.

In general and for all complexes, faster protein release is observed at higher ionic strength and at higher pH values. The faster release at higher pH is due to partial loss of positive charges on lysozyme as the pH increases¹⁷, leading to weakened electrostatic interactions between lysozyme and negative alginate chains which causes faster degradation of the complexes. In the case of BSA, which has a net negative charge at pH=7.4, only local and minimal attraction and a net repulsion between the protein and the alginate causing rapid degradation of the complex are expected. However, due to the presence of positively charged lysozyme in the matrix as well, the strong attraction forces between BSA and lysozyme seem to be able to overcome the expected rapid degradation.

Increasing the ionic strength of the release buffer from 10 mM to 150 mM also led to more rapid protein release due to the faster degradation of the complexes as a result of charge screening effects at high salt concentrations as well as ion exchange²³ and presence of larger amount of sodium ions acting to displace the crosslinkers of the network³⁹. Furthermore, at low ionic strength conditions where complex degradation is slower, protein molecular weight seems to influence the release rates as a controlling factor: the higher molecular weight of BSA compared to lysozyme resulted in slower

release of the larger protein. Additional studies with other proteins are necessary to confirm this.

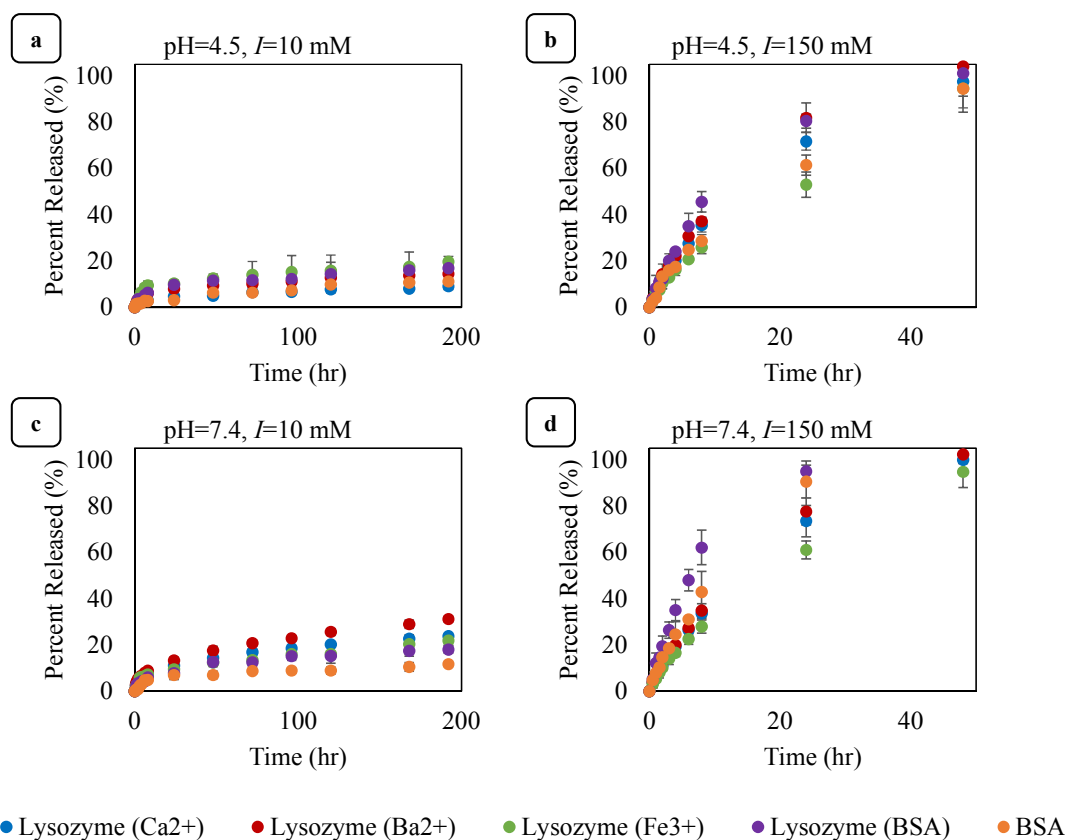


Figure 2.4. Release of proteins from protein/crosslinker-alginate complexes; (a) pH=4.5, $I=10$ mM, (b) pH=4.5, $I=150$ mM, (c) pH=7.4, $I=10$ mM, (d) pH=7.4, $I=150$ mM.

Although the type of cation used for crosslinking the matrix significantly ($p < 0.05$) affected the release kinetics, it is hard to draw conclusions by generalizing the results presented in Figure 2.4. Calcium and barium ions are divalent cations and are expected to crosslink the alginate in a planar two-dimensional manner while formation of a three-dimensional bonding structure with alginate is anticipated from the trivalent iron

cations³⁴. In addition, since the crosslinkers vary in size ($BSA \gg Ba^{2+} > Ca^{2+} > Fe^{3+}$), their diffusion rates from the complex into the release media and their exchange rates with the sodium ions in the release media is diverse as well which affects the degradation kinetics of the complex³⁴. While it can be concluded that the type of crosslinker has a great influence on the stability and degradation pattern of the complexes, further examination of the relationships is necessary for more in-depth understanding.

The results suggest that, conditions such as the nature of crosslinker can be used to control protein release and the ionic strength and pH of the release media can be a trigger to protein release from the protein-polysaccharide complexes. Therefore, depending on the protein and the application, a tailorable release is possible. However, the correlations between the parameters need to be understood and easily interpreted. Multivariate statistical analysis methods provide a tool for quantifying the effect of each of the factors on the release kinetics.

2.3.4. Multivariate Statistical Analysis

2.3.4.a. PLS Model for Physical Properties

The initial conditions, complex composition and physical properties were imported into ProMV software (ProSensus Inc.) where a model consisting of two latent variables was built. The overall R^2Y (a measure of the model fit capability) and Q^2Y (an indication of the model predictive capability) were calculated to have values of 0.715 and 0.562, respectively (Figure 2.5(a)). PLS also models the relationships among X variables and the R^2X , a measurement of how well the model fits the X data, was calculated to be

0.754 (Figure 2.5(a)). The R^2 and Q^2 values for each of the Y variables shown in Figure 2.5(b), with the exception of average size, demonstrated reasonable fit and acceptable predictive performance.

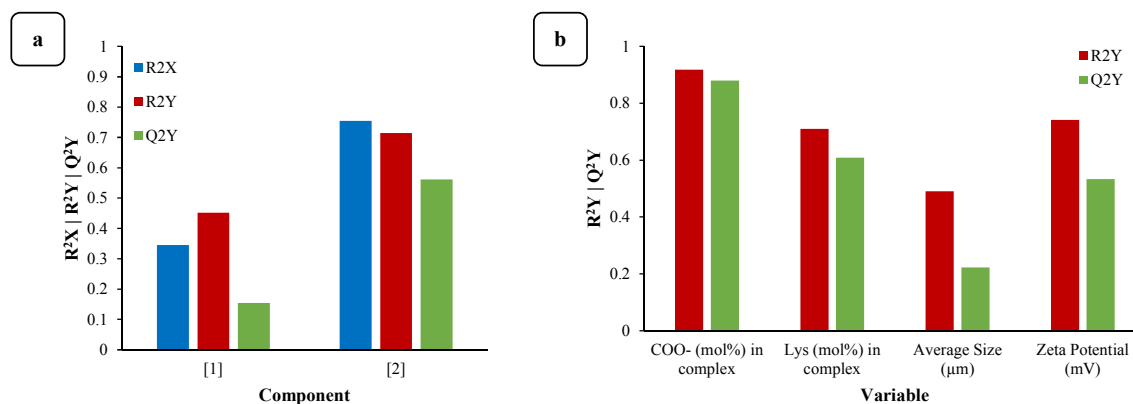


Figure 2.5. (a) Cumulative R^2X , R^2Y , and Q^2Y for the PLS model for physical properties; (b) R^2 and Q^2 for each of the Y variables.

The correlation-loading plot (Figure 2.6) explains the relationships between the X and Y variables. In this plot, the location of the variables with respect to each other is an indication of their correlation: positively correlated variables cluster together while parameters with negative correlations are located in opposite quadrants⁴⁰. For example, it can be observed that mole fraction of alginate in complexes is negatively correlated with the initial concentration of calcium ions in the mixing solution (located in opposite quadrants) and the zeta potential of complexes is strongly and positively correlated with the initial concentration of ions present in the mixing solution (cluster formation). These interpretations are in agreement with the trends observed in Figure 2.1 through Figure 2.3.

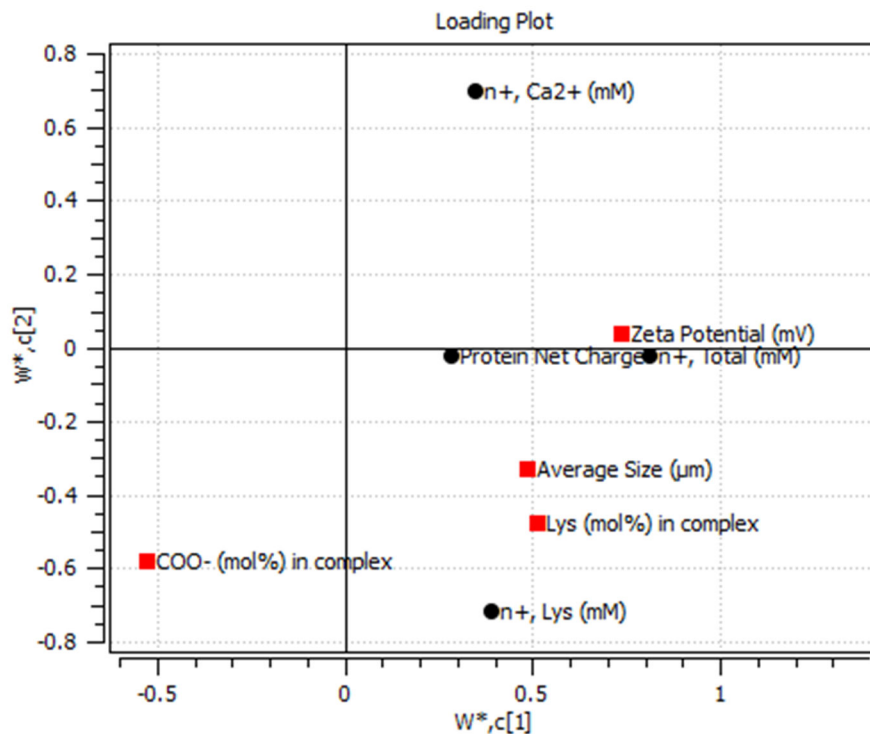


Figure 2.6. Correlation-loading plot for contributors to Y variables.

The relationships described in the correlation-loading plot (Figure 2.6) can be quantified using coefficient plots (Figure 2.7, and Figure 2.8) which show the size and direction of the influences of each of the X parameters on the Y variables.

The calcium concentration in the mixing solution played the most significant role in determining the mole fraction of alginate in the complexes (Figure 2.7(a)). As observed in Figure 2.2 and Figure 2.3 increasing the calcium concentration resulted in higher precipitation amounts of alginate, lysozyme, and calcium. Since the concentration of alginate in the initial mixing solution was kept constant for all experiments and the concentrations of positive charges varied (Sections 2.2.3.a and 2.2.3.b), the increase in the number of precipitated moles was greater for calcium due to its higher concentration in

the initial mixing solution. Therefore, increasing calcium concentration increased the mole percentage of calcium which as a result caused a lower mole fraction of alginate to be present in the complex system.

As observed in Figure 2.2 and Figure 2.3, higher calcium concentrations resulted in higher percentages of lysozyme precipitating. However, due to variations in the initial concentration of lysozyme in the mixing solutions (Section 2.2.3.b) higher precipitation did not necessarily correspond to an increase in the number of precipitated lysozyme moles or higher lysozyme mole fractions. As seen in Figure 2.7(b), the mole fraction of lysozyme in the complex was mostly dependent on the initial lysozyme concentration rather than the calcium concentration.

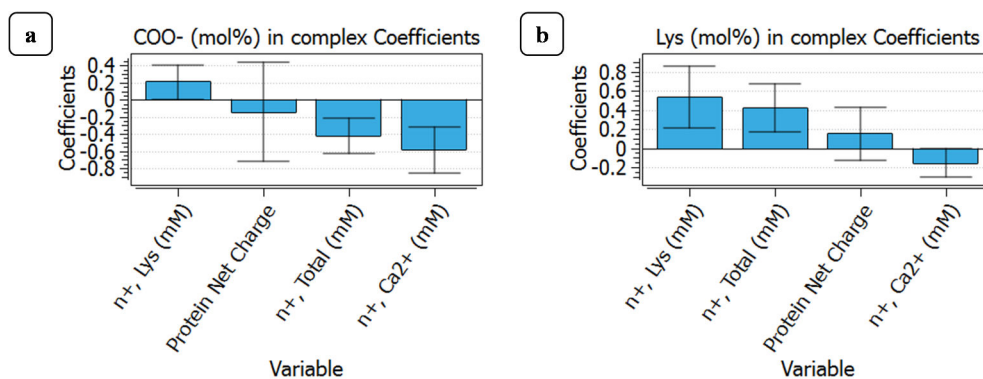


Figure 2.7. Coefficient plots showing the effect of each X parameter on complex composition and mole fractions of (a) COO⁻, (b) lysozyme.

As observed in Figure 2.8, average size of the complexes and their zeta potential were positively related to the concentration of the positive charges in the mixing solutions and were also positively dependent on protein net charge. Increasing the total concentration of positive charges led to the presence of higher amounts of alginate in the

complexes. Higher alginate precipitation was associated with a greater number of moles of alginate involved in complex formation, and with the high molecular weight of alginate, the increase in average diameter of the complex is anticipated (Figure 2.8(a)).

Increase in the initial calcium and lysozyme concentrations led to lower alginate and higher lysozyme mole fractions (Figure 2.7) which resulted in an increase in the final n^+/n^- ratio in the complex causing more positive zeta potential values (Figure 2.8(b)). The decrease in protein net charge resulted in lower n^+/n^- ratios in the final complex (Figure 2.1(b)) as well as lower zeta potential values (Table 2.1). The positive coefficient for protein net charge in Figure 2.8(b) also confirms the observed positive correlation between protein net charge and zeta potential.

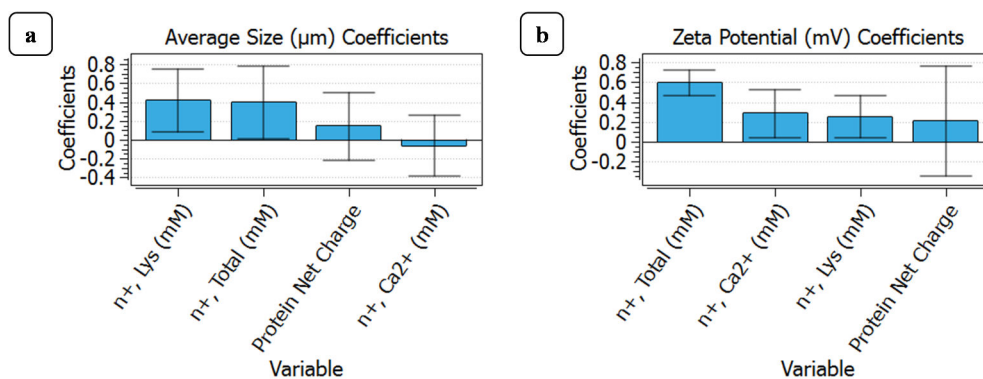


Figure 2.8. Coefficient plots showing the effect of each X parameter on (a) average size, (b) zeta potential.

2.3.4.b. PLS Model for Release Kinetics

Multivariate statistical analysis methods were applied to the release data for further understanding the effects of various factors on the release. The crosslinker charge density, protein molecular weight, electrostatic attraction forces, and the ionic strength of

the release media were imported as the X matrix. The data obtained from fitting the protein release data into the logarithmic form of the Korsmeyer-Peppas kinetic model were imported as the Y matrix. A two component model was built based on the data imported into the ProMV software (ProSensus Inc.). Figure 2.9(a) shows measures of model fit capability, R^2X and R^2Y , to have values of 0.718 and 0.890, respectively. Figure 2.9 also shows value of 0.834 for model predictive capability, Q^2Y . The high values of R^2X , R^2Y , and Q^2Y represent the excellent fit capability and reliable predictive performance of the model. In Figure 2.9(b), the R^2 and Q^2 values for each of the Y variables are shown which also demonstrate great fit and predictive performance of the model.

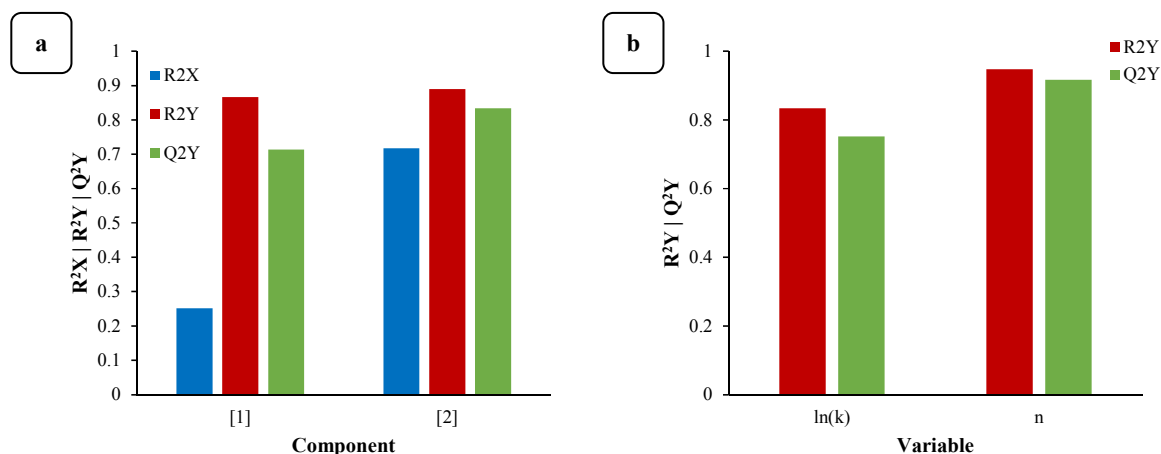


Figure 2.9. (a) Cumulative R^2X , R^2Y , and Q^2Y for the PLS model for release kinetics; (b) R^2 and Q^2 for each of the Y variables.

Figure 2.10 shows the coefficient plots which indicate the size and direction of the effect of each of the X variables on the release kinetic parameters ($\ln(k)$ and n). The high

dependency of both these parameters on the ionic strength of the release buffer is an indication of the ion-sensitivity of the release kinetics which was observed also in Figure 2.4. The kinetic constant k parameter in the Korsmeyer-Peppas model represents the structural characteristics of the drug dosage form²⁴. As seen in Figure 2.10(a), this parameter is dominantly and positively dependent on the ionic strength of the release buffer with a minor dependence on the electrostatic forces and protein molecular weight. In Figure 2.10(b), a similar trend is observed for the effect of the X variables on parameter n , which is suggestive of the release mechanism. Higher n values represent less-diffusion based kinetics and more non-Fickian transport mechanisms²⁴. The relative independence of the release kinetics from the electrostatic attraction and molecular weight as well as crosslinker properties indicate, somewhat surprisingly, that diffusion is not the limiting factor in these complexes. Rather, this proposes that the release is mainly governed by the disintegration of the complexes at conditions where the electrostatic interactions, which are the main driving force in complex formation⁴, are compromised, such as at higher ionic strength. This non-diffusion based release kinetics is also established from the high n values found from the fit of release profiles into the Korsmeyer-Peppas model (Supplementary Material).

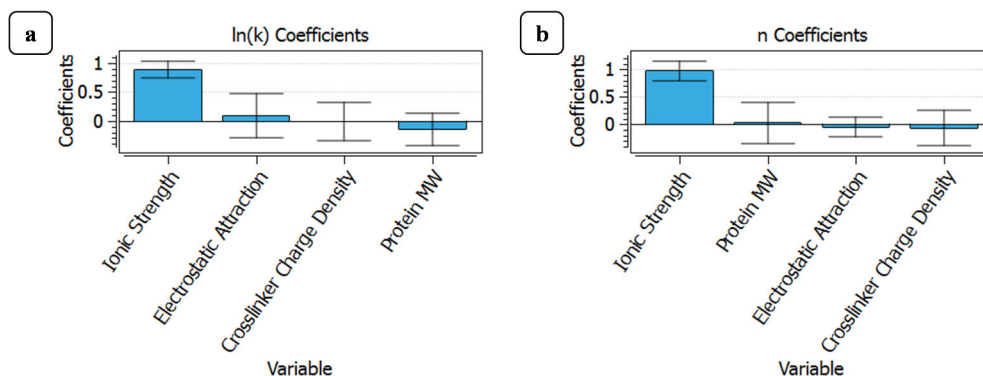


Figure 2.10. Coefficient plots showing the effect of each X parameter on release kinetic parameters; (a) $\ln(k)$, (b) n .

Since the ultimate objective of protein and drug release is delivery and release at physiological conditions, the contour plots for prediction of the release kinetic parameters were plotted as functions of their main contributing factors (other than ionic strength) obtained from Figure 2.10 and at constant ionic strength of the buffer ($I=150$ mM), mimicking typical *in vivo* conditions (Figure 2.11). The scattered data on the plots represent the observed experimental data. The acceptable distance between the experimental data and the contour plots (root mean-squared values of 0.238 and 0.049 for parameters $\ln(k)$ and n , respectively) indicate that the statistical model offers reliable performance for prediction of the release kinetics.

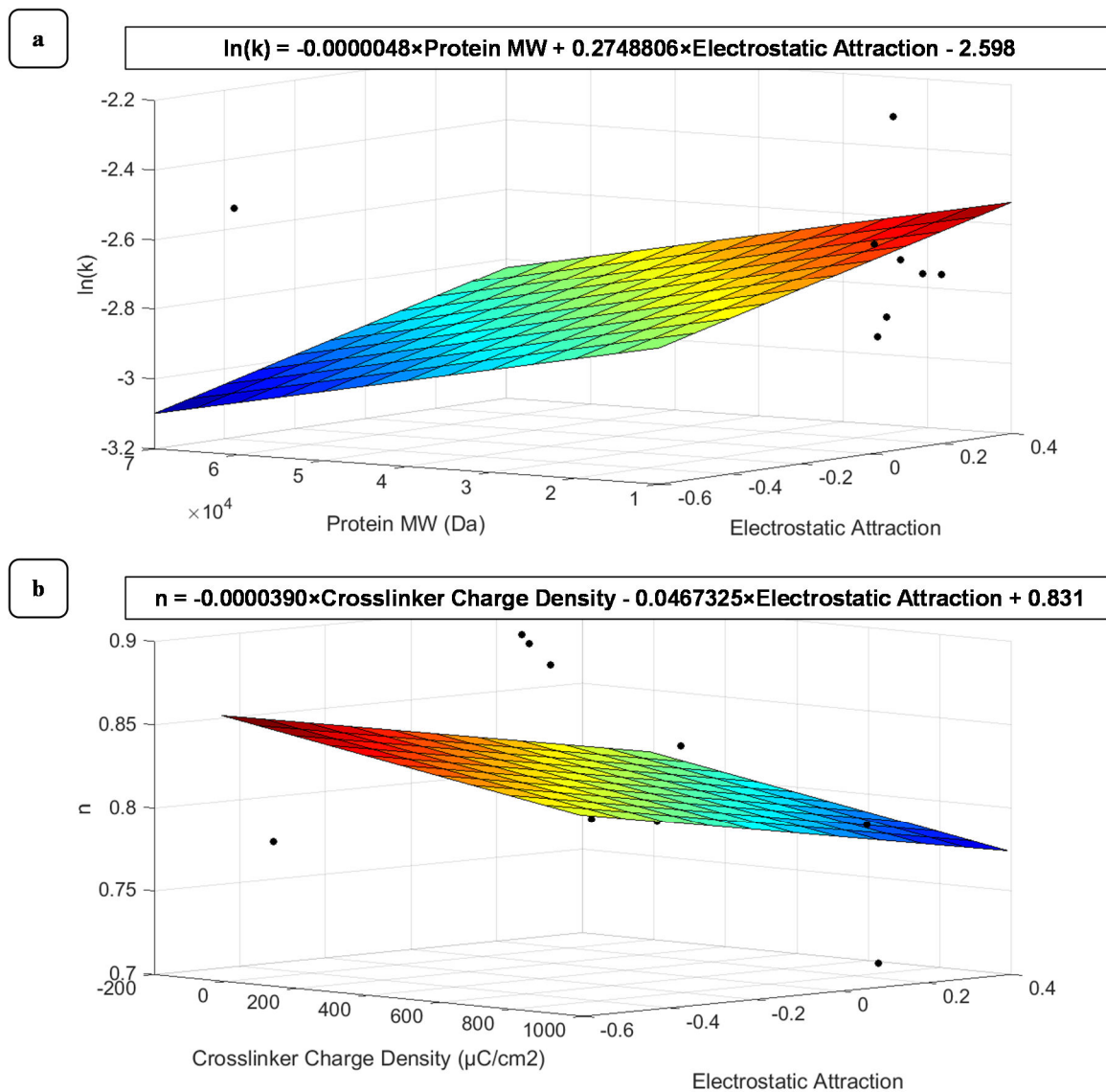


Figure 2.11. Contour surface plots from the PLS model for protein release kinetics as functions of protein properties and crosslinker charge density at physiological ionic strength ($I=150$ mM); (a) $\ln(k)$, (b) n .

2.3.4.c. Observed vs. Predicted

Figure 2.12 compares the model-predicted values with the experimental values of each of the Y variables. With the exception of the average diameter (Figure 2.12(c)), the R^2 values for all Y variables range from 0.710 (Figure 2.12(b)) to 0.948 (Figure 2.12(f))

indicate high model fitting capabilities. The maximum root mean-squared error of prediction for the values reported in percentages (Figure 2.12(a) and (b)) is calculated to be 1.247 (Figure 2.12(b)) which is considered a very small threshold in the 0 to 100 percent range. While the R^2 values for average size (Figure 2.12(c)) and zeta potential (Figure 2.12(d)) are imperfect, the root mean-squared error values of 0.249 μm and 4.071 mV are indicative that the model could still be considered effective and reliable in property predictions.

As shown in Figure 2.12(e) and Figure 2.12(f), the R^2 values for fit of the release parameters $\ln(k)$ and n are equal to 0.833 and 0.948, respectively, which are indicative of excellent fits. The root mean-squared error value of 0.306 for parameter $\ln(k)$, which ranges from -4.639 to -2.262 (Supplementary Material), and a root mean-squared error value of 0.051 for parameter n , which varies in the range of 0.343-0.891 (Supplementary Material), are considered very small thresholds in the fluctuation ranges of each of these parameters and therefore, endorse the accuracy and reliability of the model.

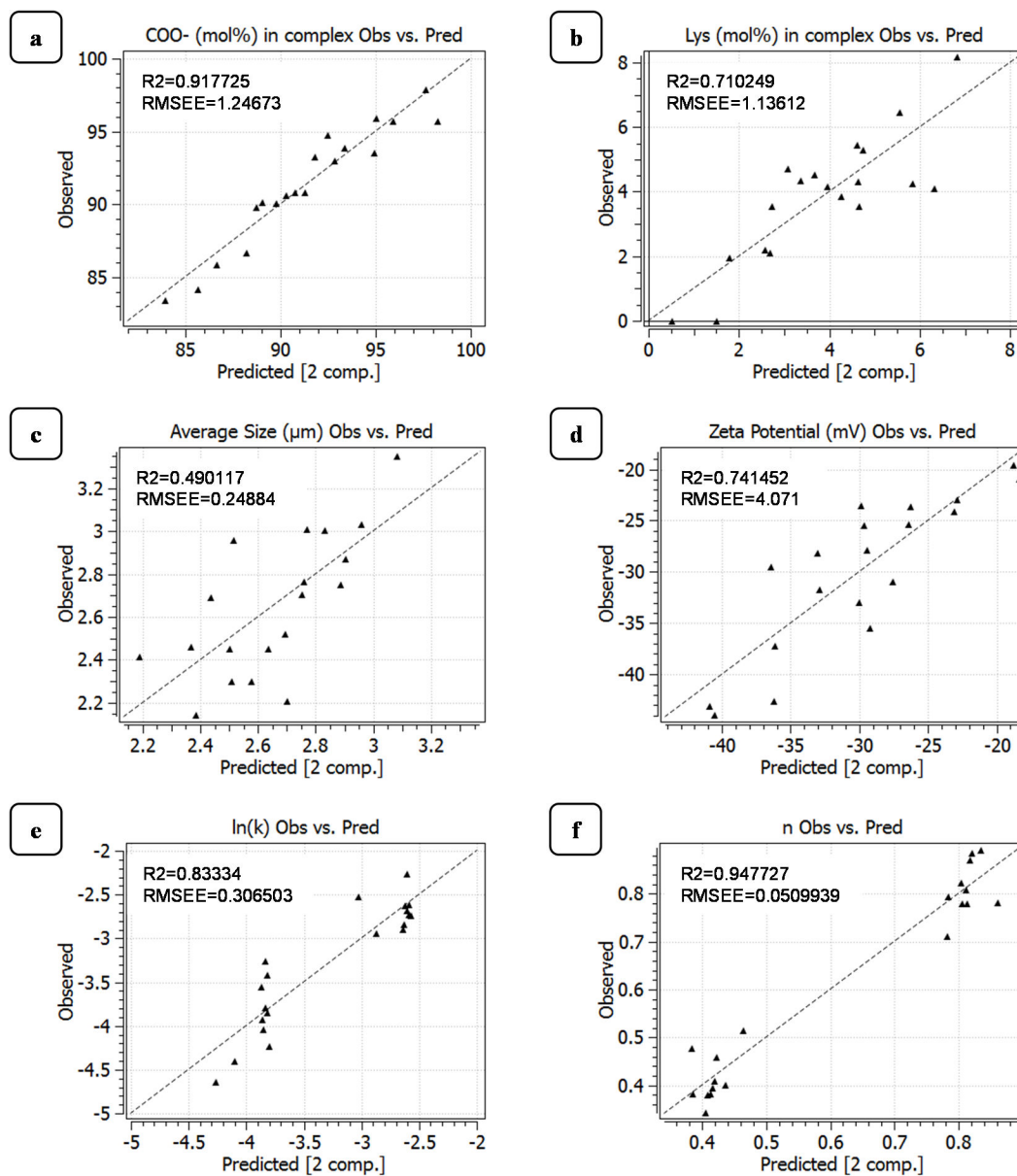


Figure 2.12. Observed vs. Predicted plots for Y variables.

2.3.5. Model Verification

The quantified correlations obtained from the PLS model, presented in Figure 2.7 and Figure 2.8, can be used for complex designs and property predictions, respectively. As seen in Figure 2.7, mole fractions of COO⁻ and lysozyme are mainly influenced by the

initial concentration of positive charges and therefore can be acceptably described as functions of their two main contributing factors. When a specific complex composition is desired (known COO^- , lysozyme, calcium mole fractions), simultaneous solution of Equation 2.6, Equation 2.7, and Equation 2.8 can be used to achieve suitable mixing conditions (n^+_{Ca} , n^+_{Lys}).

$$\text{COO}^- (\text{mol}\%) = -6.113 \times n^+_{\text{Total}}(\text{mM}) - 7.611 \times n^+_{\text{Ca}}(\text{mM}) + 103.486 \quad \text{Equation 2.6}$$

$$\text{Lys} (\text{mol}\%) = 2.945 \times n^+_{\text{Total}}(\text{mM}) + 3.357 \times n^+_{\text{Lys}}(\text{mM}) - 2.638 \quad \text{Equation 2.7}$$

$$n^+_{\text{Lys}}(\text{mM}) + n^+_{\text{Ca}}(\text{mM}) = n^+_{\text{Total}}(\text{mM}) \quad \text{Equation 2.8}$$

In order to evaluate the predictive capabilities of the model, two sets of complex compositions were selected and the required initial conditions were calculated using simultaneous solution of Equation 2.6, Equation 2.7, and Equation 2.8 (Table 2.4).

Table 2.4. Selected complex compositions and their required initial mixing conditions.

Complex	Complex composition (mol%)			Mixing conditions	
	COO^-	Lys	Ca	n^+_{Lys} (mM)	n^+_{Ca} (mM)
1	80	10	10	1.5	1.0
2	90	7	3	1.4	0.4

The comparisons between the theoretical and the measured values are reported in Table 2.5.

Table 2.5. Comparison of model predicted and measured experimental values for complex compositions and their physical properties.

Complex		Complex composition (mol%)		
		COO ⁻	Lys	Ca
1	Theoretical	80	10	10
	Measured	66.5 ± 1.6	9.0 ± 0.9	24.5 ± 0.8
2	Theoretical	90	7	3
	Measured	87.9 ± 1.3	9.2 ± 1.5	2.9 ± 0.7

As seen in Table 2.5, while the composition predictions might be imperfect, the predicted increasing/decreasing trend for each of the components from complex 1 to complex 2 is acceptably preserved in experiments. This proves that while the model is imperfect, it still can be considered reliable in achieving desired complex compositions and has the potential for improvements with the addition of more data points.

2.4. Conclusion

Lysozyme/crosslinker-alginate complexes were prepared at different pH conditions, with varying concentrations of positive charges, and in the presence of various types of crosslinkers in the mixing solutions. The resulting complex compositions and their physical properties, such as average size and zeta potential, were measured and mathematical relationships were developed between the final properties and the initial conditions. This multivariate model showed the minimal effect of the crosslinker type on protein release rates at typical *in vivo* conditions from the complexes due to the high ion-sensitivity of the polyelectrolyte complex systems and their disintegration-based release mechanisms rather than diffusion-governed kinetics. In addition to qualitatively and

quantitatively describing the correlations between the initial conditions and the final properties, the multivariate statistical approach provided an effective model for prediction of properties and design of desired complexes. The model can be extended and improved by investigating the effects of additional factors such as polysaccharide molecular weight, chain composition, and use of other model proteins. While the current literature is lacking a comprehensive understanding of the existing correlations between complex properties and their preparation conditions, this study shows that statistical approaches can be used to minimize trial and error experiments for achieving the desired properties in a complex system.

2.5. Acknowledgements

The authors would like to gratefully acknowledge NSERC for funding support and ProSensus Inc. for generous permission to use ProMV software.

References

1. Bungenberg de Jong, H. G. & Kruyt, H. R. Coacervation (Partial Miscibility in Colloid Systems). *Proc. K. Ned. Akad. van Wet.* **32**, 849–856 (1929).
2. Fioramonti, S. A., Perez, A. A., Aringoli, E. E., Rubiolo, A. C. & Santiago, L. G. Design and characterization of soluble biopolymer complexes produced by electrostatic self-assembly of a whey protein isolate and sodium alginate. *Food Hydrocoll.* **35**, 129–136 (2014).
3. Fuenzalida, J. P. *et al.* On the role of alginate structure in complexing with lysozyme and application for enzyme delivery. *Food Hydrocoll.* **53**, 239–248 (2016).
4. Schmitt, C. & Turgeon, S. L. Protein/polysaccharide complexes and coacervates in food systems. *Adv. Colloid Interface Sci.* **167**, 63–70 (2011).

5. Fuenzalida, J. & Goycoolea, F. Polysaccharide-Protein Nanoassemblies: Novel Soft Materials for Biomedical and Biotechnological Applications. *Curr. Protein Pept. Sci.* **16**, 89–99 (2015).
6. van Rijn, P. Polymer Directed Protein Assemblies. *Polymers (Basel)*. **5**, 576–599 (2013).
7. Mizrahy, S. & Peer, D. Polysaccharides as building blocks for nanotherapeutics. *Chem. Soc. Rev.* **41**, 2623–2640 (2012).
8. Bayarri, M., Oulahal, N., Degraeve, P. & Gharsallaoui, A. Properties of lysozyme/low methoxyl (LM) pectin complexes for antimicrobial edible food packaging. *J. Food Eng.* **131**, 18–25 (2014).
9. Water, J. J. *et al.* Complex coacervates of hyaluronic acid and lysozyme: Effect on protein structure and physical stability. *Eur. J. Pharm. Biopharm.* **88**, 325–331 (2014).
10. Shilpa, A., Agrawal, S. S. & Ray, A. R. Controlled Delivery of Drugs from Alginate Matrix. *J. Macromol. Sci. Part C Polym. Rev.* **43**, 187–221 (2003).
11. Joshi, A., Keerthiprasad, R., Jayant, R. D. & Srivastava, R. Nano-in-micro alginate based hybrid particles. *Carbohydr. Polym.* **81**, 790–798 (2010).
12. Lee, K. Y. & Mooney, D. J. Alginate: Properties and biomedical applications. *Prog. Polym. Sci.* **37**, 106–126 (2012).
13. Harnsilawat, T., Pongsawatmanit, R. & McClements, D. J. Characterization of β -lactoglobulin–sodium alginate interactions in aqueous solutions: A calorimetry, light scattering, electrophoretic mobility and solubility study. *Food Hydrocoll.* **20**, 577–585 (2006).
14. Takahashi, D., Uchida, K. & Izumi, T. Activities of lysozyme complexed with polysaccharides and potassium poly(vinyl alcohol sulfate) with various degrees of esterification. *Polym. Bull.* **67**, 741–751 (2011).
15. MacGregor, J. F., Bruwer, M. J., Miletic, I., Cardin, M. & Liu, Z. Latent Variable Models and Big Data in the Process Industries. *IFAC-PapersOnLine* **48**, 520–524 (2015).
16. Postnikova, G. B. & Shekhovtsova, E. A. The effect of mitochondrial and artificial bilayer phospholipid membranes on conformation of myoglobin and its affinity for oxygen. *Am. J. Biol. Chem.* **3**, 16–32 (2015).
17. Yu, G., Liu, J. & Zhou, J. Mesoscopic coarse-grained simulations of hydrophobic charge induction chromatography (HCIC) for protein purification. *AIChE J.* **61**,

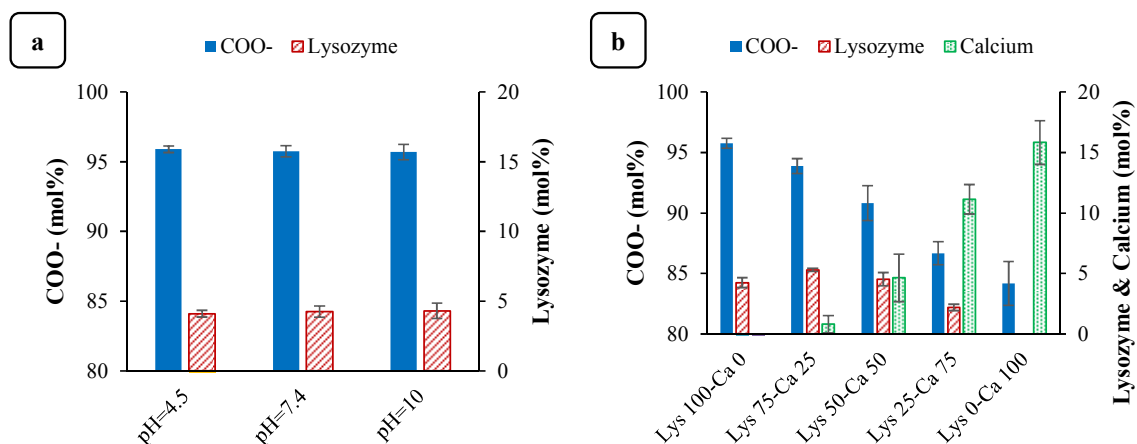
2035–2047 (2015).

18. Shi, Q., Zhou, Y. & Sun, Y. Influence of pH and Ionic Strength on the Steric Mass-Action Model Parameters around the Isoelectric Point of Protein. *Biotechnol. Prog.* **21**, 516–523 (2005).
19. Han, L., Kodama, S. & Okiji, T. Evaluation of calcium-releasing and apatite-forming abilities of fast-setting calcium silicate-based endodontic materials. *Int. Endod. J.* **48**, 124–130 (2015).
20. Jeffery, G. H., Bassett, J., Mendham, J. & Denney, R. C. *Vogel's Textbook of Quantitative Chemical Analysis. John Wiley & Sons, Inc. Fifth Edit*, (1989).
21. Wang, X., Lee, B. I. & Mann, L. Dispersion of barium titanate with polyaspartic acid in aqueous media. *Colloids Surfaces A Physicochem. Eng. Asp.* **202**, 71–80 (2002).
22. Gu, F., Amsden, B. & Neufeld, R. Sustained delivery of vascular endothelial growth factor with alginate beads. *J. Control. Release* **96**, 463–472 (2004).
23. Simonoska Crcarevska, M., Glavas Dodov, M. & Goracinova, K. Chitosan coated Ca–alginate microparticles loaded with budesonide for delivery to the inflamed colonic mucosa. *Eur. J. Pharm. Biopharm.* **68**, 565–578 (2008).
24. Costa, P. & Sousa Lobo, J. M. Modeling and comparison of dissolution profiles. *Eur. J. Pharm. Sci.* **13**, 123–133 (2001).
25. Lao, L. L., Venkatraman, S. S. & Peppas, N. A. Modeling of drug release from biodegradable polymer blends. *Eur. J. Pharm. Biopharm.* **70**, 796–803 (2008).
26. Siepmann, J. & Peppas, N. A. Modeling of drug release from delivery systems based on hydroxypropyl methylcellulose (HPMC). *Adv. Drug Deliv. Rev.* **64**, 163–174 (2012).
27. Lin, W.-C., Yu, D.-G. & Yang, M.-C. pH-sensitive polyelectrolyte complex gel microspheres composed of chitosan/sodium tripolyphosphate/dextran sulfate: swelling kinetics and drug delivery properties. *Colloids Surfaces B Biointerfaces* **44**, 143–151 (2005).
28. Gitlin, I., Carbeck, J. D. & Whitesides, G. M. Why Are Proteins Charged? Networks of Charge–Charge Interactions in Proteins Measured by Charge Ladders and Capillary Electrophoresis. *Angew. Chemie Int. Ed.* **45**, 3022–3060 (2006).
29. Tanford, C., Buzzell, J. G., Rands, D. G. & Swanson, S. A. The Reversible Expansion of Bovine Serum Albumin in Acid Solutions. *J. Am. Chem. Soc.* **77**, 6421–6428 (1955).

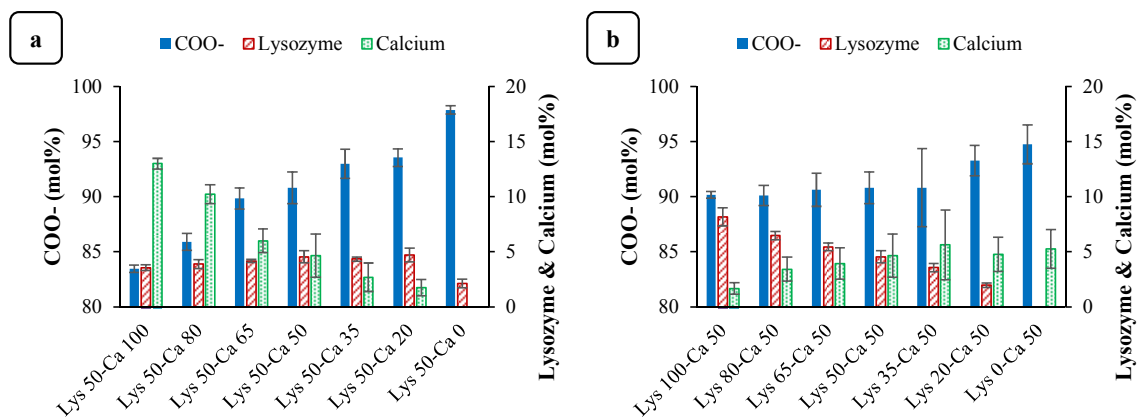
30. Baler, K. *et al.* Electrostatic Unfolding and Interactions of Albumin Driven by pH Changes: A Molecular Dynamics Study. *J. Phys. Chem. B* **118**, 921–930 (2014).
31. Nick Pace, C., Alston, R. W. & Shaw, K. L. Charge-charge interactions influence the denatured state ensemble and contribute to protein stability. *Protein Sci.* **9**, 1395–1398 (2000).
32. Echeverría, A., Barrios, E., Nussbaum, M., Améstica, M. & Leclerc, S. The atomic intrinsic integration approach: A structured methodology for the design of games for the conceptual understanding of physics. *Comput. Educ.* **59**, 806–816 (2012).
33. Roth, C. M. & Lenhoff, A. M. Electrostatic and van der Waals Contributions to Protein Adsorption: Comparison of Theory and Experiment. *Langmuir* **11**, 3500–3509 (1995).
34. Bajpai, S. K. & Sharma, S. Investigation of swelling/degradation behaviour of alginate beads crosslinked with Ca²⁺ and Ba²⁺ ions. *React. Funct. Polym.* **59**, 129–140 (2004).
35. de Araujo, T. S., de Souza, S. O. & de Sousa, E. M. B. Effect of Zn²⁺, Fe³⁺ and Cr³⁺ addition to hydroxyapatite for its application as an active constituent of sunscreens. *J. Phys. Conf. Ser.* **249**, 12012 (2010).
36. Park, J. M., Muhoberac, B. B., Dubin, P. L. & Xia, J. Effects of protein charge heterogeneity in protein-polyelectrolyte complexation. *Macromolecules* **25**, 290–295 (1992).
37. Mehler, E. L., Fuxreiter, M., Simon, I. & Garcia-Moreno E, B. The role of hydrophobic microenvironments in modulating pK_a shifts in proteins. *Proteins Struct. Funct. Genet.* **48**, 283–292 (2002).
38. Hecht, H. & Srebnik, S. Structural Characterization of Sodium Alginate and Calcium Alginate. *Biomacromolecules* **17**, 2160–2167 (2016).
39. Wells, L. A. & Sheardown, H. Extended release of high pI proteins from alginate microspheres via a novel encapsulation technique. *Eur. J. Pharm. Biopharm.* **65**, 329–335 (2007).
40. Tzoc Torres, J. M. G., Nichols, E., MacGregor, J. F. & Hoare, T. Designing multi-responsive polymers using latent variable methods. *Polymer (Guildf)*. **55**, 505–516 (2014).

Supplementary Material for Chapter 2

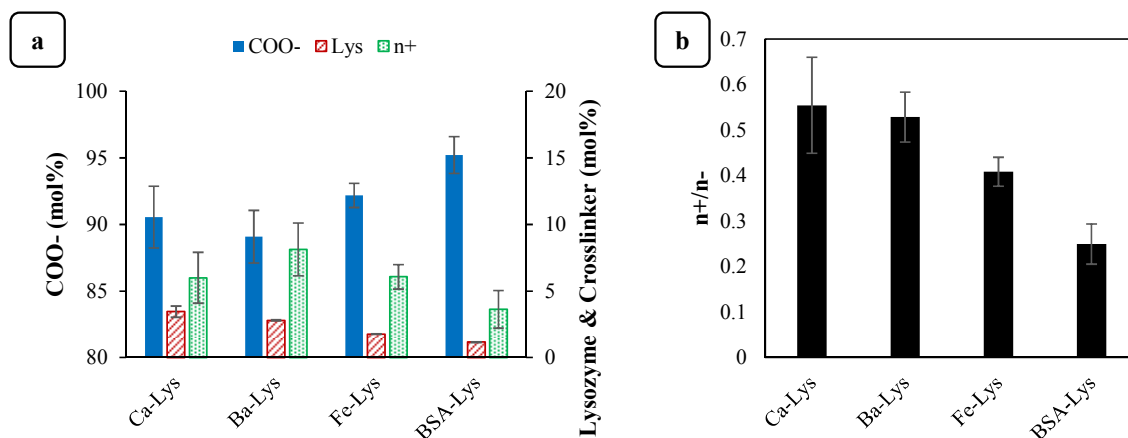
Supplementary Material 2.1: Complex Composition and Properties



SI Figure 2.1. (a) Mole composition of lysozyme-alginate complexes at various pH values; (b) Mole composition of lysozyme/calcium-alginate complexes at pH=7.4 and $[n^+]/[n^-]=1$.



SI Figure 2.2. Mole Composition of lysozyme/calcium-alginate complexes at pH=7.4; (a) constant lysozyme and varying calcium concentrations, (b) constant calcium and varying lysozyme concentrations.



SI Figure 2.3. (a) Mole composition of lysozyme/crosslinker-alginate complexes; (b) n⁺/n⁻ ratio in complex. Ca=Calcium, Ba=Barium, Fe=Iron(III), BSA=Bovine Serum Albumin, Lys=Lysozyme.

SI Table 2.1. Physical characteristics of lysozyme/crosslinker-alginate complexes; Ca=Calcium, Ba=Barium, Fe=Iron(III), BSA=Bovine Serum Albumin, Lys=Lysozyme.

Complex	Zeta potential (mV)	Mean complex size	
		Volume mean diameter (μm)	SPAN
Ca-Lys	-33.2 ± 0.8	2.7 ± 0.1	1.4 ± 0.0
Ba-Lys	-28.8 ± 1.6	2.9 ± 0.1	1.2 ± 0.1
Fe-Lys	-60.1 ± 1.6	3.1 ± 0.2	1.2 ± 0.0
BSA-Lys	-65.3 ± 1.8	3.2 ± 0.3	1.5 ± 0.0

Supplementary Material 2.2: Release Kinetics, Regression Fits, and Model**Predictions****SI Table 2.2. Values of parameters obtained from fit into the Korsmeyer-Peppas model and the PLS model-predicted values.**

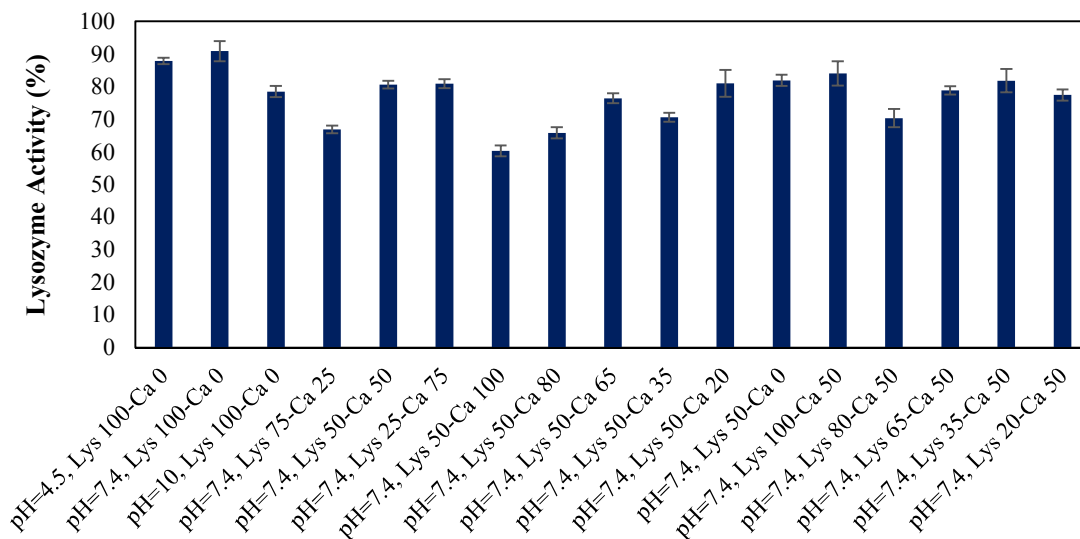
Protein	Crosslinker	pH	Buffer Ionic Strength (mM)	Korsmeyer-Peppas			Multivariate Statistical Analysis	
				ln(k)	n	R ²	ln(k)	n
Lysozyme	Ca ²⁺	4.5	10	-4.227	0.343	0.974	-3.808	0.405
Lysozyme	Ca ²⁺	4.5	150	-2.735	0.823	0.998	-2.577	0.803
Lysozyme	Ca ²⁺	7.4	10	-3.417	0.381	0.999	-3.823	0.407
Lysozyme	Ca ²⁺	7.4	150	-2.725	0.779	0.999	-2.592	0.805
Lysozyme	Ba ²⁺	4.5	10	-3.846	0.383	0.934	-3.826	0.413
Lysozyme	Ba ²⁺	4.5	150	-2.615	0.809	0.994	-2.595	0.811
Lysozyme	Ba ²⁺	7.4	10	-3.253	0.394	0.999	-3.837	0.415
Lysozyme	Ba ²⁺	7.4	150	-2.677	0.780	0.999	-2.606	0.813
Lysozyme	Fe ³⁺	4.5	10	-3.920	0.477	0.848	-3.868	0.383
Lysozyme	Fe ³⁺	4.5	150	-2.838	0.711	0.995	-2.637	0.781
Lysozyme	Fe ³⁺	7.4	10	-3.553	0.384	0.966	-3.875	0.385
Lysozyme	Fe ³⁺	7.4	150	-2.890	0.795	0.996	-2.644	0.782
Lysozyme	BSA	4.5	10	-4.035	0.459	0.923	-3.856	0.421
Lysozyme	BSA	4.5	150	-2.622	0.885	0.991	-2.625	0.819
Lysozyme	BSA	7.4	10	-3.788	0.409	0.974	-3.841	0.419
Lysozyme	BSA	7.4	150	-2.262	0.871	0.989	-2.611	0.817
BSA	Lysozyme	4.5	10	-4.404	0.401	0.961	-4.106	0.435
BSA	Lysozyme	4.5	150	-2.942	0.891	0.954	-2.875	0.833
BSA	Lysozyme	7.4	10	-4.639	0.515	0.892	-4.266	0.463
BSA	Lysozyme	7.4	150	-2.516	0.781	0.995	-3.035	0.861

Supplementary Material 2.3: Lysozyme Activity

Lysozyme was tested for its bioactivity after complexation. Lysozyme activity can be evaluated by the break-up of *Micrococcus lysodeikticus* cell walls. Enzymatic degradation by lysozyme results in a turbidity reduction of *Micrococcus lysodeikticus* cells solution and can be quantified spectrophotometrically at 450 nm^{1,2}.

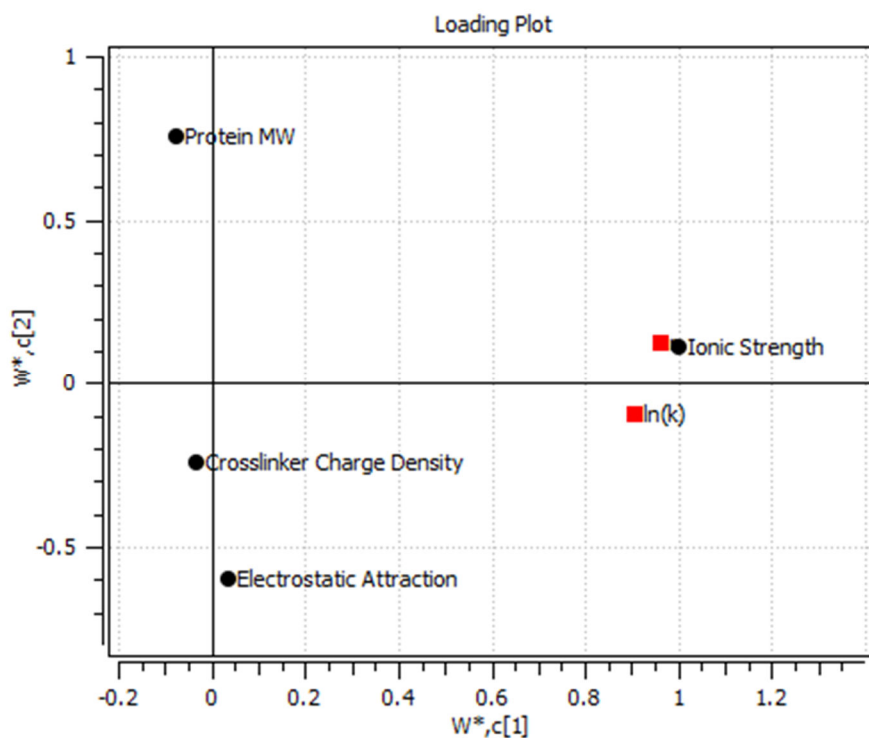
To detect the activity of the protein, complexes were dissociated in 10 mL of 1 M NaCl. The samples were added to cell suspension (0.2 mg/mL) at a sample to cell suspension volumetric ratio of 1:10 and absorbance was measured at 450 nm. The turbidity reduction of the samples were compared against fresh controls of the same concentration (using standards) and were used to determine the percent bioactivity of the complexed lysozyme.

The complexed lysozyme was tested for activity and the results are shown in SI Figure 2.4. The enzymatic activity of the protein trapped in the complex was compared to the activity of a control of the same concentration. Activities of between 60% and 90% of the control were observed, suggesting that, a decrease in the enzymatic activity of lysozyme was observed upon complexation with alginate, in general the activity of the complexed proteins was not unacceptably compromised.



SI Figure 2.4. Lysozyme activity of the complex structures.

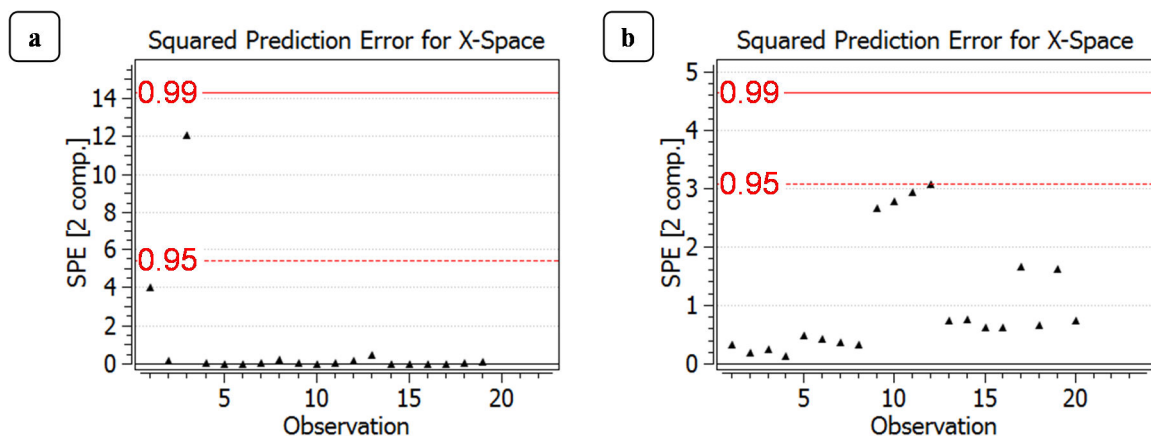
Supplementary Material 2.4: Correlation-Loading Plot for PLS Model for Release Kinetics



SI Figure 2.5. Correlation-loading plot for contributors to Y variables.

Supplementary Material 2.5: Squared Prediction Error (SPE-X)

SI Figure 2.6 shows the squared prediction error (SPE-X) and, as observed, all data points fall below the 99% confidence level. This indicates that the modeled correlations in the X space are well explained and can be reliable for predicting the behaviors of the Y variables.



SI Figure 2.6. Squared prediction error (SPE) values for the experimental observations; (a) PLS model for physical properties, (b) PLS model for release kinetics.

Supplementary Material References

1. Shugar, D. The measurement of lysozyme activity and the ultra-violet inactivation of lysozyme. *Biochim. Biophys. Acta* **8**, 302–309 (1952).
2. Wells, L. A. & Sheardown, H. Extended release of high pI proteins from alginate microspheres via a novel encapsulation technique. *Eur. J. Pharm. Biopharm.* **65**, 329–335 (2007).

Chapter 3: Protein-Alginate Complexes as pH-/Ion-Sensitive Carriers of Proteins

Vida Rahmani¹, Heather Sheardown^{1,2*}

¹ Department of Chemical Engineering, McMaster University, 1280 Main Street West, Hamilton ON L8S 4L7, Canada

² School of Biomedical Engineering, McMaster University, 1280 Main Street West, Hamilton ON L8S 4L7, Canada

* Corresponding author: sheadow@mcmaster.ca

Objectives:

Studying the potential use of protein-polysaccharide complexes as protein delivery devices which respond to environmental triggers such as pH and ionic strength, and quantifying the influencing factors for building a model on the release kinetics.

Main Scientific Contributions:

- Preparation of complexes from alginate and model proteins.
- Characterization of the complexes.
- Triggering protein release from the complexes in response to changes in pH and ionic strength of the release media.
- Applying multivariate statistical analysis for building a model and qualitatively and quantitatively describing the correlations between complex preparation conditions, complex properties, and complex degradation.

Publication Information:

Submitted to *International Journal of Pharmaceutics* (June 2017).

Author Contribution:

Vida was responsible for the experimental work (synthesis and characterization of the complexes, property measurements, protein release experiments, applying multivariate analysis) and paper write-up.

The work was done in consultation with and under the supervision of Dr. Heather Sheardown. Dr. Heather Sheardown revised the draft to the final version.

Abstract

Protein-alginate complexes were prepared with the objective of quantifying the influence of the parameters such as protein characteristics on the final complex properties and their dissociation rates. Lysozyme, chymotrypsin, and bovine serum albumin were used as model proteins for preparing the complexes and physical properties such as composition, average diameter, and zeta potential of the complexes formed were measured. In addition, protein release kinetics from the complexes in response to changes in pH and ionic strength were investigated. The results clearly demonstrated that, even in the absence of a cation, proteins could be complexed with alginate and showed a decreased release rate under the appropriate conditions. Projection to Latent Structures was applied as a multivariate statistical analysis method to mathematically describe the final properties and the protein release kinetics as functions of the influencing variables. It was found that the physical characteristics of the complexes could be accurately modelled with low error thresholds indicative of good fit and prediction capabilities of the model. The statistical model indicated that the release kinetics parameters were highly dependent on the ionic strength and the protein net charge as a function of pH, demonstrating the potential use of these complexes in ion-/pH-sensitive delivery systems.

Keywords: Alginate; Protein; Polyelectrolyte complex; Electrostatic self-assembly; Controlled release; Multivariate statistical analysis

3.1. Introduction

Based on results from Chapter 2, which revealed the promising potential of lysozyme-alginate complexes as pH-/ion-sensitive protein carriers while conserving the enzymatic activity of the complexed lysozyme, in this chapter the physicochemical properties and release kinetics of the protein-alginate complexes were further studied with the use of two additional proteins (chymotrypsin and bovine serum albumin). Multivariate statistical analysis methods in Chapter 2 quantified the effects of physicochemical properties of the complex as well as environmental triggers such as ionic strength on the protein release kinetics (kt^n) and the potential to tailor the system to obtain desired release kinetics was demonstrated. In order to further understand the effect of protein properties on the complex properties and protein release rates, in addition to lysozyme, two proteins with varying molecular weights and isoelectric points were incorporated into the complex system. A multivariate statistical model was built and a cross-validation method was carried out in order to assess the quality of the statistical model in describing the trends and its prediction ability. Additional details, not included in the publication, regarding the cross-validation method are found in Appendix C for release parameter k as an example calculation.

Pioneering studies using biomolecules such as oligonucleotides¹, oligopeptides², antibodies³, and proteins⁴ promises great opportunities for the fabrication of biomolecule-crosslinked hydrogels. These studies were followed by further investigations using biomolecules as crosslinkers^{5,6} which offered the advantage of controlled stimulus-response modulated by the biomolecule⁷. While promising, caution is required to ensure

protein structure and functionality are not compromised during the process⁸. Fabrication of protein-polymer complexes where mostly electrostatic interactions drive the self-assembly process⁹ in aqueous solutions and under ambient conditions⁸ is a potentially favorable approach for protein crosslinking compared to covalent binding in the presence of toxic chemicals involving heat or vigorous agitations¹⁰.

Polyelectrolyte complexes (PECs) have drawn increasing attention as functional ingredients in the food and pharmaceutical industries^{11,9} as well as in biomedical applications¹². These self-assembled structures are spontaneously formed as a result of strong electrostatic interactions between oppositely charged polyelectrolytes in solution⁹.

Alginate, an anionic polysaccharide composed of mannuronic (M) and guluronic (G) acid residues¹³, has been widely studied for use in various biomedical applications including drug delivery, cell encapsulation, and wound healing¹⁴ as well as for consumption in the food industry as a stabilizer, thickening and gelling agent¹⁵. This non-toxic and highly mucoadhesive¹³ polymer is capable of ionically crosslinking in the presence of multivalent cations such as calcium to form gels under ambient conditions without the need for toxic organic solvents^{16,17}.

Since alginate is an anionic polymer, it is expected to form complexes with proteins below their isoelectric point (pI) where the protein carries a net positive charge. Protein-polymer complex formation and stability are mainly influenced by factors such as protein/polymer ratio, pH, and ionic strength. The complexation is a reversible process and with changes in pH or ionic strength, the complex will dissociate¹⁸. Therefore, protein-polymer complexes offer the potential to be used as pH-/ion-sensitive drug or

protein delivery vehicles. Complex nanoparticles of insulin and amino poly(glycerol methacrylate)s¹⁰ and also insulin and block polyelectrolyte quaternized poly[3,5-bis(dimethylaminomethylene)hydroxystyrene]-b-poly(ethylene oxide)¹⁹ for example have been shown to offer potential as delivery vehicles for insulin. In another study, polyelectrolyte complexes of N,N-dimethyl chitosan and heparin were prepared and *in vitro* release of heparin from the complex matrix was evaluated²⁰.

Although alginate-protein complex systems have been studied in food industry^{21,22} and drug delivery¹¹ applications, they have not been widely investigated as efficient carriers for the delivery of the complexed protein from the alginate-based complex. Furthermore, in spite of numerous studies on protein-polysaccharide complexes, the related literature lacks a systemic approach for comprehensively understanding the correlations and relationships.

In this study, complexes of alginate and model proteins were prepared and their properties as well as their dissociation/release patterns at varying pH and ionic strength conditions were evaluated in order to assess how these systems might be applied to different delivery applications. Multivariate statistical methods were applied to this work in order to better understand how the proteins interacted with the alginate and under which conditions release could be best controlled.

The Projection to Latent Structures (PLS) method was used for multivariate statistical analysis of the data. This method uses statistically independent variables, which are linear combinations of the original variables, to build models on the variables and responses as well as to provide insight into the correlations between them²³. It is

hypothesized that the reduced dimensional space²³ of the model can be used as a beneficial tool for further understanding of the relationships and to mathematically quantify the model, making it potentially advantageous for predicting properties at other conditions. By assessing the potential of protein charges as the modulators of release and subsequently examining which parameters can be used to control release properties, a better understanding of protein release from alginate based systems can be achieved.

3.2. Materials and Methods

3.2.1. Materials

Sodium alginate from brown algae with molecular weight range of 100,000-200,000 g/mol and consisting of 65% guluronic acid and 35% mannuronic acid residues was purchased from Sigma-Aldrich (Oakville, ON). Lysozyme (from chicken egg white), chymotrypsin (from bovine pancreas), and bovine serum albumin (BSA) were used as model proteins. These and all other reagents were also purchased from Sigma-Aldrich (Oakville, ON).

3.2.2. Preparation of Protein-Alginate Complexes

The electrostatic self-assembly of alginate and proteins and the potential use of these systems to release the complexed protein was investigated using the model proteins, the properties of which are detailed in Table 3.1.

Table 3.1. Isoelectric point, net charge at physiological pH, and molecular weight of the model proteins^{24,25}.

Protein	pI / Net Charge	Molecular Weight (Da)
Lysozyme	11.0 / Positive	14,000
Chymotrypsin	9.1 / Positive	25,000
Bovine Serum Albumin (BSA)	5.4 / Negative	65,000

Complexes were prepared by mixing solutions of alginate and the protein in sodium acetate buffer (pH=4.5, $I=10$ mM) at room temperature. This ensured that all of the proteins carried a net positive charge and could crosslink the alginate. Protein-alginate complexes were prepared by the addition of 1.2 mL alginate solution to 1.8 mL protein solution under constant stirring as described by Fuenzalida *et al.*¹¹.

The concentration of alginate was fixed in all solutions and was selected to obtain a 1 mM concentration of anionic charges on alginate. The concentration of the proteins was then calculated to obtain cationic to anionic molar charge ratios of 0.5:1, 1:1, and 2:1 based on the net charge per mole of each of the proteins at pH=4.5 (+11 for lysozyme¹¹, +7.7 for chymotrypsin²⁶, +3 for BSA²⁷). Complexes were collected by centrifugation (100 × g, 90 s) and were lyophilized until further use. All complexes were prepared in triplicate and the error bars on graphs represent standard deviations.

3.2.3. Complex Composition Analysis

The polymer and protein mole fractions in the complexes were determined indirectly by determining the component content in the supernatant collected after centrifugation.

Protein concentrations were measured using Bradford assay. Bradford Reagent was added to the samples, absorbance was quantified at 595 nm (SpectraMax Plus 384 Microplate reader, Molecular Devices LLC, CA, USA), and protein concentrations were calculated based on comparison with known standards.

Alginate content was determined using the phenol-sulfuric acid assay²⁸. Briefly, 0.1 mL of distilled water was added to an equal volume of alginate sample followed by the addition of 0.2 mL of 5% (w/v) phenol plus 1 mL of concentrated sulfuric acid. The mixture was incubated at room temperature for 15 minutes and the absorbance was measured at 488 nm. Alginate concentrations were determined by comparison with known standards.

3.2.4. Physical Characterization

Physical characterization of complexes was performed by measuring the zeta potential of the complexes (Zeta PALS, Brookhaven Instruments Corp., NY, USA) and determining complex size distributions (Mastersizer 2000 equipped with Hydro 2000S, Malvern Instruments Ltd., UK). The size distribution was stated in volume mean diameter along with SPAN factor (Equation 3.1).

$$\text{SPAN} = \frac{d_{90} - d_{10}}{d_{50}}$$

Equation 3.1

In Equation 3.1, values of d_{10} , d_{50} , and d_{90} are the diameter sizes that the specified percentages (10, 50, and 90, respectively) of the complexes are smaller than that particular size. High SPAN values imply wide size distributions²⁹.

3.2.5. Protein Release

Protein release studies were carried out at pH values of 4.5 and 7.4 in sodium acetate buffer and sodium phosphate buffer, respectively. Furthermore, since it is expected that higher salt concentrations will lead to more rapid replacement of the protein charges and therefore faster release, the effect of the ionic strength of the buffer was examined. For evaluating the effect of salt concentration on the release kinetics, low ionic strength ($I=10$ mM) and high ionic strength ($I=150$ mM) buffers were used as release media at each of the pH conditions. Complexes were suspended in 1.5 mL of buffer and placed in a 37°C and 100 rpm incubator. At regular intervals, release tubes were centrifuged (2000 rpm, 2 min) and samples (0.5 mL) were taken and replaced with 0.5 mL of fresh buffer. Release was carried out until the complexes were fully degraded (100% of the theoretical protein loading was released) or no more protein release was detected.

Equation 3.2 shows the Korsmeyer-Peppas kinetic model which is commonly used for analyzing the release mechanisms³⁰. The first 60% of the protein release kinetic data were fitted to the logarithmic form of the Korsmeyer-Peppas kinetic model (Equation 3.3) in order to obtain values for parameters $\ln(k)$ and n . In Equation 3.2 and

Equation 3.3, M_t/M_∞ is the fraction of drug released at time t , k is the release rate constant and n is the release exponent.

$$\frac{M_t}{M_\infty} = kt^n \quad \text{Equation 3.2}$$

$$\ln\left(\frac{M_t}{M_\infty}\right) = \ln k + n \ln t \quad \text{Equation 3.3}$$

3.2.6. Multivariate Statistical Analysis

To better understand and model the effects of the various parameters on protein release from protein crosslinking alginate gels, multivariate statistical analysis was performed using ProMV software (ProSensus Inc.). The Projection to Latent Structures (PLS) model was applied for further understanding of the interactions involved in the formation of the complexes and in determining the release kinetics. Multivariate analysis is a statistical approach which summarizes all of the factors involved in the process in a smaller number of independent latent variables. These latent variables are linear combinations of the original variables²³.

In building the model, protein properties (net charge and molecular weight), initial $[n^+]/[n^-]$ mixing ratio, and the ionic strength of the release buffer were inputted into the ProMV software as the X matrix. The complex composition, complex physical properties (average diameter and zeta potential), and the release kinetic parameters comprised the Y matrix.

The values of protein net charge imputed into the software at pH=4.5 were +11 for lysozyme¹¹, +7.7 for chymotrypsin²⁶, and +3 for BSA²⁷. At pH=7.4, the net charges were +9 for lysozyme³¹, +3 for chymotrypsin³², and -16 for BSA³³.

3.3. Results and Discussion

3.3.1. Complex Composition Analysis

Figure 3.1 shows the complex composition and the final n^+/n^- ratios in the complexes formed. As expected, the mole fraction of protein in the complex increased with the initial protein concentration in the mixing solution. Therefore, for achieving higher protein loading, a higher concentration of protein in the initial mixing solution can be used. As a result, the final n^+/n^- ratios were also increased due to the complexation and presence of higher amounts of positive charge in the complex.

Furthermore, it is also observed in Figure 3.1 that, somewhat unexpectedly, with an increase in the molecular weight of the protein ($MW_{BSA} > MW_{Chymotrypsin} > MW_{Lysozyme}$), the formation of the alginate complex is decreased. With the net charges per mole of the model proteins at pH=4.5 being +11 for lysozyme¹¹, +7.7 for chymotrypsin²⁶, and +3 for BSA²⁷, it can be seen that the lowest molecular weight protein (lysozyme) has the highest net positive charge and the lowest net positive charge is associated with the largest protein (BSA). Therefore, the positive charge density is highest in lysozyme, followed by chymotrypsin, and is the lowest in BSA. Since electrostatic interactions are the main driving force in complex formation⁹, the high positive charge density of

lysozyme and the low positive charge density of BSA result in the complexation observed.

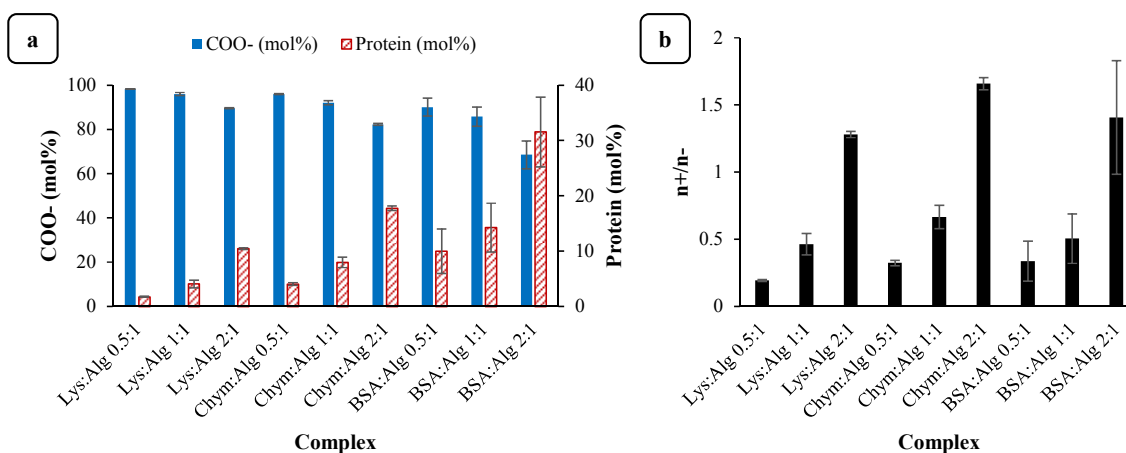


Figure 3.1. Composition of protein-alginate complexes; (a) mole compositions, (b) n^+/n^- ratio in complex. Lys=Lysozyme, Chym=Chymotrypsin, BSA=Bovine Serum Albumin.

3.3.2. Physical Characterization

The results of the zeta potential and mean size measurements are shown in Table 3.2. An increase in the initial protein:alginate mixing ratio leads to more positive zeta potential values. This is consistent with the trend observed for the final n^+/n^- ratios in the complex (Figure 3.1(b)). An increase in the initial protein concentration results in a higher degree of protein complexation suggesting that the complexes are not saturated. Thus the presence of more positive charge is associated with more positive zeta potential values. Furthermore, the average diameter of the complexes was increased as higher molecular weight proteins were used as would be expected. While the proteins act to

crosslink the polymer, complexes with slightly greater diameters are formed when the polymer chains are interacting with larger proteins.

Table 3.2. Physical properties of protein-alginate complexes.

Complex	Zeta potential (mV)	Mean complex size	
		Volume mean diameter (μm)	SPAN
Lysozyme-Alginate 0.5:1	-45.6 ± 2.2	2.5 ± 0.3	1.0 ± 0.1
Lysozyme-Alginate 1:1	-35.8 ± 1.1	2.7 ± 0.1	1.2 ± 0.1
Lysozyme-Alginate 2:1	8.0 ± 2.2	3.2 ± 0.3	2.6 ± 0.6
Chymotrypsin-Alginate 0.5:1	-37.0 ± 1.2	2.8 ± 0.7	1.3 ± 0.3
Chymotrypsin-Alginate 1:1	-28.4 ± 1.4	3.1 ± 0.6	0.9 ± 0.3
Chymotrypsin-Alginate 2:1	11.4 ± 1.4	3.5 ± 0.7	3.3 ± 0.7
BSA-Alginate 0.5:1	-32.8 ± 2.0	3.2 ± 0.2	1.1 ± 0.3
BSA-Alginate 1:1	-30.7 ± 2.1	3.6 ± 0.6	1.2 ± 0.8
BSA-Alginate 2:1	9.0 ± 1.6	4.8 ± 0.7	5.6 ± 1.0

As shown in Table 3.2, the high SPAN values of the complexes formed at protein to alginate mixing ratio of 2:1 for all of the proteins, and increasing with increasing protein size, are indicative of wide size distributions. This is likely the result of intra-complex bridge formation with the presence of more protein³⁴ leading to wider size distributions. In this study, only complexes formed at a protein to alginate mixing ratio of 0.5:1 and 1:1 were used for protein release studies due to their lower SPAN values and more narrow size distributions as it is expected that with the larger size distributions, there will be greater variability in the release rate of the protein.

3.3.3. Protein Release

The release of proteins from the complexes at varying pH and ionic strength conditions is shown in Figure 3.2. Since electrostatic interactions control the system dynamics in complex formation⁹, factors weakening this force cause faster complex degradation and lead to more rapid release of the protein. In general, the results faster protein release is observed at higher pH values irrespective of the protein used. This is due to the complete or partial loss of positive charges on the proteins leading to weakened electrostatic interactions and the degradation of the complexes. Furthermore, higher ionic strength conditions also lead to more rapid protein release as a result of the faster degradation of the complexes due to charge screening effects at high salt concentrations which replace the proteins in the complex.

At pH=7.4, BSA has a net negative charge; therefore minimal and only local interaction between the protein and the alginate would be expected. Furthermore, there would be expected to be repulsion forces with the anionic alginate resulting in the release of 100% of the complexed protein in less than 3 hours even at low ionic strength ($I=10$ mM) and in less than 2 hours with the presence of more sodium ions ($I=150$ mM). At conditions where complex degradation is lower, as a release controlling factor (at pH below the isoelectric point of the protein and at low ionic strength), protein molecular weight seems to impact the release rates although additional studies with other proteins are necessary to confirm this. The higher molecular weight of chymotrypsin compared to lysozyme resulted in slower diffusion and release of the larger protein at all pH and ionic strength conditions as expected.

Somewhat surprisingly, the protein loading amounts (the initial protein-alginate mixing ratio) did not seem to significantly affect the protein release rates. It was expected with higher amounts of protein present, a greater degree of crosslinking of the alginate would occur, resulting in slower release of protein as it was replaced by monovalent ions in the release solution. Instead it seemed that higher protein loadings caused a higher concentration gradient with the release media and therefore more rapid release which counteracted to some extent the effect of having more protein molecules crosslinking the networks. Above a certain threshold however, where no additional crosslinking was possible, a significant burst release would be expected due to the presence of weakly complexed or uncomplexed proteins in the system. It is not clear that this threshold was met in these studies however.

The results suggest that, as hypothesized, protein complexes with alginate can be used to control protein release and conditions such as the ionic strength and pH of the release media can be used to trigger protein release from the protein-polysaccharide complexes, meaning that, depending on the protein and the desired release location, a tailorable release is possible.

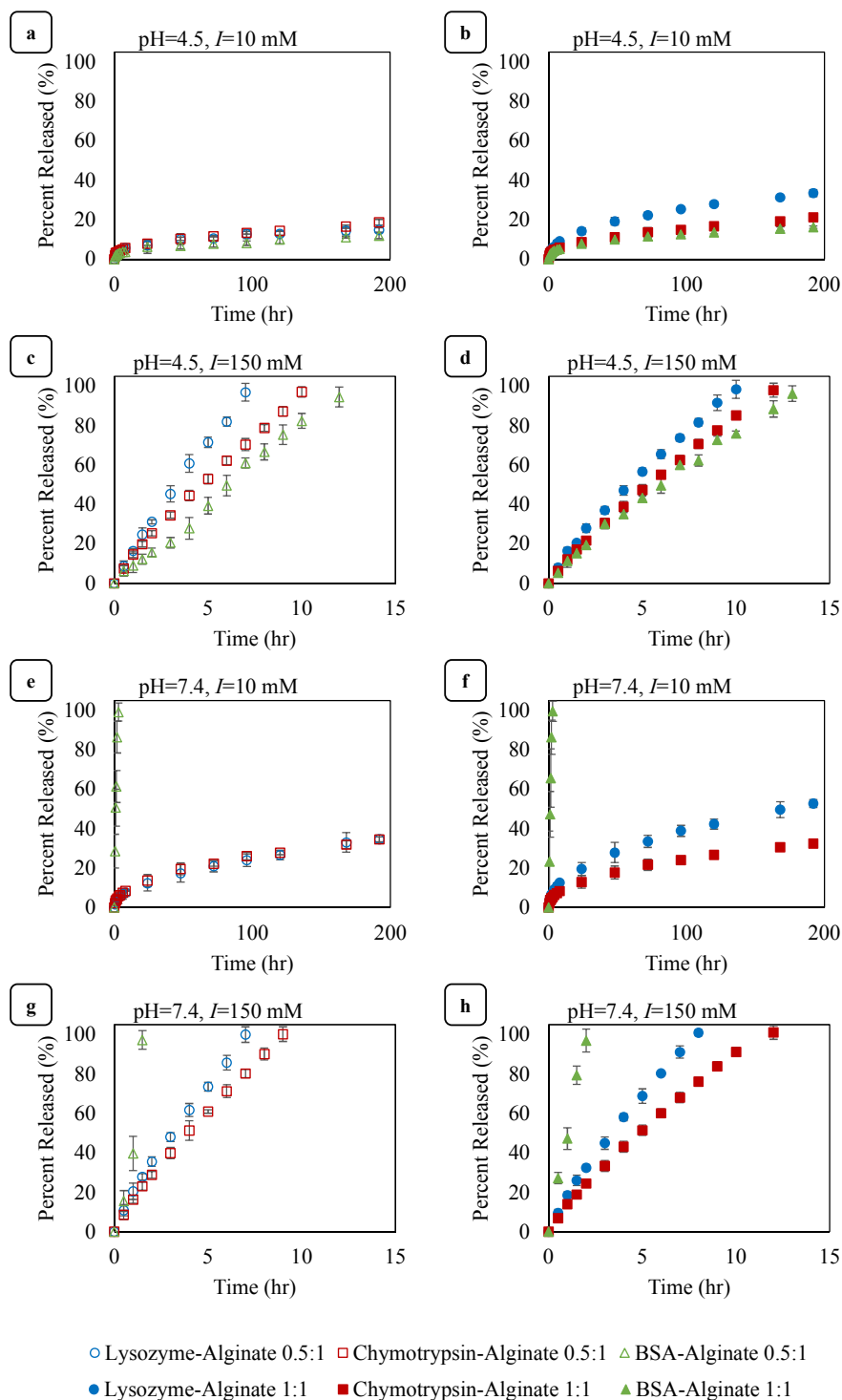


Figure 3.2. Release of proteins from protein-alginate complexes; (a) 0.5:1, pH=4.5, I=10 mM, (b) 1:1, pH=4.5, I=10 mM, (c) 0.5:1, pH=4.5, I=150 mM, (d) 1:1, pH=4.5, I=150 mM, (e) 0.5:1, pH=7.4, I=10 mM, (f) 1:1, pH=7.4, I=10 mM, (g) 0.5:1, pH=7.4, I=150 mM, (h) 1:1, pH=7.4, I=150 mM.

3.3.4. *Multivariate Statistical Analysis*

To further understand the extent of the effects of various factors in the release, multivariate statistical analysis methods were applied to the data. A three component Projection to Latent Structures (PLS) model was built based on the data imported into the ProMV software (ProSensus Inc.). Measures of model fit capability (R^2X and R^2Y) and model predictive capability (Q^2Y) are shown in Figure 3.3(a). In building the model, the initial $[n^+]/[n^-]$ mixing ratio, protein molecular weight, protein net charge (as a function of pH), and the ionic strength of the release media were imported as the X matrix. The PLS method builds a model on the X space and R^2X , representative of the fit of the model to the X data, was calculated to be 0.914. The complex properties (composition, zeta potential, and average diameter) were imported as the Y matrix. The data obtained from fitting the protein release data into the logarithmic form of the Korsmeyer-Peppas kinetic model (with R-squared values in the range of 0.968-1.000) were also included in the Y matrix. The overall R^2Y , which is indicative of model fit capability on the Y matrix and Q^2Y , a measure of model predictive capability on Y matrix were calculated to be 0.828 and 0.736, respectively. The relatively high values of R^2X , R^2Y , and Q^2Y are indicative of the excellent fit capability and reliable predictive performance of the model. In Figure 3.3(b), the R^2 and Q^2 values for each of the Y variables are shown. These also demonstrate good fit and predictive performance of the model.

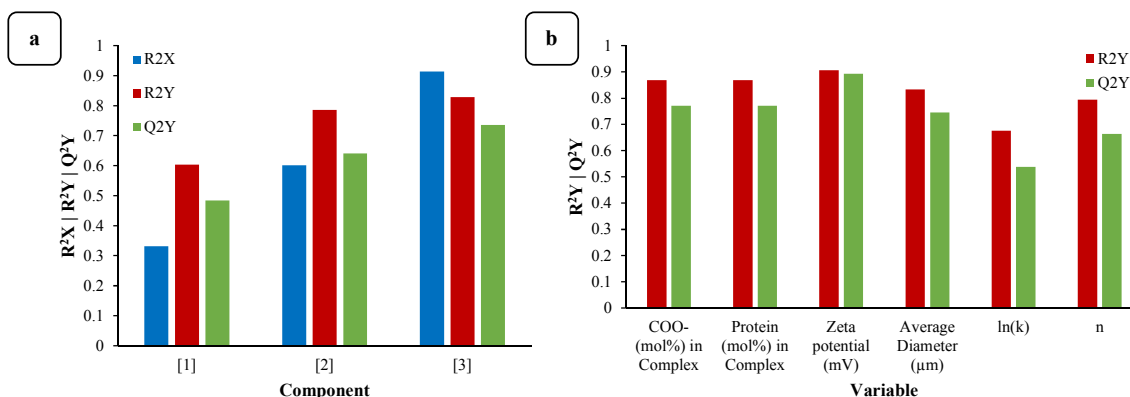


Figure 3.3. (a) Cumulative R^2X , R^2Y , and Q^2Y for the PLS model; (b) R^2 and Q^2 for each of the Y variables.

The first latent component in a PLS model represents the greatest covariance between the X and Y spaces, and each sequencing latent component explains less information³⁵. For example, as seen in Figure 3.3(a), while R^2Y based on the first component is equal to 0.604, addition of the second and third components increases the overall R^2Y by values of only 0.182 and 0.042, respectively. Therefore, a correlation-loading plot (Figure 3.4) of the first two latent components is sufficient for explaining the covariance in the X and Y spaces. In this plot, the location of the variables relative to each other is an indication of their relationships and correlations. While strongly correlated parameters are clustered together, negatively correlated variables are located in opposite quadrants. For example, as observed in Figure 3.4, the average size of the complexes is strongly and positively correlated to the protein molecular weight, meaning larger proteins result in larger complexes as would be expected. The carboxyl mole fraction is located on the opposite quadrant relative to the initial $[n^+]/[n^-]$ ratio in the mixing solution describing a negative correlation between the two factors, which, as

expected, is similar to the trend observed in Figure 3.1(a). Also observed in Figure 3.4 is the relationship between the release kinetic parameters, the protein properties, and mixing and release conditions. The plot suggests that the release parameters, $\ln(k)$ and n , both seem to be strongly/positively correlated to the ionic strength of the release buffer and negatively correlated to the net charge of the protein. The plot also indicates, somewhat surprisingly based on the release data, an absence of strong correlation between the release parameters and protein molecular weight or initial $[n^+]/[n^-]$ ratio in the mixing solution.

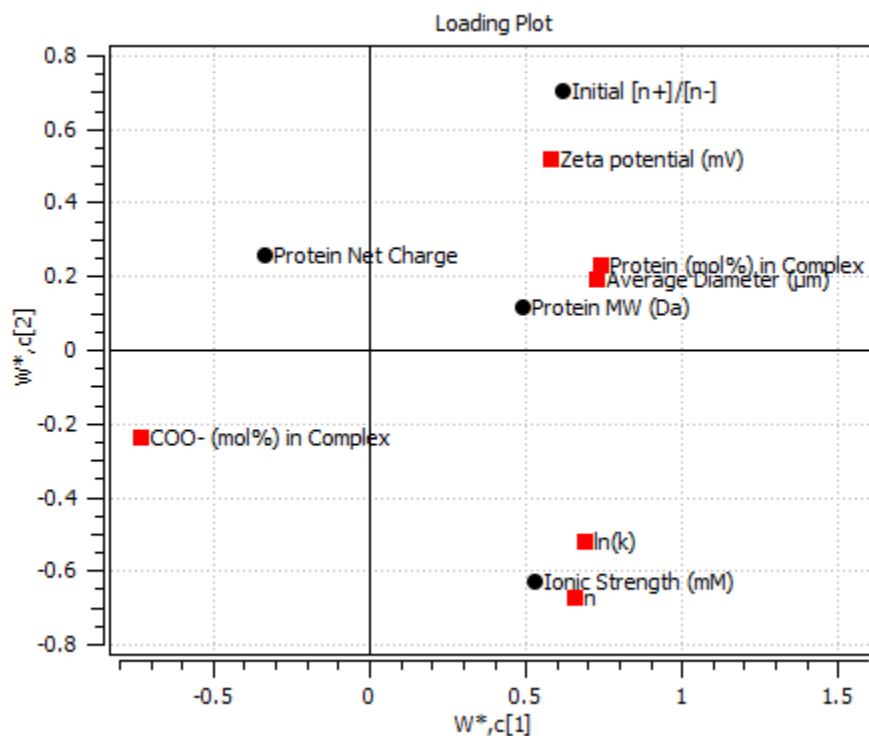


Figure 3.4. Correlation-loading plot for contributors to Y variables.

While the correlation-loading plot (Figure 3.4) represents the qualitative relationships between the parameters (also observable in Figure 3.1, Figure 3.2, and Table 3.2), coefficient plots in PLS model quantify the correlations. Figure 3.5 shows the coefficient plots which indicate the quantitative effect of each of the X parameters on the complex composition. Since the mole fraction of the protein and polymer are not independent variables, the influence of each of the X parameters on them is equal but opposite. As seen, complex composition is strongly dependent on the initial $[n^+]/[n^-]$ ratio in the mixing solution and the molecular weight of the protein. Increase in the initial $[n^+]/[n^-]$ ratio, which is due to the increase in protein concentration since the concentration of the negative charges of polysaccharide were kept constant throughout the various experimental conditions, results in higher protein complexation and therefore an increased mole fraction of protein in the complex (Figure 3.5(b)). Increase in the mole fraction of protein leads to lower mole fractions of the polysaccharide in the complex (Figure 3.5(a)). Protein molecular weight is the second influencing factor in the complex composition; larger proteins result in higher protein mole fractions (Figure 3.5(b)) and therefore lower polymer mole fractions (Figure 3.5(a)), similar to the trend observed in Figure 3.1 and explained in complex composition analysis. Surprisingly, the protein net charge seems to be an insignificant factor in determining the complex composition. This suggests that the effect of charge concentration is more dominant when higher protein concentrations are used rather than different proteins (with various net charges) at similar initial $[n^+]/[n^-]$ ratios.

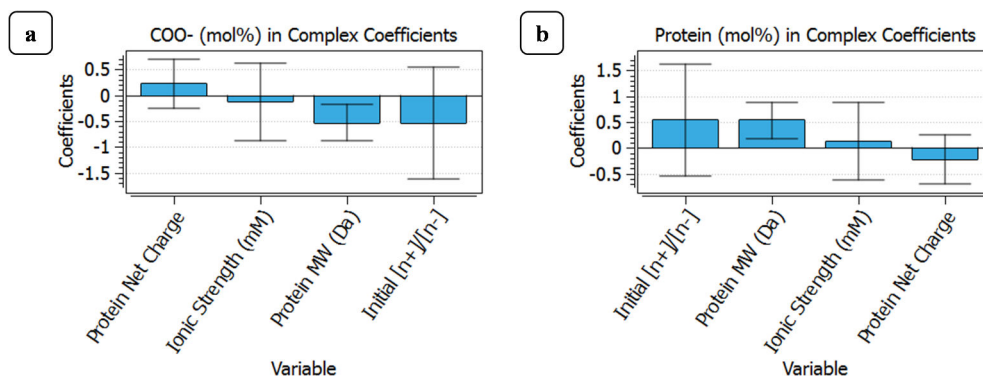


Figure 3.5. Coefficient plots showing the effect of each X parameter on complex composition and mole fractions of (a) COO⁻, (b) protein.

The size and direction of the effect of each of the X variables on the release characteristics ($\ln(k)$ and n) is shown in Figure 3.6. The high dependency of both these parameters on the ionic strength of the release buffer as well as the net charge of the protein is an indication of the ion-sensitivity and pH-dependency of the release kinetics. The k parameter in the Korsmeyer-Peppas model is the kinetic constant which represents the structural characteristics of the drug dosage form³⁰. As seen in Figure 3.6(a), this parameter is mainly and positively dependent on the ionic strength of the release buffer with a negative dependence on the protein net charge. In Figure 3.6(b) the same trend is observed for the effect of the X variables on parameter n , which is indicative of the release mechanism. Higher n values have been suggested to represent less-diffusion based kinetics and more non-Fickian transport mechanisms³⁰. The release kinetics also seem relatively independent of the initial $[n^+]/[n^-]$ and the molecular weight of the protein suggesting that diffusion is not the limiting factor in these complexes. Rather, this suggests that the release is mainly governed by the disintegration of the complexes at conditions where the electrostatic interactions, which are the main driving force in

complex formation⁹, are compromised, such as at higher ionic strength or higher pH values. This non-diffusion based release kinetics from the complexes is also concluded from the high n values obtained from the fit of release profiles into the Korsmeyer-Peppas model (Supplementary Material).

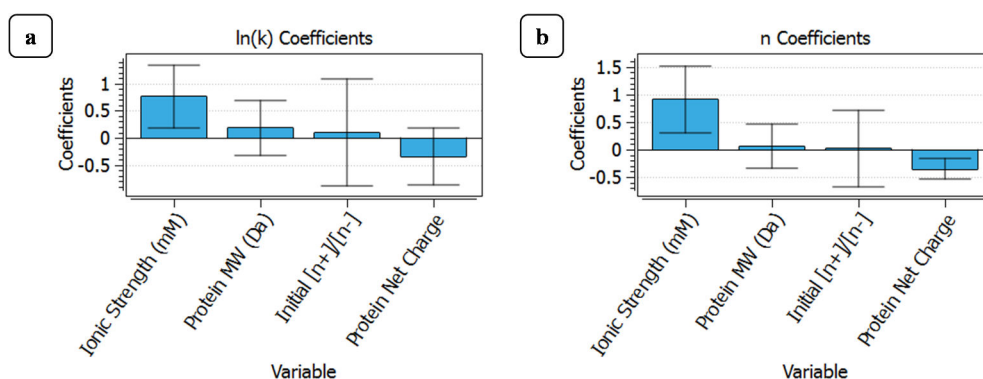


Figure 3.6. Coefficient plots showing the effect of each X parameter on release kinetic parameters; (a) $\ln(k)$, (b) n .

The experimental values and the PLS model predicted values for each of the Y variables are compared in Figure 3.7. The complex properties, such as composition, average size, and zeta potential, have R^2 values in the range of 0.834 to 0.906 (Figure 3.7(a) to (d)) which indicates high fitting capability of the model. The root mean-squared error of prediction for the mole fractions of the polymer and protein in the complex (Figure 3.7(a) and Figure 3.7(b), respectively) is 2.506, which is a very low threshold for these values which are reported in percentages. The root mean-squared error values of 0.212 μm and 4.968 mV for the average diameter (Figure 3.7(c)) and zeta potential (Figure 3.7(d)) are also considered relatively small thresholds for these parameters which fluctuate in the range of 2.489-4.773 μm and (-45.63)-(+11.38) mV,

respectively (Table 3.2). While the R^2 value for fit of the release parameter $\ln(k)$ is equal to 0.676 (Figure 3.7(e)) and is imperfect, the root mean-squared error value of 0.658 for a parameter ranging from -3.986 to -0.738 (Supplementary Material) implies that the model can still be considered relatively reliable. The R^2 value of the parameter n is calculated to be 0.794 (Figure 3.7(f)) which is an indication of a good fit and with n values in the range of 0.347-1.350 (Supplementary Material) a root mean-squared error value of 0.129 endorses the relatively acceptable fit.

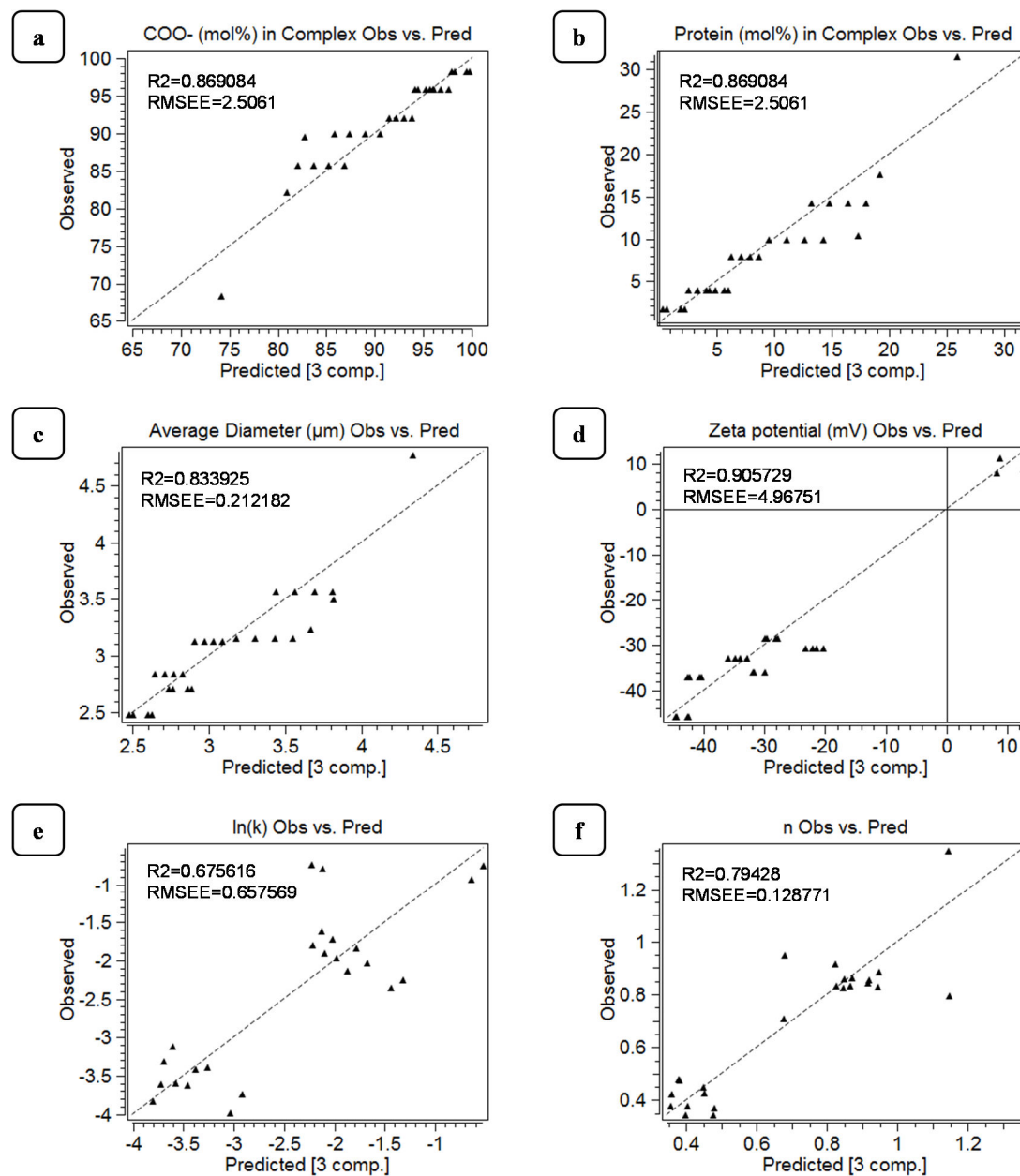


Figure 3.7. Observed vs. Predicted plots for Y variables.

Figure 3.8 shows the squared prediction error for the X space (SPE-X). As seen, all the data are located below the 99% confidence level which also confirms the reliability of the modeled correlations in the X space for prediction of the Y variables.

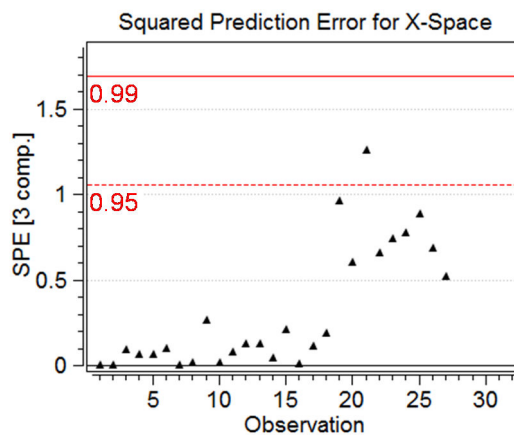


Figure 3.8. Squared prediction error (SPE) values for the experimental observations.

The contour plots in Figure 3.9 illustrate the variance in the complex properties (composition, average diameter, zeta potential) as functions of their main two contributing factors determined from the PLS model. The observed experimental data are shown with scattered data points on these plots and their distance from the contour plot represents the accuracy of the PLS model prediction. The equations describing the correlation between each property and its two main contributing factors is also shown on the plots. As observed, the scattered data fall well within an acceptable distance from the contour plot, indicating the contour plots and their respective equations can be used for reliable prediction of the complex properties.

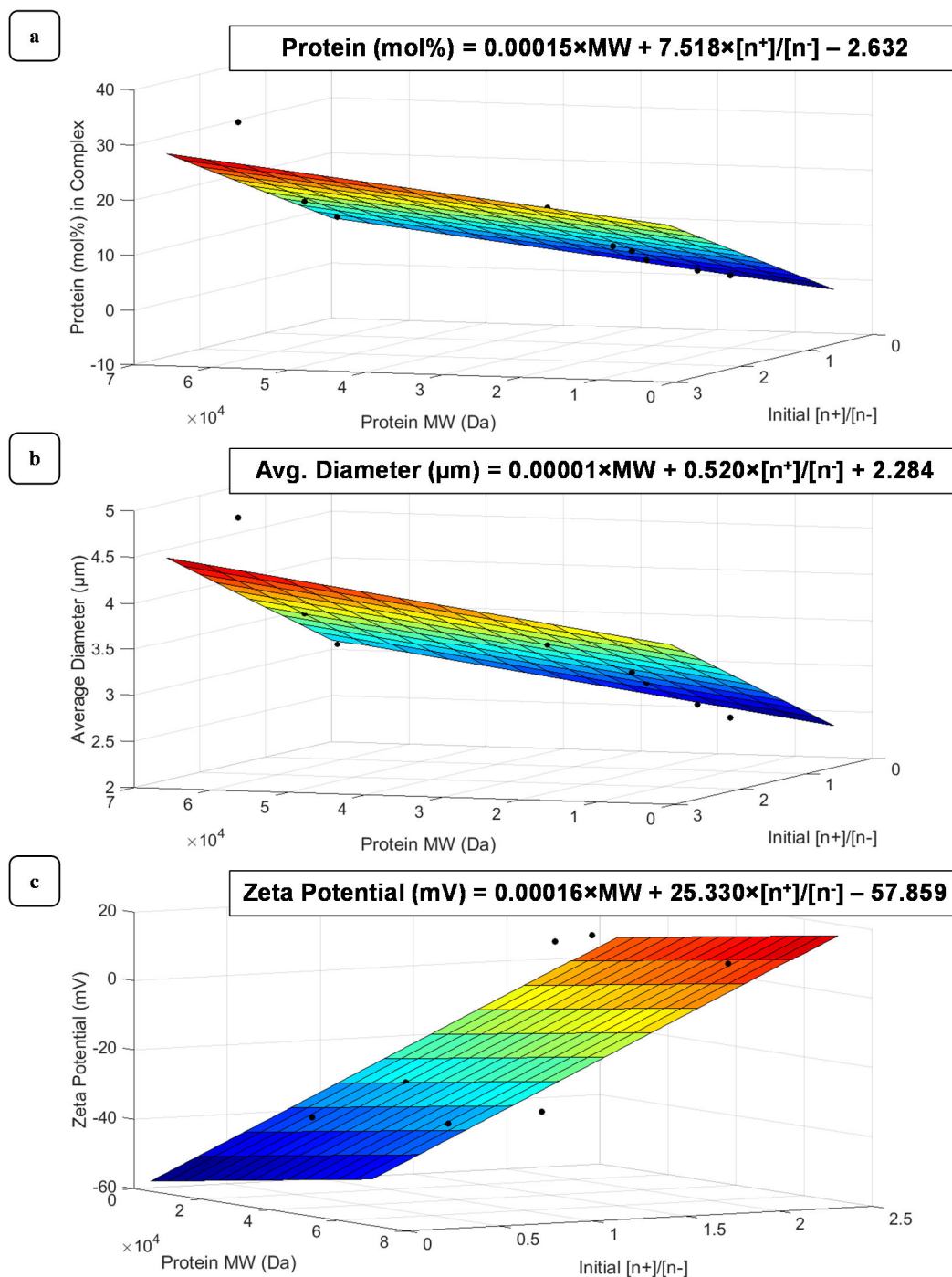


Figure 3.9. Contour surface plots from the PLS model as functions of the main two contributing factors and the experimental data for (a) protein (mol%) in complex, (b) average diameter (μm), (c) zeta potential (mV).

The ultimate objective of protein and drug release studies is delivery and release at physiological conditions. Therefore, the contour plots for prediction of the release kinetic parameters (Figure 3.10) were plotted at constant ionic strength of the buffer ($I=150$ mM), mimicking typical *in vivo* conditions, and as functions of protein properties (molecular weight and net charge). The relationships are also described in the mathematical equations shown and the scattered data on the plots represent the observed experimental data. The acceptable distance between the experimental data (root mean-squared values of 0.501 and 0.129 for parameters $\ln(k)$ and n , respectively) and the contour plots observed in Figure 3.10 as well as the observed versus predicted data in Figure 3.7(e) and Figure 3.7(f), suggest that the statistical model offers reliable predictive capabilities for the release kinetics of various proteins.

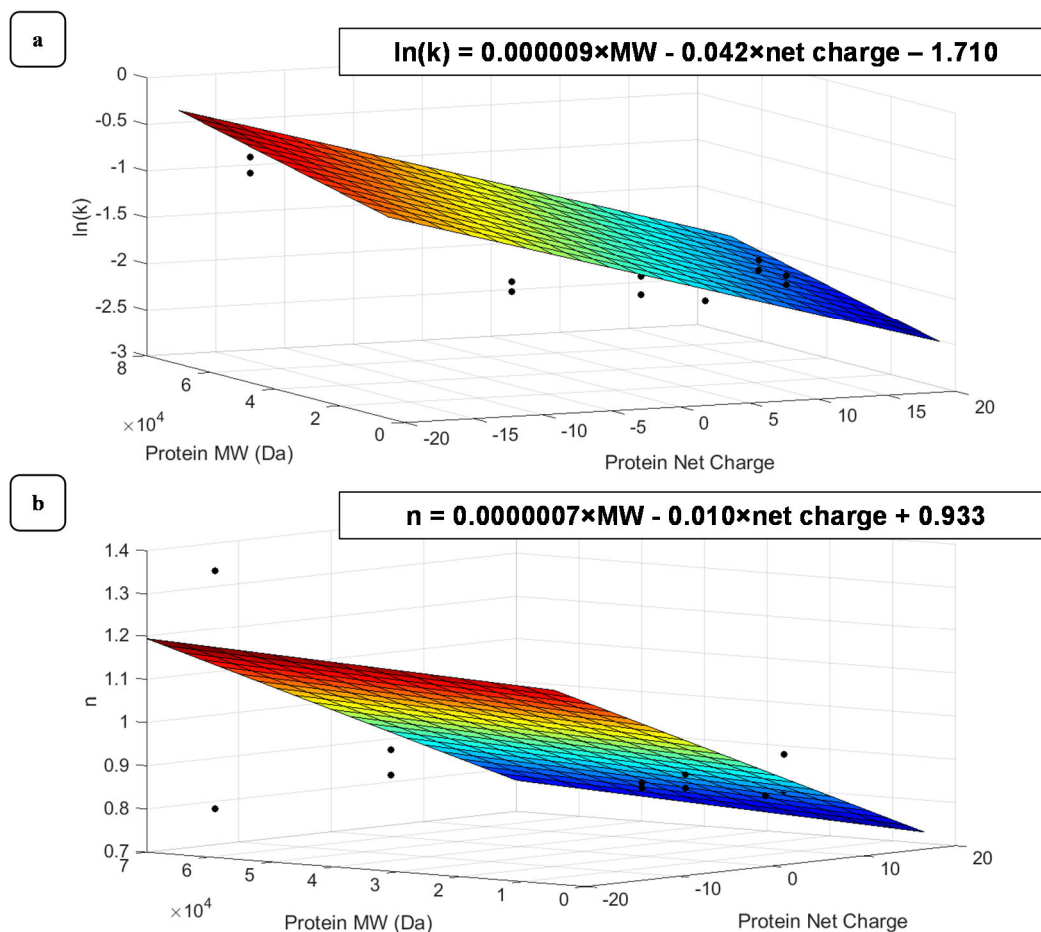


Figure 3.10. Contour surface plots from the PLS model for protein release kinetics as functions of protein properties (molecular weight and net charge) at physiological ionic strength ($I=150$ mM); (a) $\ln(k)$, (b) n .

The model can still be improved by expanding the input database using additional model proteins or release at varying pH conditions. Increasing the number of imported rows of data into the PLS model will increase the fit capability as well the prediction reliability of the model.

3.4. Conclusion

Protein-polysaccharide complexes show great promise for use as protein carriers. In the case of alginate, this study demonstrates that the protein can be used as a source of cations for gel crosslinking, depending on the protein and the surrounding conditions. The protein release is facilitated by environmental triggers such as ionic strength and pH and there is clearly the potential to tailor the system to obtain desired release kinetics. For example, it might be useful in the future to examine post crosslinking with positively charged cations such as calcium to determine how this impacts the release kinetics. To understand the nature of the various effects, a multivariate statistical analysis method was used, confirming the dependence of release properties on the ionic strength and pH of the release media while demonstrating independence from the initial charge ratio. This novel method of generating protein polysaccharide complexes and using multivariate analysis for understanding the correlations can be used to develop protein release devices offering desired release kinetics.

3.5. Acknowledgements

The authors would like to gratefully acknowledge NSERC for funding support and ProSensus Inc. for generous permission to use ProMV software.

References

1. Nagahara, S. & Matsuda, T. Hydrogel formation via hybridization of oligonucleotides derivatized in water-soluble vinyl polymers. *Polym. Gels Networks* **4**, 111–127 (1996).

2. West, J. L. & Hubbell, J. A. Polymeric Biomaterials with Degradation Sites for Proteases Involved in Cell Migration. *Macromolecules* **32**, 241–244 (1999).
3. Miyata, T., Asami, N. & Urugami, T. A reversibly antigen-responsive hydrogel. *Nature* **399**, 766–769 (1999).
4. Obaidat, A. A. & Park, K. Characterization of Glucose Dependent Gel-Sol Phase Transition of the Polymeric Glucose-Concanavalin A Hydrogel System. *Pharm. Res.* **13**, 989–995 (1996).
5. Tada, D., Tanabe, T., Tachibana, A. & Yamauchi, K. Drug release from hydrogel containing albumin as crosslinker. *J. Biosci. Bioeng.* **100**, 551–555 (2005).
6. Gawel, K. & Stokke, B. T. Logic swelling response of DNA–polymer hybrid hydrogel. *Soft Matter* **7**, 4615 (2011).
7. Sasaki, Y., Tsuchido, Y., Sawada, S. & Akiyoshi, K. Construction of protein-crosslinked nanogels with vitamin B6 bearing polysaccharide. *Polym. Chem.* **2**, 1267 (2011).
8. van Rijn, P. Polymer Directed Protein Assemblies. *Polymers (Basel)*. **5**, 576–599 (2013).
9. Schmitt, C. & Turgeon, S. L. Protein/polysaccharide complexes and coacervates in food systems. *Adv. Colloid Interface Sci.* **167**, 63–70 (2011).
10. Lu, X. *et al.* Polyelectrolyte complex nanoparticles of amino poly(glycerol methacrylate)s and insulin. *Int. J. Pharm.* **423**, 195–201 (2012).
11. Fuenzalida, J. P. *et al.* On the role of alginate structure in complexing with lysozyme and application for enzyme delivery. *Food Hydrocoll.* **53**, 239–248 (2016).
12. Fuenzalida, J. & Goycoolea, F. Polysaccharide-Protein Nanoassemblies: Novel Soft Materials for Biomedical and Biotechnological Applications. *Curr. Protein Pept. Sci.* **16**, 89–99 (2015).
13. Mizrahy, S. & Peer, D. Polysaccharides as building blocks for nanotherapeutics. *Chem. Soc. Rev.* **41**, 2623–2640 (2012).
14. Lee, K. Y. & Mooney, D. J. Alginate: Properties and biomedical applications. *Prog. Polym. Sci.* **37**, 106–126 (2012).
15. Harnsilawat, T., Pongsawatmanit, R. & McClements, D. J. Characterization of β -lactoglobulin–sodium alginate interactions in aqueous solutions: A calorimetry, light scattering, electrophoretic mobility and solubility study. *Food Hydrocoll.* **20**,

577–585 (2006).

16. Shilpa, A., Agrawal, S. S. & Ray, A. R. Controlled Delivery of Drugs from Alginate Matrix. *J. Macromol. Sci. Part C Polym. Rev.* **43**, 187–221 (2003).
17. Joshi, A., Keerthiprasad, R., Jayant, R. D. & Srivastava, R. Nano-in-micro alginate based hybrid particles. *Carbohydr. Polym.* **81**, 790–798 (2010).
18. Benichou, A., Aserin, A. & Garti, N. Double emulsions stabilized with hybrids of natural polymers for entrapment and slow release of active matters. *Adv. Colloid Interface Sci.* **108–109**, 29–41 (2004).
19. Pippa, N., Karayianni, M., Pispas, S. & Demetzos, C. Complexation of cationic-neutral block polyelectrolyte with insulin and in vitro release studies. *Int. J. Pharm.* **491**, 136–143 (2015).
20. Bueno, P. V. A. *et al.* N,N-Dimethyl chitosan/heparin polyelectrolyte complex vehicle for efficient heparin delivery. *Int. J. Biol. Macromol.* **75**, 186–191 (2015).
21. Klemmer, K. J., Waldner, L., Stone, A., Low, N. H. & Nickerson, M. T. Complex coacervation of pea protein isolate and alginate polysaccharides. *Food Chem.* **130**, 710–715 (2012).
22. Chen, L. & Subirade, M. Alginate-whey protein granular microspheres as oral delivery vehicles for bioactive compounds. *Biomaterials* **27**, 4646–4654 (2006).
23. MacGregor, J. F., Bruwer, M. J., Miletic, I., Cardin, M. & Liu, Z. Latent Variable Models and Big Data in the Process Industries. *IFAC-PapersOnLine* **48**, 520–524 (2015).
24. Wells, L. A. & Sheardown, H. Extended release of high pI proteins from alginate microspheres via a novel encapsulation technique. *Eur. J. Pharm. Biopharm.* **65**, 329–335 (2007).
25. Shi, Q., Zhou, Y. & Sun, Y. Influence of pH and Ionic Strength on the Steric Mass-Action Model Parameters around the Isoelectric Point of Protein. *Biotechnol. Prog.* **21**, 516–523 (2005).
26. Jin, L., Yu, Y.-X. & Gao, G.-H. A molecular-thermodynamic model for the interactions between globular proteins in aqueous solutions: Applications to bovine serum albumin (BSA), lysozyme, α -chymotrypsin, and immuno-gamma-globulins (IgG) solutions. *J. Colloid Interface Sci.* **304**, 77–83 (2006).
27. Tanford, C., Buzzell, J. G., Rands, D. G. & Swanson, S. A. The Reversible Expansion of Bovine Serum Albumin in Acid Solutions. *J. Am. Chem. Soc.* **77**, 6421–6428 (1955).

28. Gu, F., Amsden, B. & Neufeld, R. Sustained delivery of vascular endothelial growth factor with alginate beads. *J. Control. Release* **96**, 463–472 (2004).
29. Simonoska Crcarevska, M., Glavas Dodov, M. & Goracinova, K. Chitosan coated Ca–alginate microparticles loaded with budesonide for delivery to the inflamed colonic mucosa. *Eur. J. Pharm. Biopharm.* **68**, 565–578 (2008).
30. Costa, P. & Sousa Lobo, J. M. Modeling and comparison of dissolution profiles. *Eur. J. Pharm. Sci.* **13**, 123–133 (2001).
31. Postnikova, G. B. & Shekhovtsova, E. A. The effect of mitochondrial and artificial bilayer phospholipid membranes on conformation of myoglobin and its affinity for oxygen. *Am. J. Biol. Chem.* **3**, 16–32 (2015).
32. Hildebrand, N. *et al.* Adsorption Orientation and Binding Motifs of Lysozyme and Chymotrypsin on Amorphous Silica. *J. Phys. Chem. C* **119**, 7295–7307 (2015).
33. Baler, K. *et al.* Electrostatic Unfolding and Interactions of Albumin Driven by pH Changes: A Molecular Dynamics Study. *J. Phys. Chem. B* **118**, 921–930 (2014).
34. Hosseini, S. M. H. *et al.* β -Lactoglobulin–sodium alginate interaction as affected by polysaccharide depolymerization using high intensity ultrasound. *Food Hydrocoll.* **32**, 235–244 (2013).
35. Tzoc Torres, J. M. G., Nichols, E., MacGregor, J. F. & Hoare, T. Designing multi-responsive polymers using latent variable methods. *Polymer (Guildf)*. **55**, 505–516 (2014).

Supplementary Material for Chapter 3**Supplementary Material 3.1: Release Kinetics, Regression Fits, and Model****Predictions****SI Table 3.1. Values of parameters obtained from fit into the Korsmeyer-Peppas model and the PLS model-predicted values.**

Protein	Mixing Ratio	pH	Buffer Ionic Strength (mM)	Korsmeyer-Peppas			Multivariate Statistical Analysis	
				ln(k)	n	R ²	ln(k)	n
Lysozyme	0.5:1	4.5	10	-3.819	0.379	0.968	-3.814	0.354
Lysozyme	0.5:1	4.5	150	-1.792	0.917	0.999	-2.221	0.821
Lysozyme	0.5:1	7.4	10	-3.600	0.481	0.996	-3.729	0.375
Lysozyme	0.5:1	7.4	150	-1.618	0.826	0.998	-2.137	0.843
Lysozyme	1:1	4.5	10	-3.308	0.424	0.998	-3.700	0.358
Lysozyme	1:1	4.5	150	-1.893	0.833	0.995	-2.108	0.825
Lysozyme	1:1	7.4	10	-3.114	0.475	0.996	-3.616	0.379
Lysozyme	1:1	7.4	150	-1.723	0.859	0.998	-2.023	0.846
Chymotrypsin	0.5:1	4.5	10	-3.592	0.347	0.995	-3.580	0.396
Chymotrypsin	0.5:1	4.5	150	-1.964	0.834	0.998	-1.987	0.864
Chymotrypsin	0.5:1	7.4	10	-3.412	0.450	0.997	-3.382	0.446
Chymotrypsin	0.5:1	7.4	150	-1.873	0.845	0.999	-1.790	0.914
Chymotrypsin	1:1	4.5	10	-3.615	0.381	0.995	-3.467	0.400
Chymotrypsin	1:1	4.5	150	-2.135	0.865	0.999	-1.874	0.868
Chymotrypsin	1:1	7.4	10	-3.379	0.429	0.998	-3.269	0.450
Chymotrypsin	1:1	7.4	150	-2.031	0.857	0.998	-1.676	0.918
BSA	0.5:1	4.5	10	-3.986	0.347	0.986	-3.036	0.474
BSA	0.5:1	4.5	150	-2.355	0.830	0.972	-1.443	0.942
BSA	0.5:1	7.4	10	-0.738	0.709	0.983	-2.236	0.675
BSA	0.5:1	7.4	150	-0.924	1.350	1.000	-0.643	1.142
BSA	1:1	4.5	10	-3.740	0.370	0.996	-2.922	0.478
BSA	1:1	4.5	150	-2.247	0.888	0.996	-1.330	0.946
BSA	1:1	7.4	10	-0.784	0.950	0.997	-2.122	0.679
BSA	1:1	7.4	150	-0.750	0.797	1.000	-0.530	1.146

Chapter 4: Optimizing Electrostatic Interactions for Controlling the Release of Proteins from Anionic and Cationically Modified Alginate

Vida Rahmani¹, Rand Elshereef², Heather Sheardown^{1,3*}

¹ Department of Chemical Engineering, McMaster University, 1280 Main Street West, Hamilton ON L8S 4L7, Canada

² ProSensus Inc., 303-1425 Cormorant Road, Ancaster ON L9G 4V5, Canada

³ School of Biomedical Engineering, McMaster University, 1280 Main Street West, Hamilton ON L8S 4L7, Canada

* Corresponding author: sheadow@mcmaster.ca

Objectives:

Quantifying the factors that affect protein release from charged hydrogels and exploring the potential of manipulating electrostatic interactions for controlling protein release.

Main Scientific Contributions:

- Synthesis and characterization of cationically modified alginate.
- Characterization of microparticles prepared from calcium crosslinking of alginate and modified alginate.
- Model proteins with varying net charges and molecular weights were loaded into and were released from the microparticles.
- Applying multivariate statistical analysis for building a model on the factors affecting protein release.

Publication Information:

European Journal of Pharmaceutics and Biopharmaceutics, 117, 232-243 (2017).

Reprinted with permission from Elsevier.

Author Contribution:

Vida was responsible for the experimental work (synthesis and characterization of the materials, protein loading and release experiments, applying multivariate analysis) and paper write-up.

Dr. Rand Elshereef revised and edited the multivariate statistical sections.

The work was done in consultation with and under the supervision of Dr. Heather Sheardown. Dr. Heather Sheardown revised the draft to the final version.

Abstract

Alginate and cationically modified alginate microparticles were prepared with the goal of developing hydrogel microparticles that offer controlled release of protein drugs mainly by modification of the absolute charge of the hydrogel network. Protein loading and release studies were carried out using model proteins with different net charges (i.e. low, high, and neutral isoelectric points) covering a broad range of molecular weights. The Projection to Latent Structures (PLS) method was used for qualitatively and quantitatively describing the relationships between the properties of proteins such as net charge and molecular weight, polymer properties including degree of substitution and microparticle size, and the release kinetics (kt^n). It was found that electrostatic interactions and protein molecular weight had the greatest impact on parameter k while parameter n was mostly affected by polymer and buffer properties. In addition to understanding the current trends, the multivariate statistical method also provided an effective and reliable model as a beneficial tool for predicting and optimizing protein delivery systems.

Keywords: Controlled release; Protein delivery; Alginate; Hydrogel microparticles; Electrostatic interactions; Multivariate statistical analysis

4.1. Introduction

Delivery of proteins remains a significant challenge in the field of drug delivery. One promising method for optimizing and controlling protein release from hydrogels

involves taking advantage of the electrostatic interactions between the protein and hydrogel^{1,2}. The distinct surface composition of proteins imparts a charge and depending on the pH of the solution and the isoelectric point (pI) of the protein, a different net charge may be displayed at its surface³. At pH values below the isoelectric point, proteins carry a net positive charge, due to a high degree of protonation of the amine groups and a low degree of dissociation of the carboxyl groups. At pH values higher than the isoelectric point, proteins carry a net negative charge, as a result of the high degree of dissociation of the carboxyl groups and the low degree of protonation of the amine groups⁴. However, it should be noted that the surface charge may be very different than the net overall charge⁵.

Electrostatic interactions between hydrogels and proteins must however be optimized in order to control the protein release. Attractive interactions hinder protein release whereas repulsive interactions can increase the rate of release³. Charged hydrogels including ionic polymers such as agarose⁶, gelatin^{7,8}, carrageenan^{1,9} and alginate^{10,11} or hydrogels modified with amino¹², sulfonyl¹³ or phosphate¹⁴ functional groups have been used for drug and protein delivery³ although there are limited studies on the effect of electrostatic interactions between the charged hydrogel networks and proteins on the protein release.

Alginate is an anionic polysaccharide¹⁵ composed of mannuronic (M) and guluronic (G) acid residues¹⁶. Alginate is a non-toxic and degradable polymer¹⁵ and has been broadly studied for microsphere preparation¹⁷. Furthermore, in the presence of multivalent cations, alginate ionically crosslinks to form a gel at room temperature and

under mild conditions, a process free from the use of organic and toxic solvents^{15,17}.

Among the different cation-alginate gels, calcium-alginate hydrogels are the most widely used carriers in enzyme, protein and drug delivery applications and are considered to be clinically safe^{15,18}.

Chemical modifications of alginate have been extensively studied for various applications. For example, sulfated alginate shows great blood compatibility due to its structural similarity to heparin, which is known as an anticoagulant agent¹⁹. Oxidization of alginate is known to offer control over its *in vivo* degradability²⁰, an important aspect in controlled drug delivery applications. Amidation of alginate has been carried out for introducing amphiphilic properties to the polymer network²¹. Through amide bond linkages, Tan *et al.*²² synthesized aminated alginate grafted with thermo-sensitive polymer for assessing its potential in tissue engineering applications. Li *et al.*²³ have also reported on synthesis of aminated alginate using aqueous carbodiimide chemistry for enzyme immobilization.

While alginate is an anionic polymer, grafting amine groups on its backbone leads to synthesis of positively modified alginate. To the best of our knowledge, the possibility to control the release rate of proteins by modification of the absolute charge and the charge density of the hydrogel network has not been studied thoroughly to date.

Understanding the mechanisms and extent of effects involved in drug release is fundamental for design of drug delivery carriers which can fulfill the therapeutic needs. In this work, the Projection to Latent Structures (PLS) method is used as a multivariate statistical analysis method to provide insight into relationships and correlations between

the protein and polymer properties and the release kinetics. The reduced dimensional space (the latent variable space)²⁴ provides a beneficial tool for understanding the trends, predicting future kinetics, and optimizing the delivery carriers for efficient protein deliveries.

In this study the relationship between protein release kinetics from anionic and cationically modified alginate microparticles was studied considering factors such as net charge and molecular weight of the investigated proteins. Using multivariate statistical methods, the work is extended by predicting the release profiles of other proteins. It is hypothesized that an appropriate protein delivery vehicle can be developed by understanding and developing relationships between the release profiles of the studied proteins and their net charge and molecular weight and adapting the vehicle accordingly.

4.2. Materials and Methods

4.2.1. Materials

Sodium alginate from brown algae was purchased from Sigma-Aldrich (Oakville, ON). The molecular weight of this alginate is in the range of 100,000-200,000 g/mol. This alginate consisted of 65% guluronic acid 35% mannuronic acid residues. 1-(3-Dimethylaminopropyl)-3-ethylcarbodiimide (EDC) was purchased from Carbosynth Limited (Berkshire, UK). 1-hydroxybenzotriazole (HOBt) was obtained from Toronto Research Chemicals (Toronto, ON). N,N-Dimethylethylenediamine (DMEN) was purchased from Sigma-Aldrich (Oakville, ON). All other reagents and proteins (insulin,

bovine serum albumin, lysozyme, chymotrypsin, myoglobin, horseradish peroxidase) were also obtained from Sigma-Aldrich (Oakville, ON).

The phosphate buffered saline 1X was composed of NaCl (138 mM), KCl (2.7 mM), NaH₂PO₄ (1.9 mM), and Na₂HPO₄ (8.1 mM). This buffer is also referred to as PBS 10 mM in literature, which is the concentration of the phosphate ions. In this study, the 10-times dilution of the PBS 1X is denoted as PBS 0.1X (or PBS 1 mM).

4.2.2. Alginate Modification

Cationically modified alginate were prepared by grafting amine groups onto the alginate backbone using aqueous carbodiimide chemistry. Alginate was dissolved in deionized water to obtain a 1.5% (w/v) alginate solution. Prescribed amounts of EDC (5 molar excess relative to carboxyl groups) and HOBt (1:1 mole:mole EDC) were added to the alginate solution and the pH of the solution was adjusted to 5 using 1 M HCl. The mixture was stirred (500 rpm) at room temperature for 30 minutes for full activation of the carboxyl groups on the alginate. During the reaction, the pH of the solution was monitored and if necessary, adjusted to 5 using 1 M HCl. Then, various amounts of DMEN (for achieving 20, 40, 60, 80 and 100% theoretical degree of substitution of carboxyl groups) were added to the mixture and the reaction was left to proceed for 12 hrs under constant stirring (500 rpm) at room temperature. The resulting product was dialyzed against a 1 M NaCl solution in deionized water using a 12,000-14,000 MWCO dialysis tube. The synthesized amine modified alginate was then lyophilized followed by

storage in sealed containers at room temperature. Figure 4.1 illustrates the mechanism of the reaction.

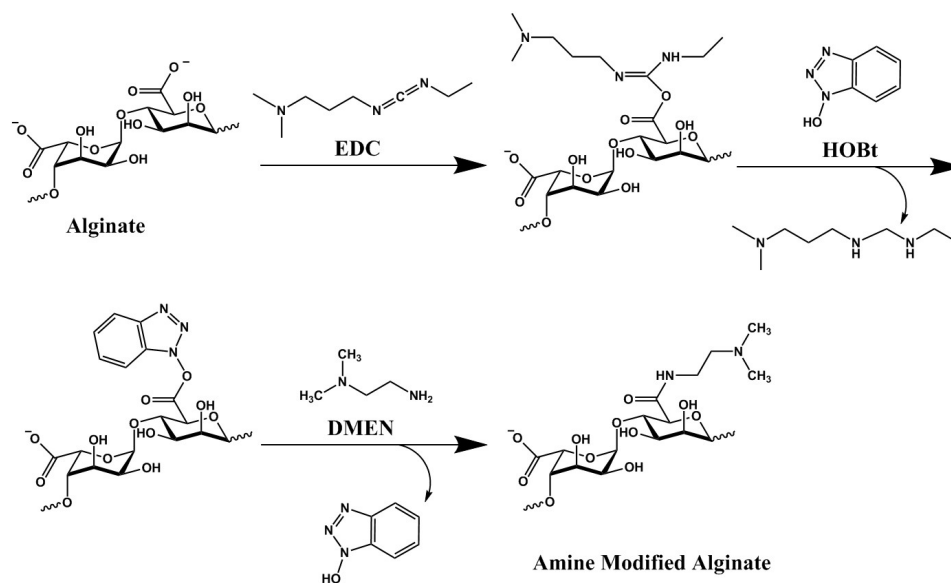


Figure 4.1. Synthesis of amine modified alginate.

4.2.3. Characterization of the Modified Alginates

The synthesized amine modified alginate polymers (Am-Alg) were characterized by FT-IR and ^1H NMR for determination of amine conjugation.

FTIR spectra were collected by applying 64 scans with a resolution of 4 cm^{-1} to lyophilized polymers and data between 370 and 5000 cm^{-1} were recorded (Hyperion 3000 FT-IR Microscope, Bruker Corporation, MA, USA).

For ^1H NMR spectroscopy, polymer solutions (10 mg/mL) were prepared in D_2O and their ^1H NMR spectra were recorded on the 600 MHz spectrometer (Bruker 600 MHz spectrometer, Bruker Corporation, MA, USA). The degree of substitution (DS) was

determined from the areas (I_{CH_3}) of the signal at δ 2.96 ppm due to the resonance of the methyl group and of the signals attributed to the proton on carbon-1 of guluronic acid, H_1 , (signal at 5.10 ppm)^{25,26}, based on Equation 4.1.

$$\text{DS} = \frac{I_{\text{CH}_3}/6}{I_{H_1}/0.65} \quad \text{Equation 4.1}$$

In Equation 4.1, division by 0.65 is done to account for all monomeric units; since the signal at δ 5.10 ppm corresponds to H_1 of only G blocks, which according to supplier (Sigma-Aldrich) make up for ~65% of the alginate molecule.

4.2.4. Synthesis of Microparticles

Alginate microparticles were prepared by the modified emulsification and external gelation methods²⁷. A 1.5% or 3% (w/v) solution of alginate in deionized water was prepared and dispersed into paraffin oil containing 5% Span 80 with a ratio of 1:4. After stirring at 1000 rpm for 30 minutes, a solution of calcium chloride (CaCl_2) (0.1 M or 1 M) was added dropwise to the emulsion mixture. The mixture was continuously stirred for 2 hours, followed by the addition of isopropyl alcohol for hardening the formed microparticles. Microparticles were collected by centrifugation, washed with isopropyl alcohol and water, and dried at 37°C.

Microparticles from amine modified alginate polymers were prepared by a similar emulsification and external gelation method. The amine modified alginate and the CaCl_2

solutions used in preparation of the particles had concentrations of 1.5% (w/v) and 1 M, respectively.

4.2.5. Particle Characterization

Physical characterization of resulting particles was carried out by measuring particle size distributions (Mastersizer 2000 equipped with Hydro 2000S, Malvern Instruments Ltd., UK) and investigating the zeta potential of the microparticles (Zeta PALS, Brookhaven Instruments Corp., NY, USA).

The morphological structure of the particles was examined using scanning electron microscopy (SEM, Vega II LSU, TESCAN, Czech) on gold sputtered samples.

4.2.6. Protein Quantification

Protein amounts were quantified using Bradford assay. Bradford Reagent was added to the protein samples and the absorbance was read at 595 nm (SpectraMax Plus 384 Microplate Reader, Molecular Devices LLC, CA, USA). Protein concentration was determined from comparison with known standards.

4.2.7. Protein Loading

Protein loading and release studies were carried out using the model proteins listed in Table 4.1. The selection of the model proteins was done based on the attempt to cover a broad range of protein molecular weights as well as different net charges (low, high, and neutral isoelectric points).

Table 4.1. Isoelectric point (pI), net charge at physiological pH, and molecular weight of the model proteins.

Protein	pI / Net Charge	Molecular Weight (Da)
Insulin	5.3 / Negative	6,000
Bovine Serum Albumin (BSA)	5.4 / Negative	65,000
Lysozyme	11.0 / Positive	14,000
Chymotrypsin	9.1 / Positive	25,000
Myoglobin	7.2 / Neutral	17,000
Horseradish Peroxidase (HRP)	7.2 / Neutral	44,000

Proteins were loaded into the particles by soaking blank particles in 5 mg/mL protein solutions in phosphate buffered saline (PBS 2 mM, pH=7.4). This method allows for uptake of protein by partially degrading the alginate particles and is followed by immersion in a 1 M CaCl₂ solution to ensure complete re-crosslinking of particles²⁸. After various periods of time, loaded microparticles were dissolved in 5% sodium citrate and the solution was analyzed for protein content.

4.2.8. Protein Release

Phosphate buffered saline (PBS), 7 ml, was added to a batch containing approximately 30 mg of particles. The release study was carried out in 15 mL tubes, placed in a 37°C and 100 rpm incubator. Samples (1 mL) were taken at regular intervals and replaced with 1 mL of fresh release medium. Prior to sampling, tubes were centrifuged at 100×g for 90 seconds. Samples were initially taken at 30 min intervals and the sampling intervals were gradually increased. Release was carried out until no more drug release was detected and/or the microparticles were totally degraded. Protein release

studies were carried out in PBS 1X (pH=7.4) and PBS 0.1X (pH=7.4) in order to understand the effect of salt concentration in the medium on the release kinetics.

4.2.9. Protein Release Kinetics

The Korsmeyer-Peppas kinetic model²⁹ (Equation 4.2) was used for modeling the release kinetics and the data obtained from the protein release studies were fitted to the logarithmic form of the Korsmeyer-Peppas kinetic model (Equation 4.3).

$$\frac{M_t}{M_\infty} = kt^n \quad \text{Equation 4.2}$$

$$\ln\left(\frac{M_t}{M_\infty}\right) = \ln k + n \ln t \quad \text{Equation 4.3}$$

In Equation 4.2 and Equation 4.3, M_t/M_∞ is the fraction of drug released at time t , k is the release rate constant and n is the release exponent. The first 60% of drug release data are used for the fit.

4.2.10. Statistical Analysis

All experiments were performed in triplicate and error bars on graphs represent standard deviations. Statistical comparisons for the protein release data were made using two-way repeated-measures analysis of variance (ANOVA) with $p < 0.05$ used as the level of significance. Statistical significance for protein loading was determined using a two-way ANOVA test ($p < 0.05$ used as the level of significance).

4.2.11. Multivariate Statistical Analysis

Multivariate analysis, also known as latent variable modeling, is a statistical data modeling approach that provides unique advantages over traditional empirical modeling methods such as multiple linear regression and neural networks. Multivariate analysis models find the hidden (or latent) independent factors that summarize all of the factors affecting the process. These are described mathematically as linear combinations of the original variables. Typically the number of such significant latent variables that are truly driving the observed process behavior is small compared to the number of the process variables measured during the experiment²⁴.

ProSensus' latent variable modeling software (ProMV) was used to extract these latent variables from the data for further understanding the interactions between the net charges of the proteins and polymers, and the molecular weights of proteins and their effect on the release kinetics. The data set consists of 48 experimental runs arising from a series of release experiments which were imported into the software for analysis and model development. Electrostatic attractions between the proteins and polymers, protein molecular weight, polymer degree of substitution, average size of microparticles, and buffer concentration were inputted into ProMV as the X matrix. The release constants obtained from the logarithmic Korsmeyer-Peppas ($\ln(k)$ and n) were inputted as the Y matrix.

The partial least squares (PLS) method was used for interpretation of the hidden relationships among X and Y variables as well as the relationship between the X and Y. PLS is performed by projecting and distilling data into low dimensional latent variable

space and is represented by only a few statistically significant latent variables that summarize all of the factors affecting the process²⁴. The PLS model was used for assessing the relative importance and quantifying the impact of the X variables on the protein release constants.

In building the model, the following assumptions were made:

- The net charge of the unmodified alginate was assigned with a value of -1, and the net charges of the cationically modified alginates were calculated relatively. For example, Am-Alg 40 (40% positively charged amine groups and 60% negatively charged carboxyl groups) would have a net charge equal to -0.2, as calculated in Equation 4.4.

$$\text{Net Charge of Am-Alg 40} = +0.4 + (-0.6) = -0.2$$

Equation 4.4

- At pH=7.4, the net charge of the proteins were considered as follows: -3 for insulin³⁰, -16 for BSA³¹, +9 for lysozyme³², +3 for chymotrypsin³³, 0 for myoglobin, 0 for HRP.
- The electrostatic contributions of all the ionized groups of all the amino acids making up a protein and also the distributions of the exposed and the buried charges are complicated to quantify³⁴ and are beyond the scope of this study. In this model, only the net charge was considered in the calculations.
- Based on Coulomb's law, the magnitude of the electrostatic forces between charged objects is directly proportional to the product of their charges³⁵. A positive value is an indication of repulsive interactions (same signed charges) and a negative value suggests presence of attraction forces (oppositely signed charges). In this study, the

electrostatic attraction between the polymer and the protein was defined based on Coulomb's law and as shown in Equation 4.5.

$$\text{Electrostatic Attraction} = - (\text{Polymer Charge}) \times (\text{Protein Charge}) \quad \text{Equation 4.5}$$

4.3. Results and Discussion

4.3.1. Characterization of the Modified Alginates

In the FT-IR spectrum of alginate, shown in Figure 4.2, the broad peak at 3310 cm^{-1} was assigned to the stretching vibrations of O-H and the small peak at 2920 cm^{-1} was a result of the C-H stretching vibrations of methylene groups. The peaks at 1090 cm^{-1} and 1030 cm^{-1} can be related to the C-O-C stretching vibrations. Also, the peaks at 1610 cm^{-1} and 1410 cm^{-1} were attributed to stretching vibrations of carboxyl groups²¹. It can be seen that in amine modified alginates, the carbonyl peaks at 1610 cm^{-1} shift to 1660 cm^{-1} , suggesting the formation of amidic groups^{21,36}. In addition, the peaks at 1530 cm^{-1} are due to the N-H bending vibrations of the amide groups³⁷.

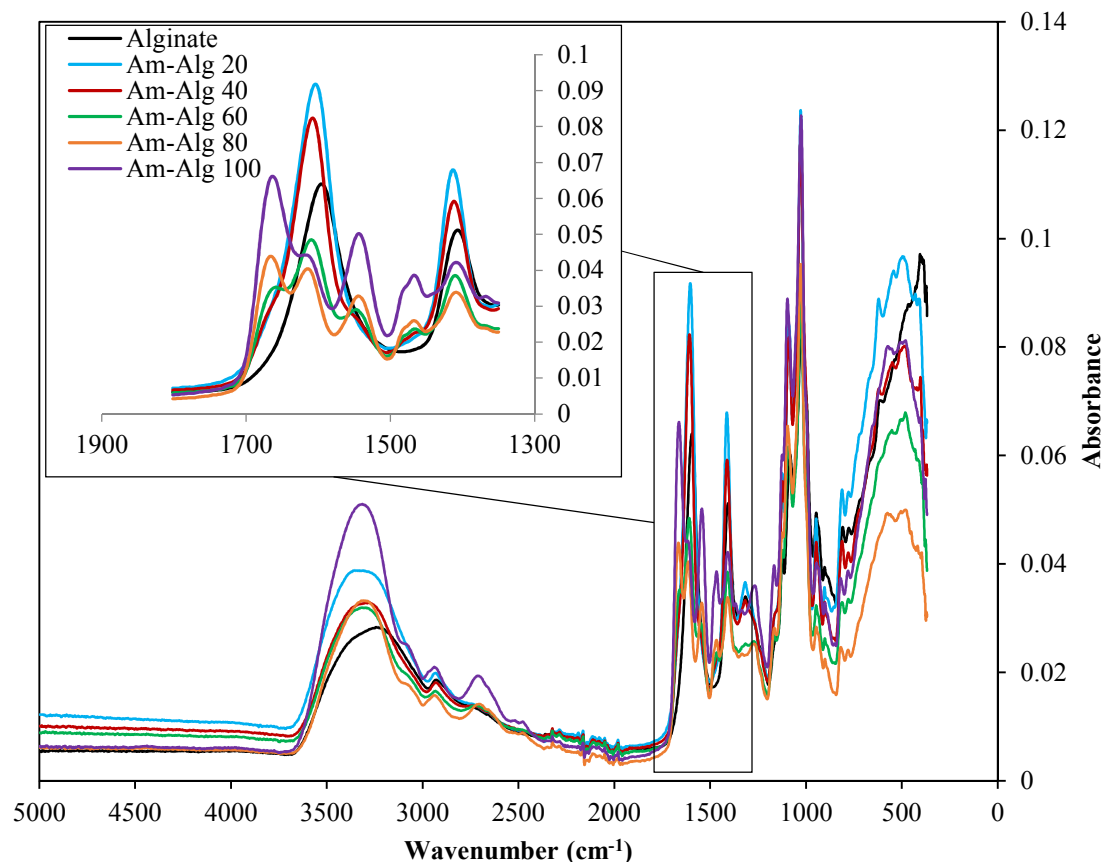


Figure 4.2. FT-IR spectra of the amine modified alginates.

For ^1H NMR spectroscopy, polymers were dissolved in D_2O and their ^1H NMR spectra were recorded (Figure 4.3). In Figure 4.3, proton peaks in the range of 3.8 to 5.1 ppm are assigned to protons present in alginate, as also observed in previously reported ^1H NMR spectra for alginate in the literature^{21,26}. In comparison with the spectrum of alginate, additional peaks were observed in the range of 2.9 to 3.7 ppm, which were attributed to the methyl and methylene protons of the dimethylethylenediamine (DMEN), as designated in Figure 4.3(a).

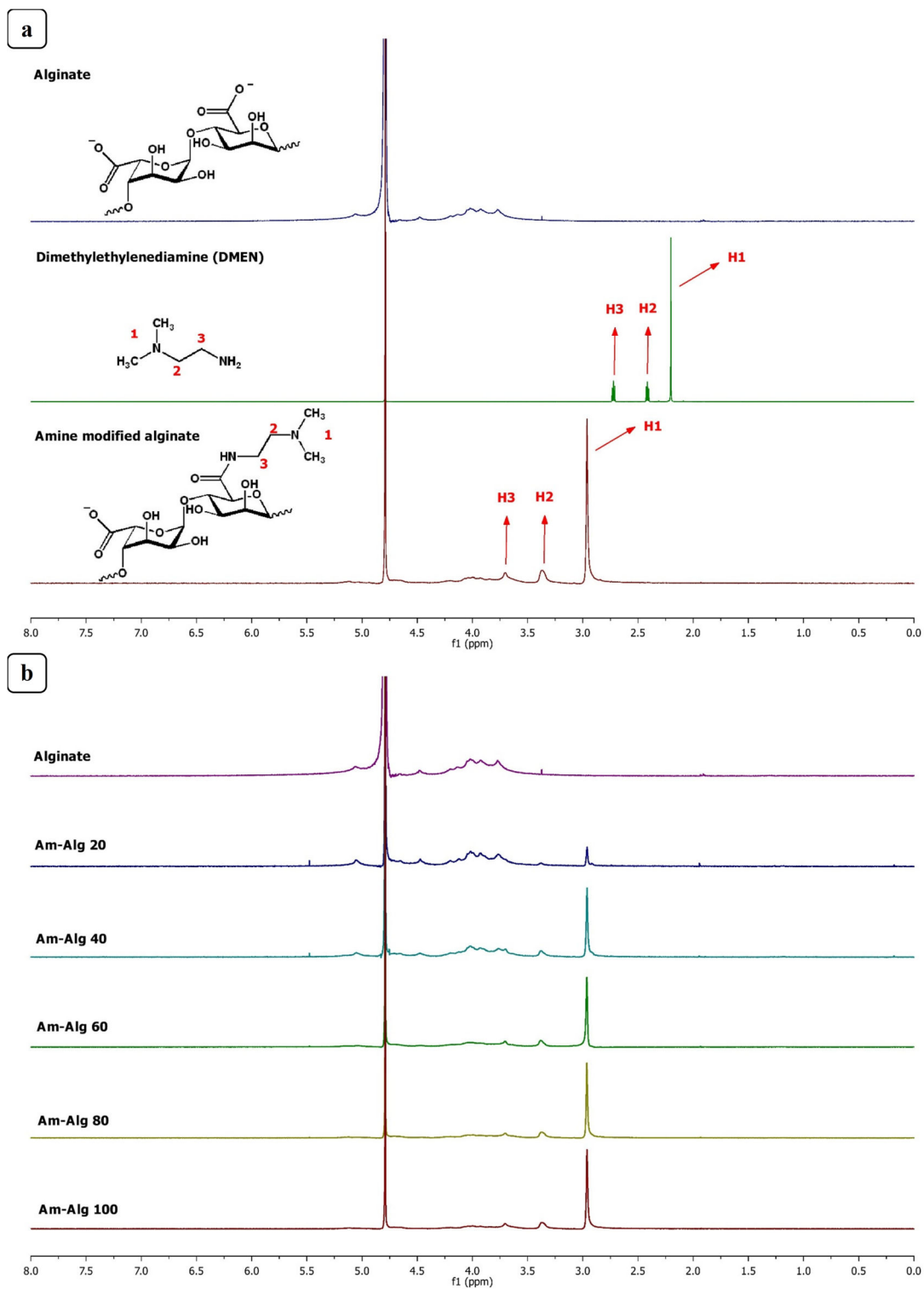


Figure 4.3. ^1H NMR spectra; (a) spectra of alginate, DMEN, and amine modified alginates in D_2O , (b) spectra of alginate and amine modified alginates in D_2O .

Table 4.2 shows the molar amine content of the amine modified polymers calculated based on ^1H NMR.

Table 4.2. Values of amine content of the amide functionalized alginates determined by ^1H NMR.

Sample	Theoretical amine content (%)	Calculated amine content (%)
Am-Alg 20	20	12.4
Am-Alg 40	40	37.5
Am-Alg 60	60	53.5
Am-Alg 80	80	80.5
Am-Alg 100	100	101.4

4.3.2. Particle Characterization

The concentration of the alginate and CaCl_2 solutions affected the shape and size of the microparticles (Supplementary Material). Particle size was increased when the concentration of alginate was increased, and the use of higher concentrations of CaCl_2 resulted in decreased particle diameter. The 1.5% (w/v) alginate and 1 M CaCl_2 solutions were selected as the optimized concentrations and were used for all subsequent experiments.

Microparticles were prepared with amine modified alginate polymers by the emulsification and external gelation method described. The differences in the morphological structure of the particles were examined through SEM (Figure 4.4) and the size distribution of the particles was measured by a laser diffraction particle size analyzer (Figure 4.5). As shown, with an increase in the amine content of the polymer, the prepared formulations lose their structure as particles and tend to develop larger

continuous assemblies. This is presumably due to the presence of fewer available carboxyl groups which are required for crosslinking of the polymer with calcium ions. Am-Alginates 20, 40, and 60 were used for protein loading and release experiments due to their ability to form particle-shaped structures.

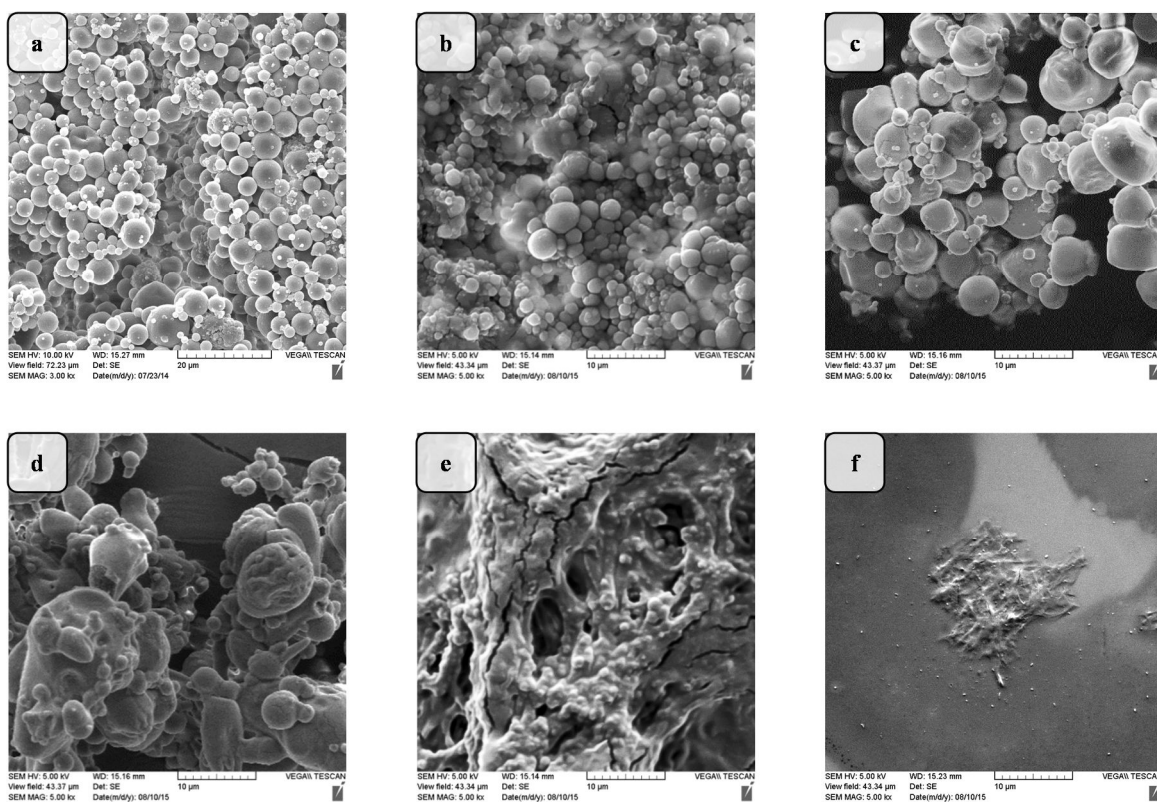


Figure 4.4. SEM images of amine modified alginate assemblies; (a) Alg, (b) Am-Alg 20, (c) Am-Alg 40, (d) Am-Alg 60, (e) Am-Alg 80, (f) Am-Alg 100.

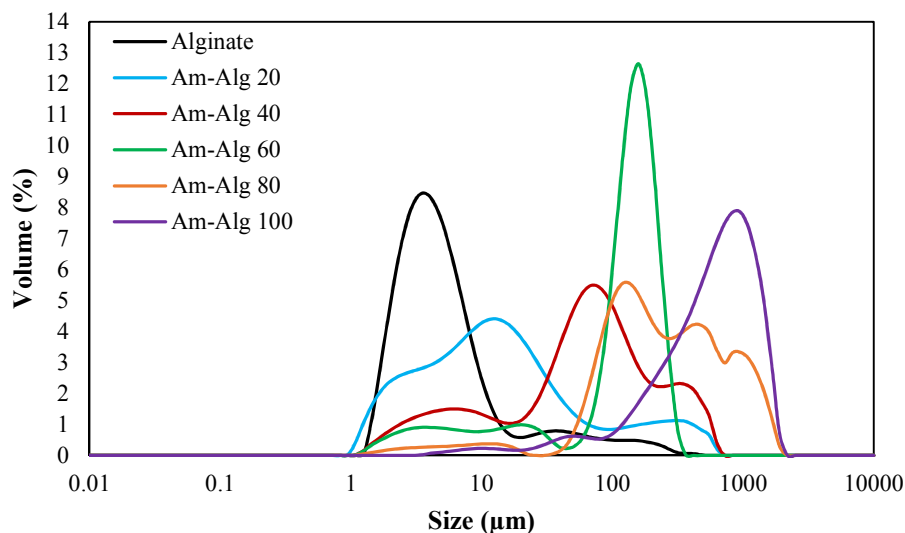


Figure 4.5. Size distributions of alginate and modified alginate microparticles.

The results of the zeta potential measurements of the alginate and modified alginate microparticles are reported in Table 4.3. Increasing the modification degree resulted in higher zeta potential values as expected. However, in the case of Am-Alg 80 and Am-Alg 100, the increasing trend did not seem to continue. While positive zeta potential values were observed for Am-Alg 80 and Am-Alg 100, the relatively small values of zeta potential are thought to be related to the instability and agglomeration of the colloid system³⁸ which is due to the presence of fewer available carboxyl groups for crosslinking and for the formation of stable particles.

Table 4.3. Zeta potential measurements of alginate and modified alginate microparticles.

Microparticle	Electrophoretic Mobility $\times 10^{-8}$ ($\text{m}^2\text{s}^{-1}\text{V}^{-1}$)	Zeta potential (mV)
Alginate	-2.90 ± 0.09	-57.85 ± 1.83
Am-Alg 20	-2.50 ± 0.12	-49.89 ± 2.36
Am-Alg 40	-1.28 ± 0.07	-24.56 ± 1.43
Am-Alg 60	0.84 ± 0.06	16.70 ± 1.16
Am-Alg 80	0.32 ± 0.07	6.33 ± 1.37
Am-Alg 100	0.26 ± 0.14	5.23 ± 2.73

4.3.3. Protein Loading

Figure 4.6 shows the loading amounts of protein into the anionic and cationically modified alginate microparticles. In the case of anionic alginate microparticles, higher protein loading amounts were observed with insulin and lysozyme compared to the other proteins due to the relatively low molecular weight of insulin and the positive nature of lysozyme. The electropositivity of chymotrypsin also resulted in an attractive electrostatic interaction with the anionic alginate, promoting a higher amount of protein loading. In the case of the electronegative BSA, the relatively larger molecular weight of the protein is also a limiting factor inhibiting its diffusion into the alginate particles.

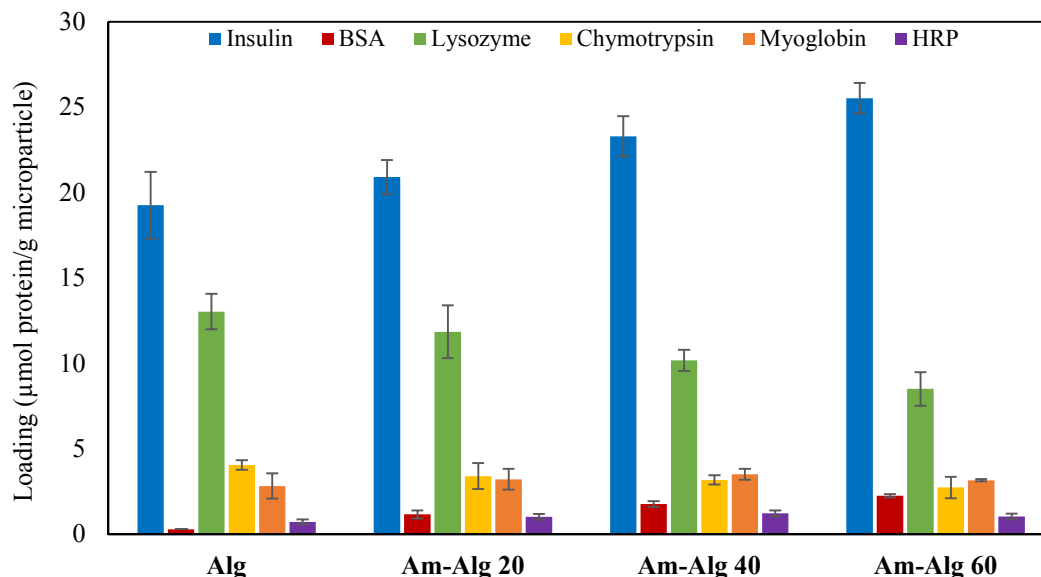


Figure 4.6. Loading of proteins in microparticles of Alg, Am-Alg 20, Am-Alg 40, and Am-Alg 60 after soaking time of 2 hours.

The loading trend observed with the Am-Alg 20 and Am-Alg 40 microparticles is similar to protein loading observed with anionic alginate microparticles. Insulin shows the highest loading, presumably due to its small size. The positive nature of lysozyme and chymotrypsin and their electrostatic attractions with the anionic polymers act as a driving force resulting in higher loading. Although, due to the positive modification of Am-Alg 20 and Am-Alg 40 polymers, loading seemed to be lower compared with that observed in unmodified alginate microparticles. On the contrary, the loading of the negative insulin and BSA was higher than in the control particles as a result of the positive modification.

Electrostatic interactions play an important role in protein diffusion into the particles. Therefore, with the Am-Alg 60 carrying the most positive charge among the modified polymers, the negative insulin and BSA show the highest and the electropositive lysozyme and chymotrypsin show the lowest loading efficiencies compared to their

uptake into the other polymeric microparticles. The relatively high molecular weight of BSA is a limiting factor controlling its diffusion into the particles of all materials.

The loading amounts of the neutral myoglobin and horseradish peroxidase is consistent between the different polymeric microparticles, suggesting their molecular weight is the major factor controlling protein uptake into these particles.

It is evident from these results that protein net charge and molecular weight have a significant effect on protein loading efficiency. On the other hand, soaking time did not greatly affect the loading of the proteins into the particles (Supplementary Material). For all the materials, equilibrium seemed to have been reached after 60 minutes and longer soaking times did not significantly impact protein uptake. For microparticles prepared for release studies, soaking times of 2 hours were used to ensure complete loading of protein to equilibration.

4.3.4. Protein Release

Release of proteins from the alginate and modified alginate microparticles in low and high buffer concentrations is shown in Figure 4.7. In general, a higher concentration of buffer resulted in faster release of proteins due to ion exchange and faster matrix degradation³⁸. However, trends in protein release from each type of polymeric particles were conserved regardless of the buffer concentrations.

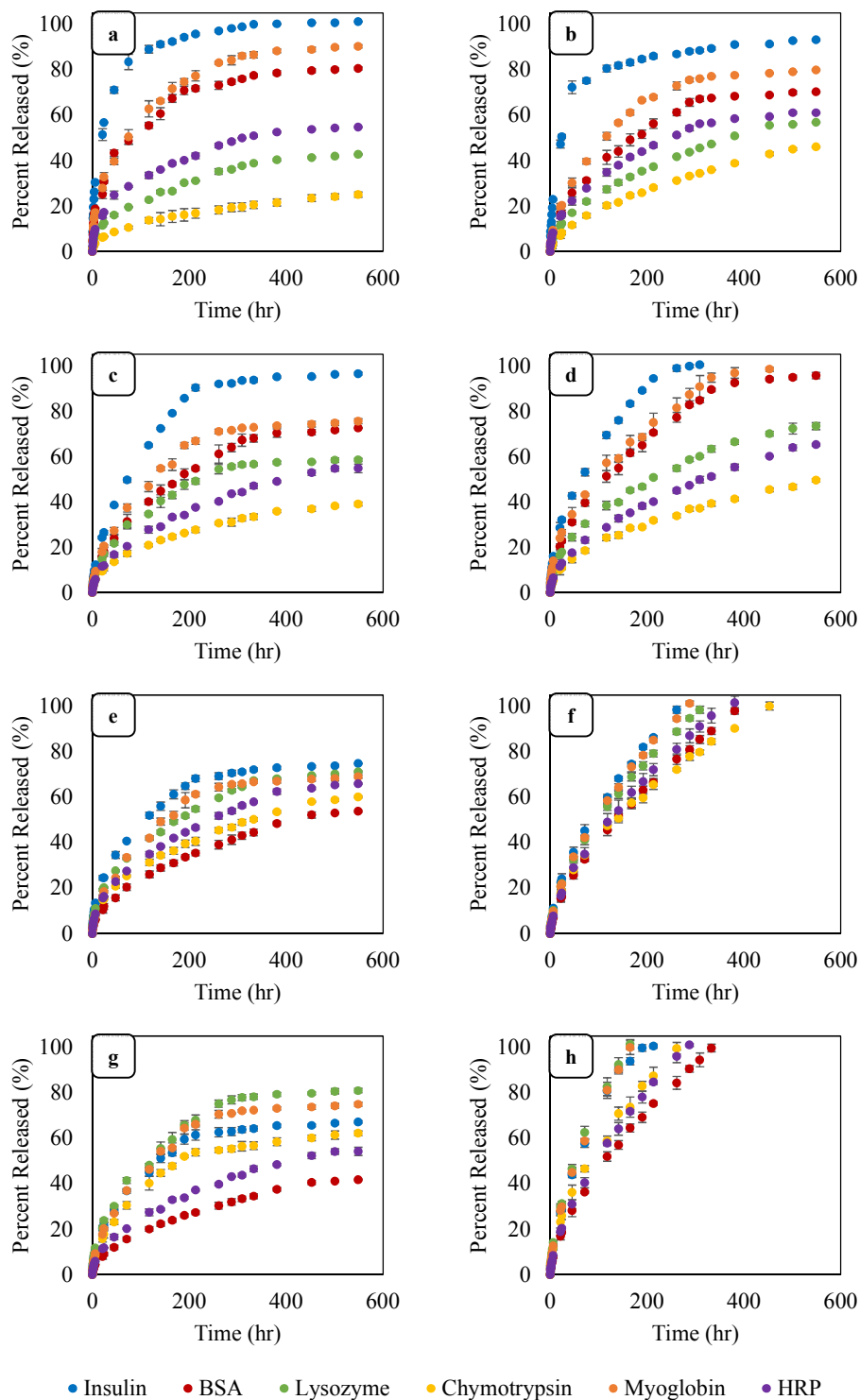


Figure 4.7. Release of proteins from microparticles; (a) Alg, PBS 0.1X, (b) Alg, PBS 1X, (c) Am-Alg 20, PBS 0.1X, (d) Am-Alg 20, PBS 1X, (e) Am-Alg 40, PBS 0.1X, (f) Am-Alg 40, PBS 1X, (g) Am-Alg 60, PBS 0.1X, (h) Am-Alg 60, PBS 1X.

In release from the alginate microparticles (Alg) in both concentrations of buffer, the highest burst release was observed with insulin, due to both its negative charge, which results in repulsion forces with the anionic alginate, and its smaller size. A more sustained release was observed with lysozyme and chymotrypsin compared to the other proteins as expected due to their positive nature and the presence of attractive forces with the alginate matrix. It seems that positive proteins have the potential to act as physical crosslinks for the alginate network leading to slower diffusion rates within the network for positive proteins compared to proteins with negative charge.

With an increase in the degree of substitution and the number of electropositive amine groups on the polymer, release rates of the electronegative insulin and BSA show a decreasing trend due to attractive electrostatic interactions with the positively modified alginate polymers. The reverse pattern was observed with the positive proteins lysozyme and chymotrypsin which would have greater repulsion forces as the cationic modification of the alginate is increased.

Slower diffusion of proteins with higher molecular weights compared to lower molecular weight proteins of similar net charge was also observed. The results suggest that, as hypothesized, the net charge and molecular weight of proteins have significant effect on protein release kinetics from a polymer matrix. However, understanding the detailed relationships between the parameters needs to be presented in a way that is easily interpreted. Multivariate statistical analysis methods provide a great tool for understanding the contribution of each of the factors and their extent of effect on the release kinetics.

4.3.5. Multivariate Statistical Analysis

The data obtained from the protein release studies were fitted into the logarithmic form of the Korsmeyer-Peppas kinetic model and the R-squared values of the fits were in the range of 0.957-0.999 (Supplementary Material), indicating excellent fits. The PLS model built using ProMV software (ProSensus Inc.) contains 3 latent variables with overall R^2Y (measure of model fit capability) and Q^2Y (representative of model predictive capability) values of 0.566 and 0.442, respectively (Figure 4.8(a)). PLS also builds a model on X space and the R^2X (indication of how well the model fits the X data) was calculated to be 0.710 (Figure 4.8(a)). The R^2 and Q^2 values for each of the Y variables is shown in Figure 4.8(b). These R^2 and Q^2 values demonstrate that the overall model has relatively good fit and reliable predictive performance.

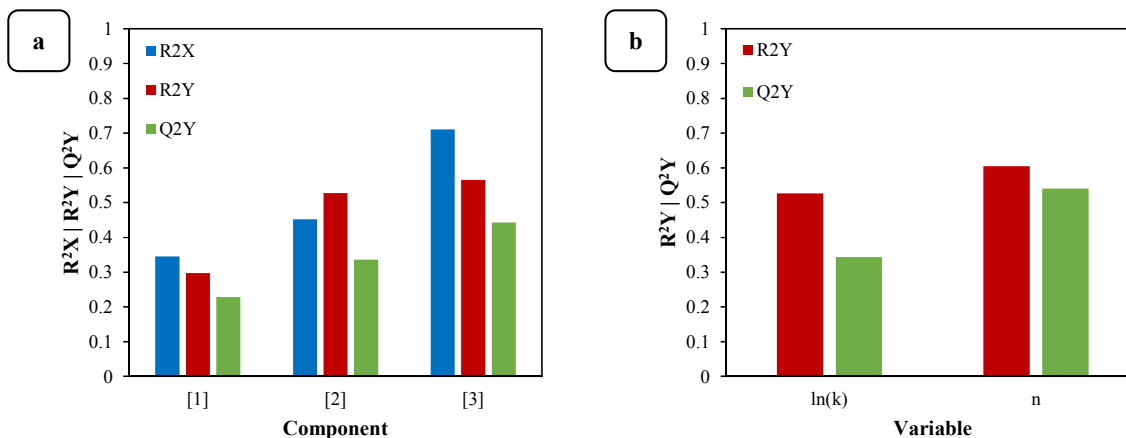


Figure 4.8. (a) Cumulative R^2X , R^2Y , and Q^2Y for each of the latent variable components of the PLS model; (b) R^2 and Q^2 for each of the Y variables.

In a PLS model, the first latent component explains the greatest covariance between X and Y spaces, and each following latent variable captures less information³⁹

(Figure 4.8(a)). Therefore, in this model, a correlation-loading plot of only the first two variables (Figure 4.9) describes the most significant relationships between the X variables (electrostatic attraction, protein molecular weight, polymer degree of substitution, particle size, buffer concentration) and the Y matrix (release characteristics: $\ln(k)$ and n). The location of each of the variables relative to each other explains the relationships between the parameters. Variables that cluster together are positively correlated, while the parameters that are located on opposite quadrants relative to each other have a negative correlation³⁹.

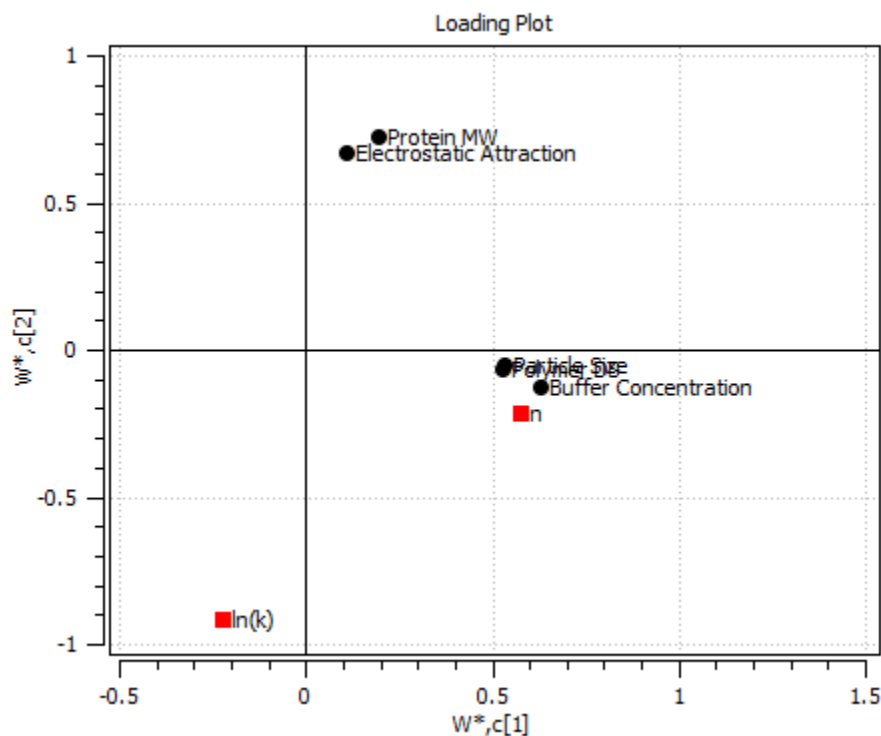


Figure 4.9. Correlation-loading plot for contributors to protein release.

It can be observed that while n has a strong positive correlation with the polymer and buffer properties (cluster and group formation), $\ln(k)$ is negatively correlated to electrostatic attractions and protein molecular weight (located on opposite quadrants). These interpretations are in agreement with the release trends observed in Figure 4.7. Proteins with higher molecular weights and electrostatic attraction will diffuse more slowly through the network (lower k values), while with the increase in the polymer degree of substitution and buffer concentration, the release exponent was increased (higher n values). Also, it is observed that n is mostly described by the first latent variable while $\ln(k)$ dominates the second latent component. In other words, n and $\ln(k)$ seem to be clearly independent from each other and accordingly, X variables that affect n have little or weak correlation to the X variables affecting $\ln(k)$.

Figure 4.10 represents the size and direction of the influences of each of the X variables on the release characteristics $\ln(k)$ and n . While k is mostly affected by protein properties and has very low dependency on polymer characteristics and release media, parameter n is greatly and positively influenced by polymer properties such as size of the microparticles and in general by the polymer degree of substitution. Buffer concentration also significantly impacts the n parameter and higher buffer concentrations result in larger n values.

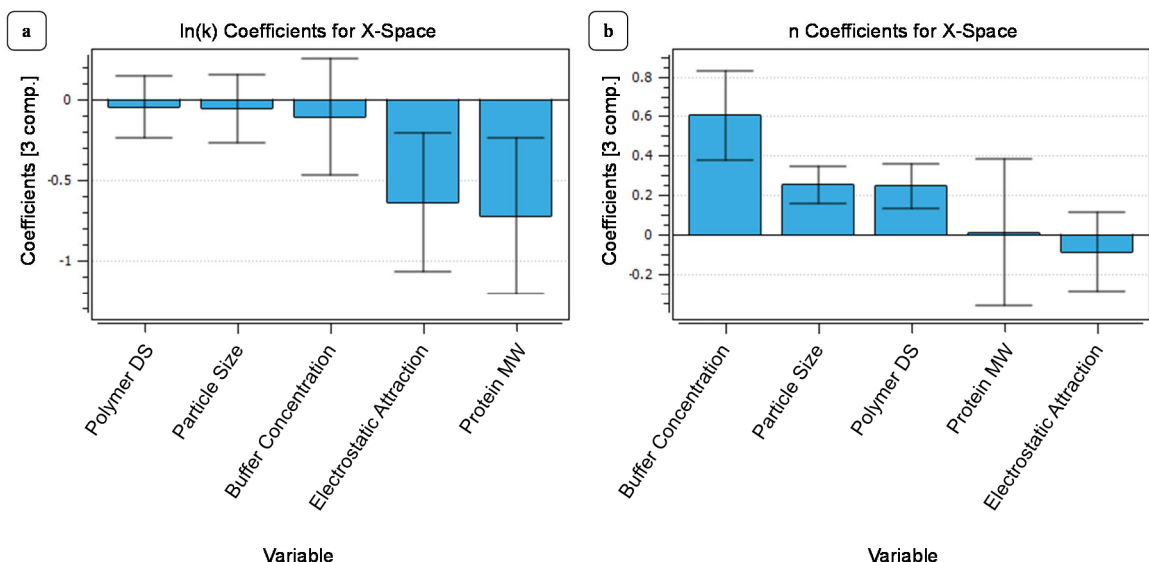


Figure 4.10. Coefficients plot showing the effect of each X variable on release kinetic parameters; (a) $\ln(k)$, (b) n .

The k parameter in the Korsmeyer-Peppas model is a constant which incorporates the structural and geometric characteristics of the drug dosage form²⁹. As seen in Figure 4.10(a), this parameter is strongly defined by the protein properties and the main contributing factor to variations in parameter $\ln(k)$ is molecular weights of proteins, followed by electrostatic attractions between the polymer and the proteins. This means, an increase in any of these two parameters will result in a decrease in $\ln(k)$ and therefore also a decrease in k .

In the Korsmeyer-Peppas model, n values are representative of the release mechanism with higher n values being indicative of less diffusion-based kinetics and more non-Fickian transport²⁹. Figure 4.10(b) suggests that n and the release mechanism are highly dependent on polymer characteristics and buffer concentration and less influenced by protein properties. Higher polymer degree of substitution results in fewer

available carboxyl groups which are required for forming stronger hydrogel networks. The looser networks formed make the hydrogel more prone to degradation, especially in higher concentrations of buffer where larger amount of sodium ions act to displace the calcium ions of the hydrogel network²⁸ and also higher concentration of calcium chelating compounds (such as phosphate ions) cause the gel to degrade faster²⁰.

Figure 4.11(a) and (b) compare the experimental values and model-predicted values of $\ln(k)$ and n . The root mean-squared error of prediction for $\ln(k)$ is calculated to be 0.31, which can be considered a relatively small threshold with observed $\ln(k)$ data ranging from -2.00 to -4.31. The observed data range for n is from 0.42 to 0.65 and while a root mean-squared value of 0.04 is imperfect, the model could still be considered effectively reliable for prediction of n . Figure 4.11(c) shows the squared prediction error (SPE-X) and as seen, all the data points fall below the 99% confidence level which means the modeled relationships between the X variables are well capable of predicting the behaviors of the Y parameters.

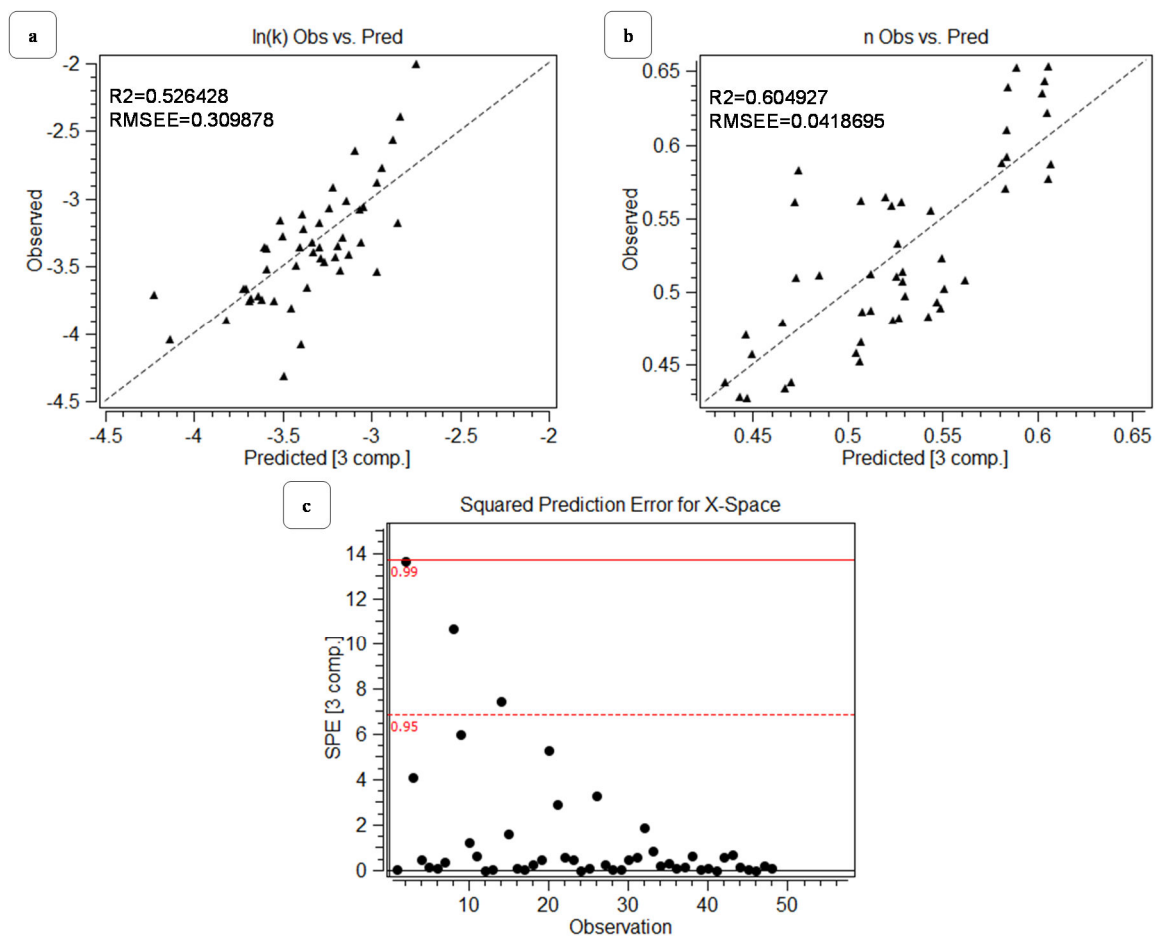


Figure 4.11. Observed vs. Predicted plots for (a) $\ln(k)$ and (b) n ; (c) squared prediction error (SPE) values for the observations.

The contour plot in Figure 4.12(a) represents variance in $\ln(k)$ as a function of the electrostatic attraction and protein molecular weight, the main two contributing factors. Figure 4.12(b) illustrates the contour plot of variances in n as a function of buffer concentration and the average microparticle diameter, the dominant two contributing variables. The scattered data in both these plots represent the experimental observed data and their distance from the contour surface is an indication of the prediction abilities of

the model. As seen, the experimental data lie within an acceptable range from the contour surfaces, which specifies effective and reliable predictions from the model.

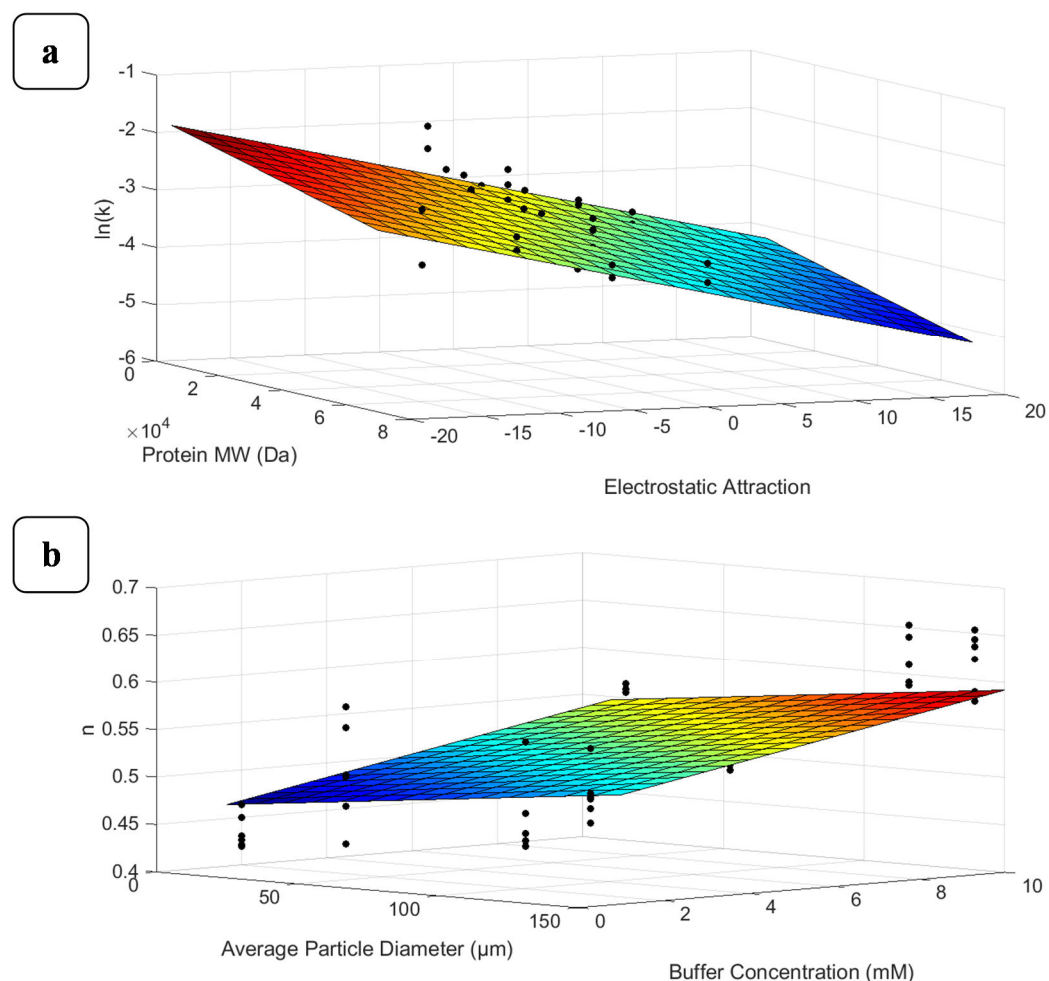


Figure 4.12. Contour surface plots from the PLS model as functions of the main two contributing factors and the experimental data for (a) $\ln(k)$ and (b) n .

4.4. Conclusion

The electrostatic interactions between alginate and proteins as well as the molecular weight of the protein have a significant influence on protein loading and release. Attractive interactions hinder protein release leading to slower diffusion rates

within the network whereas repulsive interactions can increase the rate of release as expected. Therefore, electrostatic interactions between hydrogels and proteins can be optimized as a means of controlling protein release by understanding the relationships between the release profiles of proteins and their properties and polymer characteristics. In this case, multivariate statistical methods described the quality and quantity of effects involved in the protein release kinetics (kt^n) and demonstrated that while parameter k is mostly affected by protein properties (net charge and molecular weight), parameter n is mostly influenced by polymer and buffer properties. Multivariate analysis provides a great tool for understanding the trends, predicting future kinetics, and optimizing the delivery carriers for efficient protein deliveries.

4.5. Acknowledgements

The authors would like to gratefully acknowledge NSERC for funding support, ProSensus Inc. for generous permission to use ProMV software, Dr. Dan Chen and Ashutosh Kulkarni for useful discussions, Dr. Megan Dodd for her assistance in cytotoxicity tests, Fei Xu for performing SEM imaging, and Salwa Farooqi and Karishma Manji for their assistance in preparing the microparticles.

References

1. Hirota, N., Kumaki, Y., Narita, T., Gong, J. P. & Osada, Y. Effect of Charge on Protein Diffusion in Hydrogels. *J. Phys. Chem. B* **104**, 9898–9903 (2000).
2. Schillemans, J. P., Hennink, W. E. & van Nostrum, C. F. The effect of network charge on the immobilization and release of proteins from chemically crosslinked dextran hydrogels. *Eur. J. Pharm. Biopharm.* **76**, 329–335 (2010).

3. Branco, M. C., Pochan, D. J., Wagner, N. J. & Schneider, J. P. The effect of protein structure on their controlled release from an injectable peptide hydrogel. *Biomaterials* **31**, 9527–9534 (2010).
4. Siddiqui, O., Sun, Y., Liu, J.-C. & Chien, Y. W. Facilitated Transdermal Transport of Insulin. *J. Pharm. Sci.* **76**, 341–345 (1987).
5. Beurer, E., Venkataraman, N. V., Sommer, M. & Spencer, N. D. Protein and Nanoparticle Adsorption on Orthogonal, Charge-Density-Versus-Net-Charge Surface-Chemical Gradients. *Langmuir* **28**, 3159–3166 (2012).
6. Johnson, E. M., Berk, D. A., Jain, R. K. & Deen, W. M. Diffusion and partitioning of proteins in charged agarose gels. *Biophys. J.* **68**, 1561–1568 (1995).
7. Sutter, M., Siepmann, J., Hennink, W. E. & Jiskoot, W. Recombinant gelatin hydrogels for the sustained release of proteins. *J. Control. Release* **119**, 301–312 (2007).
8. Yamamoto, M., Tabata, Y. & Ikada, Y. Growth factor release from gelatin hydrogel for tissue engineering. *J. Bioact. Compat. Polym.* **14**, 474–489 (1999).
9. Garcia, A. M. & Ghaly, E. S. Preliminary spherical agglomerates of water soluble drug using natural polymer and cross-linking technique. *J. Control. Release* **40**, 179–186 (1996).
10. Schweizer, D., Schönhammer, K., Jahn, M. & Göpferich, A. Protein–Polyanion Interactions for the Controlled Release of Monoclonal Antibodies. *Biomacromolecules* **14**, 75–83 (2013).
11. Gu, F., Amsden, B. & Neufeld, R. Sustained delivery of vascular endothelial growth factor with alginate beads. *J. Control. Release* **96**, 463–472 (2004).
12. Hua, Z., Chen, Z., Li, Y. & Zhao, M. Thermosensitive and Salt-Sensitive Molecularly Imprinted Hydrogel for Bovine Serum Albumin. *Langmuir* **24**, 5773–5780 (2008).
13. Cai, C., Bakowsky, U., Rytting, E., Schaper, A. K. & Kissel, T. Charged nanoparticles as protein delivery systems: A feasibility study using lysozyme as model protein. *Eur. J. Pharm. Biopharm.* **69**, 31–42 (2008).
14. Sato, T., Uchida, R., Tanigawa, H., Uno, K. & Murakami, A. Application of polymer gels containing side-chain phosphate groups to drug-delivery contact lenses. *J. Appl. Polym. Sci.* **98**, 731–735 (2005).
15. Shilpa, A., Agrawal, S. S. & Ray, A. R. Controlled Delivery of Drugs from Alginate Matrix. *J. Macromol. Sci. Part C Polym. Rev.* **43**, 187–221 (2003).

16. Leng, B., Jiang, F., Lu, K., Ming, W. & Shao, Z. Growth of calcium carbonate mediated by slowly released alginate. *CrystEngComm* **12**, 730–736 (2010).
17. Joshi, A., Keerthiprasad, R., Jayant, R. D. & Srivastava, R. Nano-in-micro alginate based hybrid particles. *Carbohydr. Polym.* **81**, 790–798 (2010).
18. Fundueanu, G., Nastruzzi, C., Carpov, A., Desbrieres, J. & Rinaudo, M. Physico-chemical characterization of Ca-alginate microparticles produced with different methods. *Biomaterials* **20**, 1427–1435 (1999).
19. Ronghua, H., Yumin, D. & Jianhong, Y. Preparation and in vitro anticoagulant activities of alginate sulfate and its quaterized derivatives. *Carbohydr. Polym.* **52**, 19–24 (2003).
20. Boontheekul, T., Kong, H.-J. & Mooney, D. J. Controlling alginate gel degradation utilizing partial oxidation and bimodal molecular weight distribution. *Biomaterials* **26**, 2455–2465 (2005).
21. Yang, J. S., Ren, H. B. & Xie, Y. J. Synthesis of Amidic Alginate Derivatives and Their Application in Microencapsulation of λ -Cyhalothrin. *Biomacromolecules* **12**, 2982–2987 (2011).
22. Tan, R. *et al.* Thermo-sensitive alginate-based injectable hydrogel for tissue engineering. *Carbohydr. Polym.* **87**, 1515–1521 (2012).
23. Li, J. *et al.* Facile Fabrication of Organic–Inorganic Hybrid Beads by Aminated Alginate Enabled Gelation and Biomimetic Mineralization. *J. Biomater. Sci. Polym. Ed.* **24**, 119–134 (2013).
24. MacGregor, J. F., Bruwer, M. J., Miletic, I., Cardin, M. & Liu, Z. Latent Variable Models and Big Data in the Process Industries. *IFAC-PapersOnLine* **48**, 520–524 (2015).
25. Davis, T. A. *et al.* $^1\text{H-NMR}$ Study of Na Alginates Extracted from *Sargassum* spp. in Relation to Metal Biosorption. *Appl. Biochem. Biotechnol.* **110**, 75–90 (2003).
26. Saha, S. *et al.* Rhodamine–alginate conjugate as self indicating gel beads for efficient detection and scavenging of Hg^{2+} and Cr^{3+} in aqueous media. *Chem. Commun.* **48**, 1659–1661 (2012).
27. Zhai, P., Chen, X. B. & Schreyer, D. J. Preparation and characterization of alginate microspheres for sustained protein delivery within tissue scaffolds. *Biofabrication* **5**, 15009 (2013).
28. Wells, L. A. & Sheardown, H. Extended release of high pI proteins from alginate microspheres via a novel encapsulation technique. *Eur. J. Pharm. Biopharm.* **65**,

329–335 (2007).

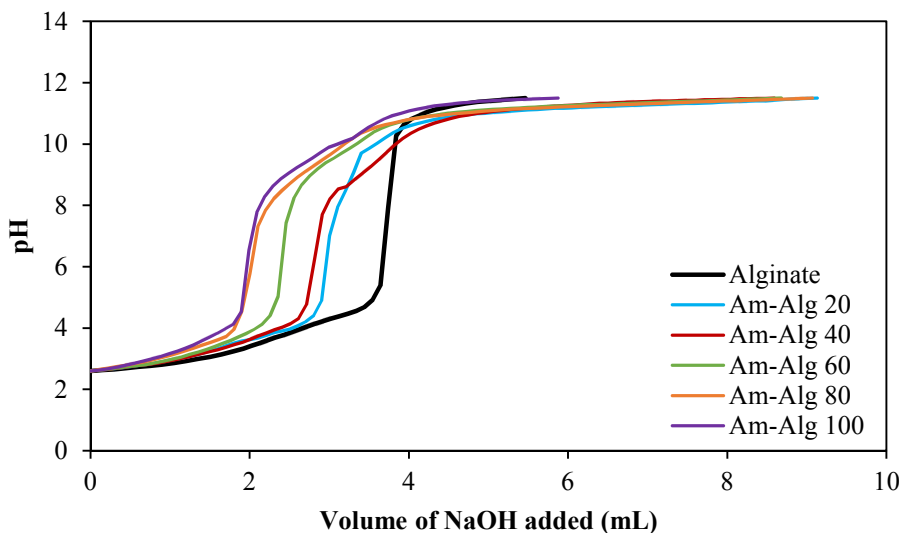
29. Costa, P. & Sousa Lobo, J. M. Modeling and comparison of dissolution profiles. *Eur. J. Pharm. Sci.* **13**, 123–133 (2001).
30. Gao, J., Mrksich, M., Gomez, F. A. & Whitesides, G. M. Using capillary electrophoresis to follow the acetylation of the amino groups of insulin and to estimate their basicities. *Anal. Chem.* **67**, 3093–3100 (1995).
31. Baler, K. *et al.* Electrostatic Unfolding and Interactions of Albumin Driven by pH Changes: A Molecular Dynamics Study. *J. Phys. Chem. B* **118**, 921–930 (2014).
32. Postnikova, G. B. & Shekhovtsova, E. A. The effect of mitochondrial and artificial bilayer phospholipid membranes on conformation of myoglobin and its affinity for oxygen. *Am. J. Biol. Chem.* **3**, 16–32 (2015).
33. Hildebrand, N. *et al.* Adsorption Orientation and Binding Motifs of Lysozyme and Chymotrypsin on Amorphous Silica. *J. Phys. Chem. C* **119**, 7295–7307 (2015).
34. Gitlin, I., Carbeck, J. D. & Whitesides, G. M. Why Are Proteins Charged? Networks of Charge–Charge Interactions in Proteins Measured by Charge Ladders and Capillary Electrophoresis. *Angew. Chemie Int. Ed.* **45**, 3022–3060 (2006).
35. Nick Pace, C., Alston, R. W. & Shaw, K. L. Charge-charge interactions influence the denatured state ensemble and contribute to protein stability. *Protein Sci.* **9**, 1395–1398 (2000).
36. Leone, G., Torricelli, P., Chiumiento, A., Facchini, A. & Barbucci, R. Amidic alginate hydrogel for nucleus pulposus replacement. *J. Biomed. Mater. Res. Part A* **84A**, 391–401 (2008).
37. Abu-Rabeah, K., Polyak, B., Ionescu, R. E., Cosnier, S. & Marks, R. S. Synthesis and Characterization of a Pyrrole–Alginate Conjugate and Its Application in a Biosensor Construction. *Biomacromolecules* **6**, 3313–3318 (2005).
38. Simonoska Crcarevska, M., Glavas Dodov, M. & Goracinova, K. Chitosan coated Ca–alginate microparticles loaded with budesonide for delivery to the inflamed colonic mucosa. *Eur. J. Pharm. Biopharm.* **68**, 565–578 (2008).
39. Tzoc Torres, J. M. G., Nichols, E., MacGregor, J. F. & Hoare, T. Designing multi-responsive polymers using latent variable methods. *Polymer (Guildf)*. **55**, 505–516 (2014).

Supplementary Material for Chapter 4

Supplementary Material 4.1: Characterization of the Modified Alginates

The synthesized amine modified alginate polymers (Am-Alg) were characterized by potentiometric-conductometric titrations for determination of amine conjugation and calculation of the degree of modification. Potentiometric-conductometric titrations of samples were performed by dissolving 50 mg of polymer into 50 mL NaCl (0.001 M). HCl was added drop-wise to adjust the initial solution to pH~2.5. Samples were titrated with NaOH 0.1 M, recording pH and conductivity as a function of the volume of base added (Mandel PC-Titrate, Mandel Scientific Company Inc., ON, Canada).

SI Figure 4.1 shows the potentiometric titration curves of the amine modified polymers and the unmodified alginate.



SI Figure 4.1. Potentiometric titration curves of the native alginate and the amine modified alginates.

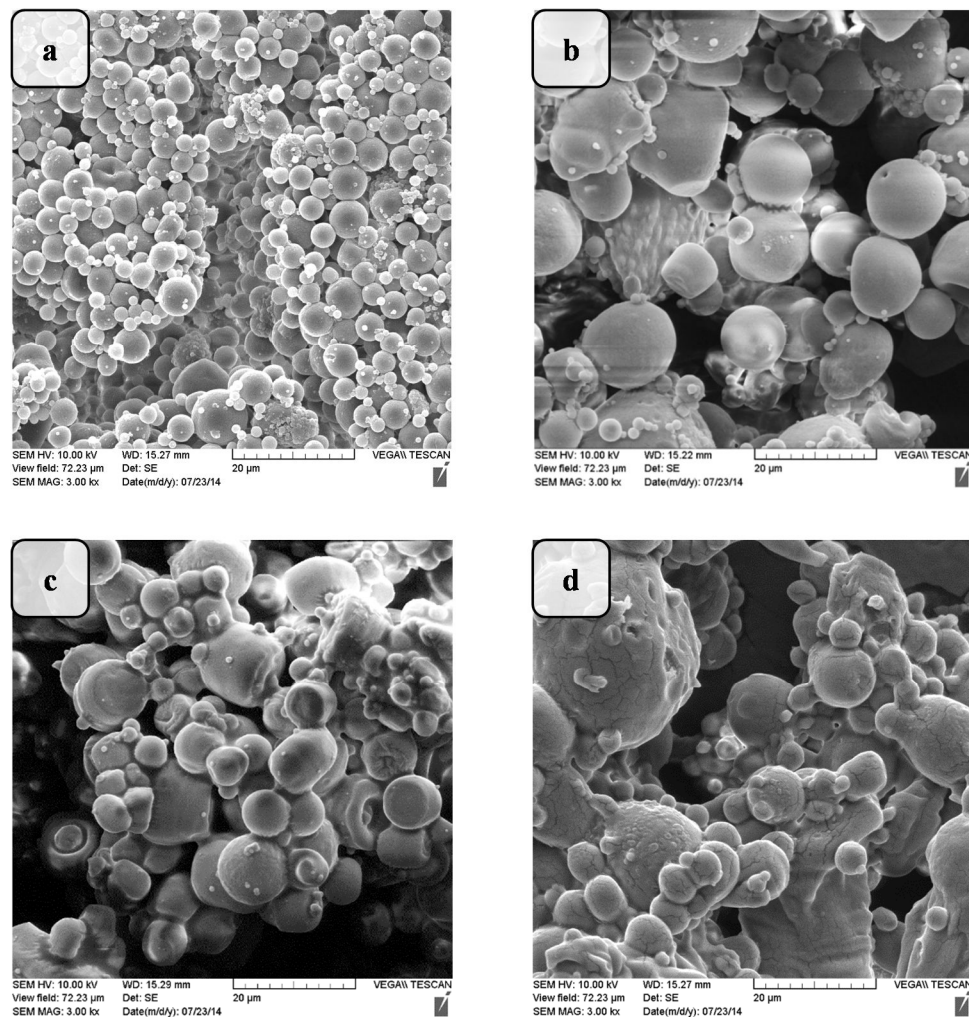
The values of the equivalent volumes obtained from the titration curves were used to calculate the carboxyl and amine contents of the polymer. SI Table 4.1 shows the molar amine content of the amine modified polymers calculated based on potentiometric-conductometric titrations.

SI Table 4.1. Values of amine content of the amide functionalized alginates determined by titration.

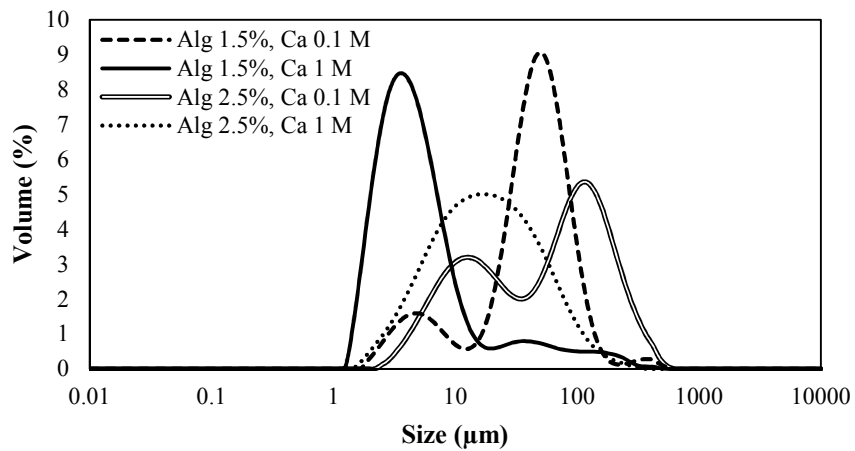
Sample	Theoretical amine content (%)	Calculated amine content (%)
Am-Alg 20	20	30.3
Am-Alg 40	40	42.0
Am-Alg 60	60	57.4
Am-Alg 80	80	71.6
Am-Alg 100	100	79.9

Supplementary Material 4.2: Particle Characterization

The shape and morphology of alginate microspheres were visualized by scanning electron microscopy (SEM) and are illustrated in SI Figure 4.2. The size distribution of the prepared alginate particles was measured by a laser diffraction particle size analyzer (SI Figure 4.3). As seen in SI Figure 4.2 and SI Figure 4.3, the concentration of the alginate and CaCl_2 solutions have effects on the shape and size of the microparticles, suggesting that particle size increased when the concentration of alginate was increased, and that the use of higher concentrations of CaCl_2 resulted in decreased particle diameter. The 1.5% (w/v) alginate and 1 M CaCl_2 solutions were selected as the optimized concentrations for achieving spherical microparticles with narrow size distribution and were used for all subsequent experiments.

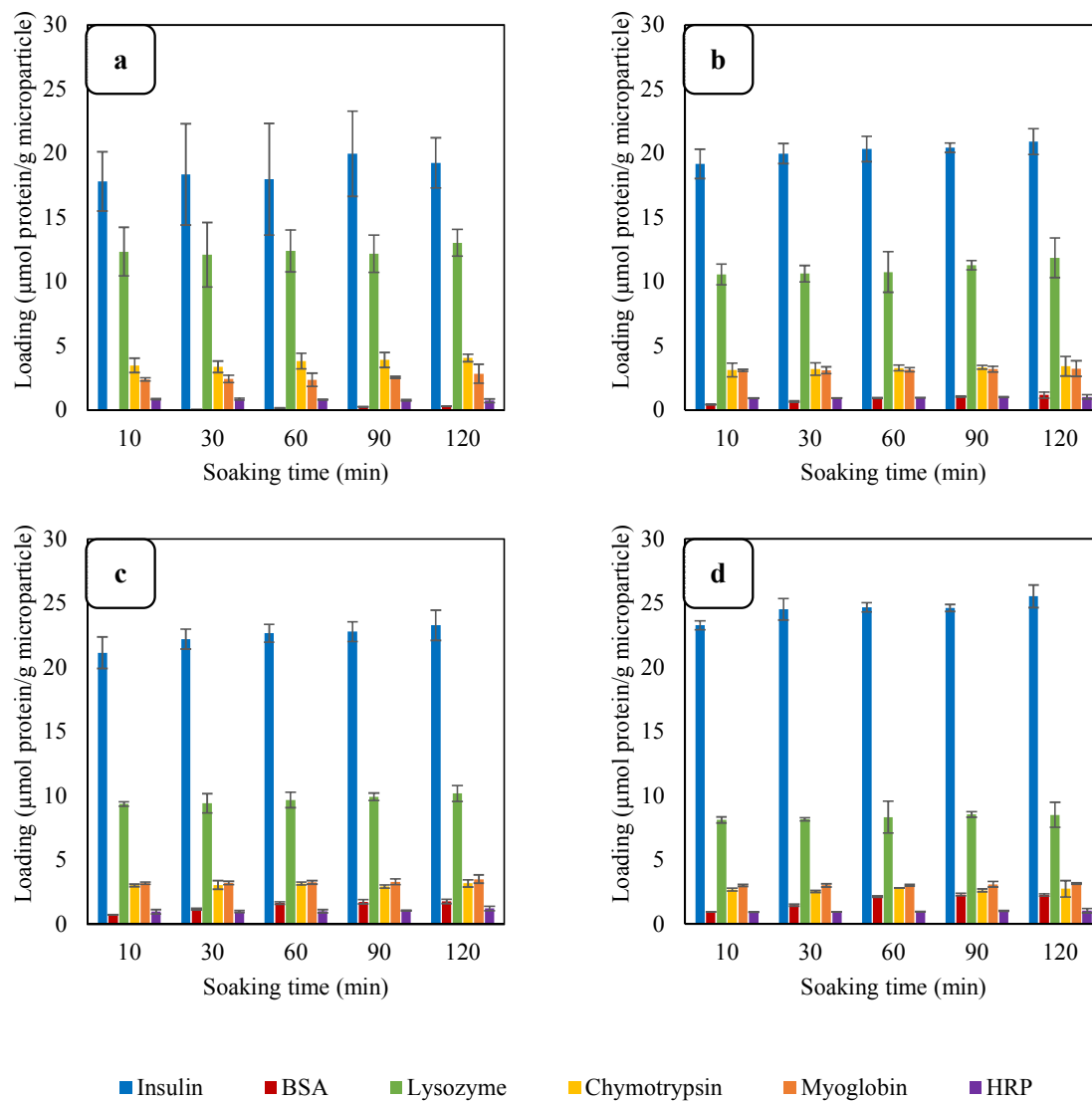


SI Figure 4.2. SEM images of alginate microparticles prepared with varying concentrations of alginate and calcium chloride solutions; (a) Alginate 1.5% (w/v), CaCl₂ 1 M, (b) Alginate 1.5% (w/v), CaCl₂ 0.1 M, (c) Alginate 2.5% (w/v), CaCl₂ 1 M, (d) Alginate 2.5% (w/v), CaCl₂ 0.1 M.



SI Figure 4.3. Size distributions of alginate microparticles prepared with varying concentrations of alginate and calcium chloride solutions.

Supplementary Material 4.3: Protein Loading



SI Figure 4.4. Loading of proteins in microparticles at various soaking times; (a) Alg, (b) Am-Alg 20, (c) Am-Alg 40, (d) Am-Alg 60.

Supplementary Material 4.4: Release Kinetics, Regression Fits, and Model**Predictions****SI Table 4.2. Values of parameters obtained from fit into the Korsmeyer-Peppas model and the PLS model-predicted values.**

Polymer	Buffer	Protein	Korsmeyer-Peppas			Multivariate Statistical Analysis	
			ln(k)	n	R ²	ln(k)	n
Alg	0.1X	Insulin	-2.002	0.458	0.984	-2.750	0.449
Alg	0.1X	BSA	-2.560	0.434	0.957	-2.884	0.466
Alg	0.1X	Lysozyme	-3.514	0.438	0.979	-3.593	0.435
Alg	0.1X	Chymotrypsin	-4.079	0.429	0.991	-3.403	0.442
Alg	0.1X	Myoglobin	-2.643	0.471	0.978	-3.100	0.446
Alg	0.1X	HRP	-3.156	0.427	0.962	-3.518	0.447
Alg	1X	Insulin	-2.389	0.533	0.995	-2.842	0.526
Alg	1X	BSA	-3.535	0.555	0.997	-2.976	0.543
Alg	1X	Lysozyme	-3.736	0.513	0.998	-3.685	0.512
Alg	1X	Chymotrypsin	-4.312	0.565	0.995	-3.496	0.519
Alg	1X	Myoglobin	-3.344	0.559	0.994	-3.192	0.523
Alg	1X	HRP	-3.352	0.480	0.993	-3.610	0.524
Am-Alg 20	0.1X	Insulin	-3.174	0.583	0.991	-2.855	0.474
Am-Alg 20	0.1X	BSA	-3.352	0.512	0.999	-3.301	0.485
Am-Alg 20	0.1X	Lysozyme	-3.354	0.479	0.961	-3.410	0.465
Am-Alg 20	0.1X	Chymotrypsin	-3.653	0.439	0.988	-3.365	0.470
Am-Alg 20	0.1X	Myoglobin	-3.411	0.561	0.994	-3.133	0.472
Am-Alg 20	0.1X	HRP	-3.747	0.510	0.997	-3.551	0.473
Am-Alg 20	1X	Insulin	-2.764	0.503	0.999	-2.948	0.550
Am-Alg 20	1X	BSA	-3.106	0.508	0.999	-3.393	0.561
Am-Alg 20	1X	Lysozyme	-3.275	0.483	0.998	-3.503	0.542
Am-Alg 20	1X	Chymotrypsin	-3.806	0.493	0.999	-3.457	0.547
Am-Alg 20	1X	Myoglobin	-2.909	0.489	0.997	-3.226	0.549
Am-Alg 20	1X	HRP	-3.715	0.523	0.998	-3.643	0.549
Am-Alg 40	0.1X	Insulin	-2.877	0.466	0.997	-2.973	0.507
Am-Alg 40	0.1X	BSA	-3.660	0.487	0.998	-3.730	0.512
Am-Alg 40	0.1X	Lysozyme	-3.062	0.458	0.997	-3.241	0.504
Am-Alg 40	0.1X	Chymotrypsin	-3.318	0.453	0.996	-3.339	0.506
Am-Alg 40	0.1X	Myoglobin	-3.523	0.562	0.992	-3.179	0.506
Am-Alg 40	0.1X	HRP	-3.367	0.487	0.999	-3.597	0.507
Am-Alg 40	1X	Insulin	-3.319	0.592	0.989	-3.065	0.584
Am-Alg 40	1X	BSA	-3.891	0.653	0.979	-3.822	0.588
Am-Alg 40	1X	Lysozyme	-3.389	0.588	0.988	-3.333	0.581
Am-Alg 40	1X	Chymotrypsin	-3.488	0.570	0.994	-3.431	0.583

Am-Alg 40	1X	Myoglobin	-3.458	0.611	0.982	-3.271	0.583
Am-Alg 40	1X	HRP	-3.755	0.640	0.981	-3.689	0.584
Am-Alg 60	0.1X	Insulin	-3.074	0.483	0.998	-3.072	0.527
Am-Alg 60	0.1X	BSA	-4.040	0.511	0.998	-4.140	0.525
Am-Alg 60	0.1X	Lysozyme	-3.060	0.498	0.997	-3.052	0.530
Am-Alg 60	0.1X	Chymotrypsin	-3.436	0.514	0.981	-3.294	0.529
Am-Alg 60	0.1X	Myoglobin	-3.422	0.562	0.994	-3.206	0.528
Am-Alg 60	0.1X	HRP	-3.743	0.508	0.997	-3.624	0.529
Am-Alg 60	1X	Insulin	-3.285	0.643	0.973	-3.164	0.604
Am-Alg 60	1X	BSA	-3.705	0.636	0.978	-4.233	0.602
Am-Alg 60	1X	Lysozyme	-3.012	0.587	0.986	-3.144	0.607
Am-Alg 60	1X	Chymotrypsin	-3.218	0.577	0.995	-3.386	0.606
Am-Alg 60	1X	Myoglobin	-3.176	0.622	0.980	-3.298	0.605
Am-Alg 60	1X	HRP	-3.665	0.654	0.971	-3.716	0.605

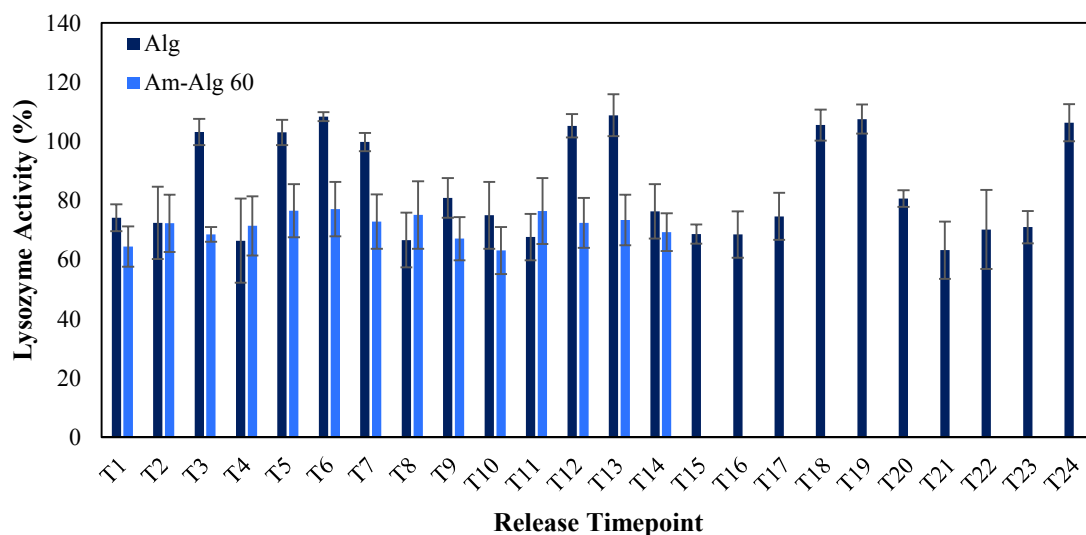
Supplementary Material 4.5: Protein Activity

Lysozyme was tested for its bioactivity after release from microparticles to determine whether the particles had any impact on the biological effects of the released proteins. The lysozyme activity can be evaluated by the break-up of *Micrococcus lysodeikticus* cell walls^{1,2} and specifically, by cleavage of the β -(1 \rightarrow 4) glycosidic linkages of the murein cell wall³. This hydrolysis and enzymatic degradation by lysozyme results in turbidity reduction of *Micrococcus lysodeikticus* cells solution and can be quantitatively measured using a spectrophotometer at 450 nm^{1,2}.

To detect the activity of the released protein, lysozyme samples were added to cell suspension (0.2 mg/mL) and absorbance was measured at 450 nm. The volumetric ratio of the lysozyme sample to cell suspension was 1:20 and 1:10 for lysozyme concentrations above and below 100 μ g/mL, respectively. The measured turbidity reduction in the samples was compared to that of fresh controls of the same concentration (using

standards) and this was used to determine the percent bioactivity of the released lysozyme.

The activity of the lysozyme released from Alg and Am-Alg 60 microparticles was measured to determine the effect of the materials on protein activity (SI Figure 4.5). The enzymatic activity of the samples drawn during the release was compared to the activity of a control of the same concentration. Activities of between 60% and 110% of the control were observed, suggesting overall that the activity of the protein encapsulated in these gels is preserved.



SI Figure 4.5. Lysozyme activity of the release studies from Alg and Am-Alg 60 microparticles in PBS 1X.

Supplementary Material 4.6: *In Vitro* Cytotoxicity

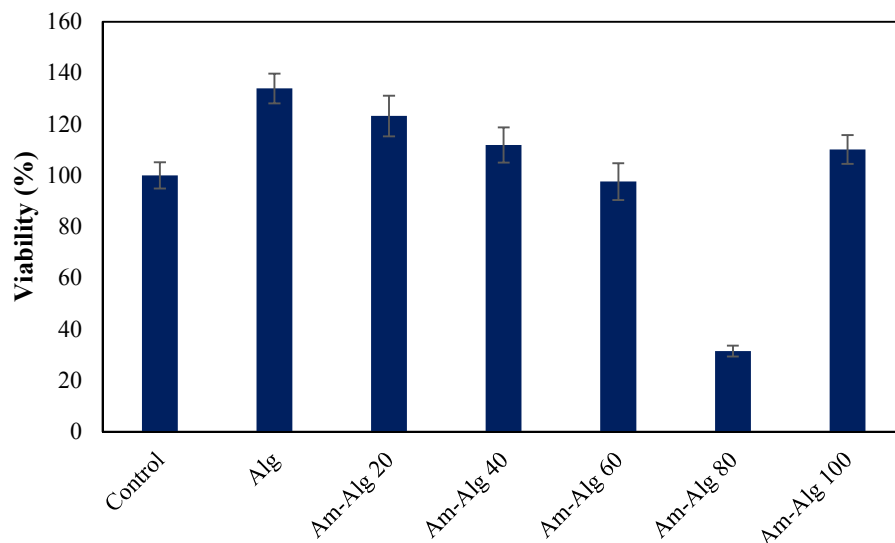
An MTT assay was performed to evaluate the compatibility of the alginate and modified alginate microparticles on a 3T3 cell line. This assay can be used to assess cell

population and viability when cells were grown with the microparticles as opposed to controls. Cells were seeded in 96-well plates at the density of 10^4 cells per well and 100 μL of DMEM with 10% fetal bovine serum were added. After 6 hours of incubation at 37°C and 5% CO_2 , 50 μL samples containing suspensions of alginate and modified alginate microparticles were added to the cells. For the control wells, 50 μL of PBS solution was added. Cells were incubated for 48 hours and then washed with PBS buffer before addition of 100 μL of PBS buffer and 10 μL MTT reagent. After 2 hours, the PBS and MTT reagent were removed and 50 μL of DMSO (dimethyl sulfoxide) was added to the wells. The viability was evaluated after 10 minutes of incubation at 37°C and 5% CO_2 by measuring absorbance at 540 nm. The controls in the assay were untreated cells (assumed to be 100% viable) and all values from the experiment were compared with this set of data.

In addition, the Live/Dead assay, which simultaneously determines the live and dead cells using a two-color fluorescence cell viability assay, was utilized to investigate any disruption in cell membranes. Cells were seeded, grown, and incubated with alginate and modified alginate microparticles similar to the methods described for the MTT assay. After 48 hours of incubation, cells were washed with PBS buffer, followed by addition of 50 μL of PBS buffer and 50 μL of solution containing both calcein acetoxymethyl (AM) (2 μM) and ethidium homodimer-1 (EthD-1) (4 μM) to each well. 50 μL of only calcein AM and 50 μL of only EthD-1 solutions were added to control wells for labelling the live control and dead control, respectively. The dead control was generated by incubating

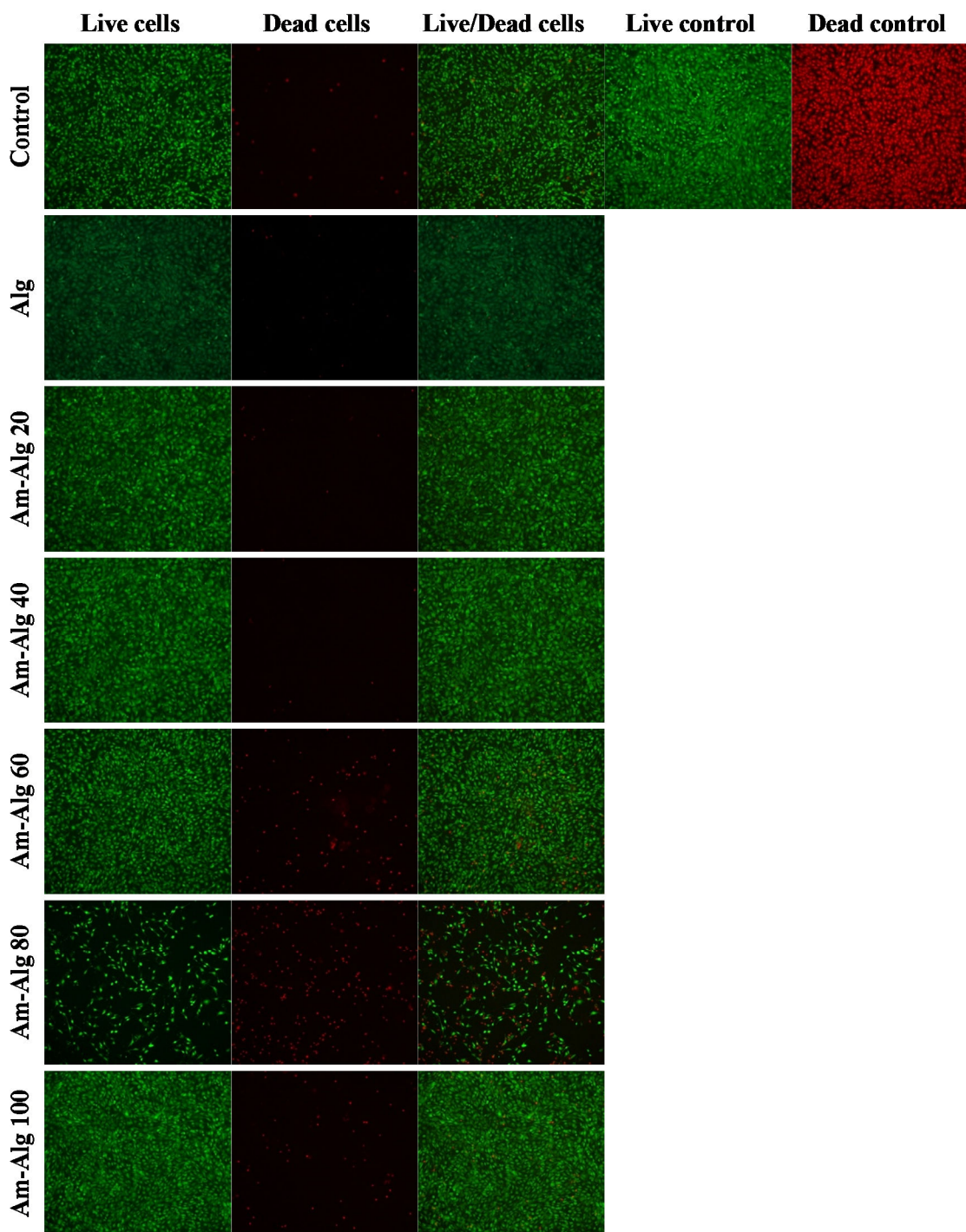
control cells in 70% ethanol for 10 min. After incubation for 30 mins at 37°C in a dark place, the labelled cells were observed by fluorescence microscopy.

Cytotoxicity of the alginate and modified alginate microparticles was tested in a 3T3 cell line using the MTT assay. The MTT assay tests cell viability through the reduction of water-soluble MTT (3-[4,5-dimethylthiazol-2-yl]-2,5-diphenyltetrazolium bromide) to a non-soluble formazan⁴ by viable cell mitochondria⁵. The purple-to-dark blue MTT-formazan⁴ is then extracted and photometrically quantified⁵. As observed in SI Figure 4.6, alginate and up to 60% modified alginate microparticles did not compromise cell viability; although, a reduction in cell viability was seen as the modification was increased. A significant decrease in cell viability to 31% was observed from 80% modified alginate samples. However, at the highest degree of modification (100%), a high level of viability was observed. This could be a result of low concentration of microparticles in the sample suspension. With a high degree of modification, fewer carboxyl groups of alginate are available for crosslinking and for the formation of microparticles, which leads to a lower number of microparticles formed.



SI Figure 4.6. MTT assay results of 3T3 cells growth with varying alginate modification degrees over 48 hours.

The Live/Dead assay is another well-established method for the evaluation of viability of the cells. Live cells are represented by the green fluorescence (ex/em ~495 nm/~515 nm) as a result of the intercellular activity of the cells which enzymatically convert the non-fluorescent cell-permeating calcein AM to the fluorescent calcein. On the other hand, the cells with damaged membranes allow entrance of the EthD-1 into the cells which produces a bright red fluorescent (ex/em ~495 nm-635 nm) upon binding to the nucleic acids of the dead cells⁶. SI Figure 4.7 shows the images of the stained cells observed by fluorescence microscopy. Similar to the results observed from the MTT assay (SI Figure 4.6), no signs of significant cell cytotoxicity were observed from the materials being used in protein release studies (alginate with modification up to 60%).



SI Figure 4.7. Live/Dead assay results of 3T3 cells growth with varying alginate modification degrees over 48 hours.

Supplementary Material References

1. Shugar, D. The measurement of lysozyme activity and the ultra-violet inactivation of lysozyme. *Biochim. Biophys. Acta* **8**, 302–309 (1952).
2. Wells, L. A. & Sheardown, H. Extended release of high pI proteins from alginate microspheres via a novel encapsulation technique. *Eur. J. Pharm. Biopharm.* **65**, 329–335 (2007).
3. Mörsky, P. Turbidimetric determination of lysozyme with *Micrococcus lysodeikticus* cells: Reexamination of reaction conditions. *Anal. Biochem.* **128**, 77–85 (1983).
4. Ahmad, S., Ahmad, A., Schneider, B. & White, C. Cholesterol Interferes with the MTT Assay in Human Epithelial-Like (A549) and Endothelial (HLMVE and HCAE) Cells. *Int. J. Toxicol.* **25**, 17–23 (2006).
5. Wörle-Knirsch, J. M., Pulskamp, K. & Krug, H. F. Oops They Did It Again! Carbon Nanotubes Hoax Scientists in Viability Assays. *Nano Lett.* **6**, 1261–1268 (2006).
6. Maltaris, T. *et al.* Comparison of xenografting in SCID mice and LIVE/DEAD assay as a predictor of the developmental potential of cryopreserved ovarian tissue. *In Vivo (Brooklyn)*. **20**, 11–16 (2006).

Chapter 5: Summary and Conclusions

In this work, the hypothesis that protein release could be controlled by taking advantage of molecular interactions, specifically electrostatic interactions, was evaluated and statistical methods were applied for mathematical modelling these interactions and used for the prediction of trends.

The first step of studying the electrostatic interactions between proteins and polysaccharides was done by simply mixing solutions of lysozyme, a net positively charged protein at physiological pH, and alginate, an anionic polysaccharide. Lysozyme-alginate complexes were prepared with different positive to negative charge ratios in the mixing solutions, in the absence and presence of calcium, and also at varying pH conditions. Complex composition, average diameter, and zeta potential were measured and Projection to Latent Structures was applied for developing mathematical relationships between these final properties (Y data) and the initial preparation conditions (X data). Furthermore, crosslinkers calcium, barium, iron(III), and bovine serum albumin (BSA), were used alongside lysozyme for forming complexes with alginate and multivariate analysis was applied for investigating the influence of crosslinker charge density on protein release kinetics (kt^n) from the alginate-based complex. The generated model revealed that while both release kinetic parameters (k and n) were highly dependent on the ionic strength of the release media, parameter k was dependent on protein properties while parameter n, which is suggestive of the release mechanism, showed a slight

dependency on the charge density of the crosslinker. It was also shown that at typical *in vivo* conditions the effect of the nature of the crosslinker on release rates was minimal due to the high ion-sensitivity of these complex systems and their disintegration-governed release mechanisms rather than diffusion-based kinetics. In addition to offering a comprehensive understanding of the trends, the Projection to Latent Structures model also provided a platform for prediction of complex properties and minimizing trial and error experiments for achieving the desired properties in a complex system. The overall R^2Y (a measure of the model fit capability of the Y data) and Q^2Y (an indication of the model predictive capability) were calculated to have values of 0.715 and 0.562, respectively. The R^2X , a measurement of how well the model fits the X data, was calculated to be 0.754. These values demonstrated reasonable fit and acceptable predictive performance for the model. In addition, with the exception of the average diameter, the R^2 values for all Y variables ranged from 0.710 to 0.948 which indicated high model fitting capabilities.

Since the enzymatic activity of the complexed lysozyme was shown to be acceptably conserved at between 60% and 90% of the control and the electrostatic complexation is a reversible process, the potential use of these protein-polysaccharide complexes as pH-/ion-sensitive protein carriers which dissociate in response to changes in environmental conditions (such as pH or ionic strength) was investigated. Multivariate statistical methods were applied not only for further understanding the ongoing correlations, but also for achieving a reliable model for prediction of future release kinetics and optimization of complex properties. The multivariate statistical analysis

quantified the parameters affecting the release kinetics (kt^n) and proved the high dependence of both parameters k and n on the ionic strength and pH of the release media. The root mean-squared error value of 0.658 for parameter $\ln(k)$, which fluctuates in the range of -3.986 to -0.738, and root mean-squared error value of 0.129 for parameter n , which ranges from 0.347 to 1.350, indicate that the model can be reliably used for prediction of protein release kinetics from the complex systems. The model also had R^2 values in the range of 0.834 to 0.906 for the complex properties (complex composition, average diameter, and zeta potential) which indicated high fitting capabilities of the model.

In addition to investigating the influencing factors on the disintegration-controlled protein release from the self-assembled protein-polysaccharide complexes, studies were also done on mainly diffusion-controlled protein release from calcium-alginate microparticles. It was shown that electrostatic interactions between the alginate microparticles and the proteins and also the molecular weight of the protein have a significant effect on protein loading and release. While attractive interactions hinder protein release and cause slower protein diffusion rates, repulsive interactions were found to increase the release rate as expected. For further understanding the correlations between the protein release kinetics, protein properties as well as polymer characteristics, multivariate statistical analysis was used. The statistical method quantified the observed qualitative trends in protein release kinetics (kt^n) in terms of mathematical relationships. It was shown that while the parameter k is mostly influenced by protein properties (net charge and molecular weight), the parameter n is mostly affected by polymer and buffer

properties. Therefore, it was concluded that electrostatic interactions between hydrogels and proteins can be optimized as a means of achieving desired protein release kinetics and multivariate analysis can be applied for understanding the trends and predicting future release patterns.

While acceptably reliable statistical models were achieved in this work, future work should focus on improving and extending the statistical models. Expanding the input database will provide a platform for better recognition of the correlations and patterns and therefore, will likely increase the fit capability and prediction reliability of the model. The input database can be extended for protein molecular weight and net charge by using additional model proteins. Also, the effects of such factors as chain composition of the alginate and polysaccharide molecular weight on complex properties and dissociation kinetics can be investigated. Design of experiment algorithms can be applied for optimizing the number of experiments which need to be carried out for achieving output data that can be analyzed to yield valid and objective conclusions. In addition, model evaluations should be carried out for examining the validity of the model for prediction purposes. This would include comparing the model predicted Y values and the observed experimental Y values for a new and independent set of X data. The model can also be evaluated by obtaining corresponding X values for desired values of Y, carrying out experiments based on the predicted X values, measuring the experimental Y values, and comparing the obtained Y values with the initial Y values.

In conclusion, Projection to Latent Structure modelling is a powerful tool for uncovering the obvious and non-obvious correlations between the X data and Y values.

The lower-dimensional working space of latent variable methods simplifies the extraction of the underlying factors which influence the process and explain the data variance.

Therefore, in optimizing processes and when aiming for desired results, taking advantage of this powerful modelling tool results in saving time as well as resources compared to traditional trial-and-error methods.

Appendix A – Bradford Assay

Bradford assay is a well-established, quick, and sensitive method used in protein detections. In this assay, Coomassie Brilliant Blue binds to lysine and arginine amino acid groups of proteins and changes from a red form to a blue form. The magnitude of the color change can be quantified using spectrophotometry at 595 nm¹. The ratio of the Bradford reagent to sample has to be varied until calibration curves with acceptable linearity can be achieved. Table A 1 lists the volumetric ratios between the sample and the Bradford reagent that were used to detect the ranges of concentrations. Samples were plated into 96-well plates and measurements were made no longer than 30 minutes following the addition of the reagent to the samples to ensure accurate results.

Table A 1. The sample:reagent volumetric ratios used in Bradford assay for different media and various concentration ranges.

	Milli-Q Water		PBS 1X (10 mM)		Sodium Citrate
	1-10 µg/mL	10-100 µg/mL	1-10 µg/mL	10-100 µg/mL	10-100 µg/mL
Insulin	4:1	1:6	4:1	1:6	1:6
BSA	1:1	1:4	1:1	1:4	1:4
Lysozyme	1:1	1:4	1:1	1:4	1:4
Chymotrypsin	1:1	1:4	1:1	1:4	1:4
Myoglobin	1:1	1:6	1:1	1:6	1:6
HRP	2:1	1:1	2:1	1:1	1:1

Reference

1. Sapan, C. V, Lundblad, R. L. & Price, N. C. Colorimetric protein assay techniques. *Biotechnol. Appl. Biochem.* **29 (Pt 2)**, 99–108 (1999).

Appendix B - Potentiometric-Conductometric Titration

In Figure B 1, potentiometric-conductometric titration curves of alginate and amine modified alginate with 40% theoretical degree of substitution are provided as examples for calculation of the change in the number of titratable functional groups before and after amine modification. The volume of base added (and thus the number of titratable functional groups of polymer) was found based on using the conductometric titration curves; where the end point of the titration corresponds to the intersection of the extrapolated linear portions of the conductometric titration curve. The determined equivalence points were also checked for by the potentiometric curves; in which the spikes in the first derivative (dpH/dV) curve correspond to equivalence points.

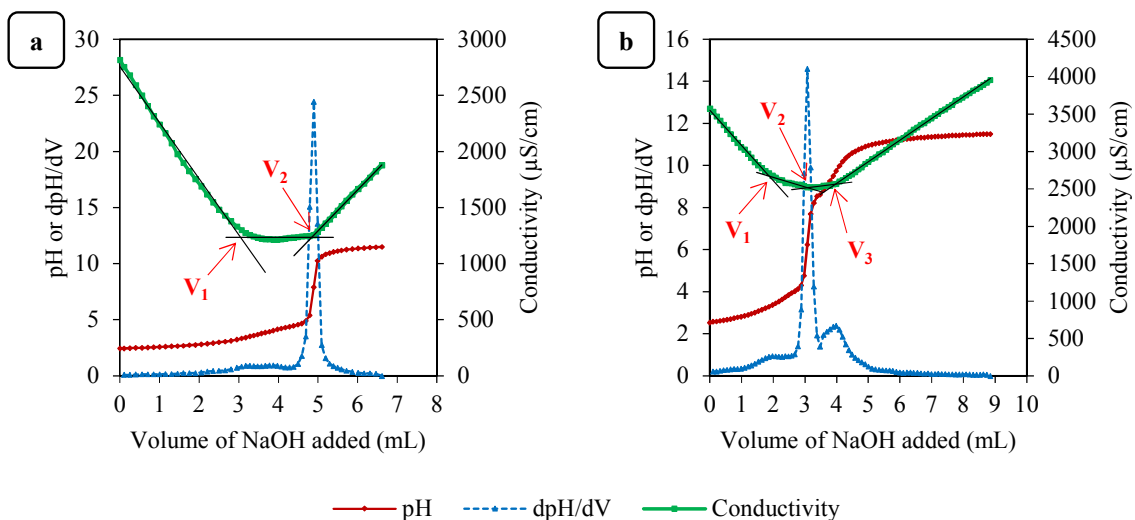


Figure B 1. Potentiometric-conductometric titration curves; (a) alginate, (b) Am-Alg 40.

In Figure B 1, the first linear branch of the conductometric curve ($V=0$ to V_1) indicate the volume of base added for the neutralization of the stronger acid (H_3O^+) present in the solution. The difference V_2-V_1 is the volume of base necessary to neutralize the COOH groups. In Figure B 1(b), the third equivalence point is achieved at V_3 and the difference V_3-V_2 is the volume of base necessary to neutralize the tertiary amine groups on the polymer. The third linear branch in Figure B 1(a) and the fourth linear branch of the curve in Figure B 1(b) correspond to the presence of the excess NaOH. The values of the equivalent volumes obtained from the titration curves were used to calculate the carboxyl and amine contents of the polymer (Table B 1).

Table B 1. Calculation of determination of carboxyl and amine content of the theoretically 40% amine modified alginate as an example calculation.

V_1 (mL)	1.879
V_2 (mL)	3.089
V_3 (mL)	3.966
V_2-V_1 (mL)	1.210
V_3-V_2 (mL)	0.877
Concentration of NaOH used (M)	0.1
Moles of carboxyl	1.210×10^{-4} (= $1.210 \text{ mL} \times 1 \text{ L}/1000 \text{ mL} \times 0.1 \text{ M}$)
Moles of amine	0.887×10^{-4} (= $0.887 \text{ mL} \times 1 \text{ L}/1000 \text{ mL} \times 0.1 \text{ M}$)
Total number of moles	2.087×10^{-4} (= $1.210 \times 10^{-4} + 0.887 \times 10^{-4}$)
Molar carboxyl content (%)	58.0 (= $1.210 \times 10^{-4} / 2.087 \times 10^{-4} \times 100\%$)
Molar amine content (%)	42.0 (= $0.887 \times 10^{-4} / 2.087 \times 10^{-4} \times 100\%$)

Appendix C – PLS Cross-Validation

Cross-validation is the main strategy in assessing the quality of a model and is represented through the values of different quality parameters such as R^2 and Q^2 . While R^2 is a measure of the goodness of the fit, Q^2 indicates the predictive ability of the model. The values of R^2 and Q^2 being equal to 1 show perfect fit of the data by the model and perfect predictability, respectively¹.

Cross-validation estimates the ability of a model to correctly predict the Y response matrix of new data inputs in the X matrix¹. In this thesis, cross-validation for all PLS models was done by splitting the dataset into 7 different subsets where each subset is created by selecting one row every seven rows in the dataset. Then, the Y values of all individuals in each subset were predicted using a submodel built with the 6 other subsets. The Q^2 calculation is done using Equation C 1; where y_i is the observed value, \hat{y}_i is the predicted value, and \bar{y} is the mean value².

$$Q^2 = 1 - \frac{\sum_{i=1}^n (y_i - \hat{y}_i)^2}{\sum_{i=1}^n (y_i - \bar{y})^2} \quad \text{Equation C 1}$$

An example calculation of the Q^2 value for parameter $\ln(k)$ in Chapter 2 is shown in Table C 1.

Table C 1. Calculation of Q^2 using a 7-fold cross-validation procedure for parameter $\ln(k)$ in Chapter 2.

Subset	Protein	Crosslinker	pH	Buffer Ionic Strength (mM)	ln(k)		$(y_i - \hat{y}_i)^2$	$(y_i - \bar{y})^2$
					Observed (y_i)	Predicted (\hat{y}_i)		
#1	Lysozyme	Ca ²⁺	4.5	10	-4.227	-3.755	0.223	0.869
#2	Lysozyme	Ca ²⁺	7.4	10	-3.417	-3.908	0.241	0.015
#3	Lysozyme	Ca ²⁺	4.5	150	-2.735	-2.554	0.033	0.313
#4	Lysozyme	Ca ²⁺	7.4	150	-2.725	-2.612	0.013	0.325
#5	Lysozyme	Ba ²⁺	4.5	10	-3.846	-3.764	0.007	0.304
#6	Lysozyme	Ba ²⁺	7.4	10	-3.253	-3.804	0.304	0.002
#7	Lysozyme	Ba ²⁺	4.5	150	-2.615	-2.591	0.001	0.462
#1	Lysozyme	Ba ²⁺	7.4	150	-2.677	-2.629	0.002	0.383
#2	Lysozyme	Fe ³⁺	4.5	10	-3.920	-3.775	0.021	0.390
#3	Lysozyme	Fe ³⁺	7.4	10	-3.553	-3.906	0.124	0.066
#4	Lysozyme	Fe ³⁺	4.5	150	-2.838	-2.635	0.041	0.209
#5	Lysozyme	Fe ³⁺	7.4	150	-2.890	-2.758	0.017	0.164
#6	Lysozyme	BSA	4.5	10	-4.035	-3.849	0.034	0.547
#7	Lysozyme	BSA	7.4	10	-3.788	-3.843	0.003	0.242
#1	Lysozyme	BSA	4.5	150	-2.622	-2.664	0.002	0.453
#2	Lysozyme	BSA	7.4	150	-2.262	-2.748	0.236	1.068
#3	BSA	Lysozyme	4.5	10	-4.404	-4.025	0.143	1.229
#4	BSA	Lysozyme	7.4	10	-4.639	-3.933	0.499	1.807
#5	BSA	Lysozyme	4.5	150	-2.942	-2.911	0.001	0.125
#6	BSA	Lysozyme	7.4	150	-2.516	-3.453	0.879	0.608
					$\bar{y} = -3.295$		SUM = 2.826	SUM = 9.583
							$Q^2 = 1 - 2.826/9.583 =$ 0.705	

References

1. Triba, M. N. *et al.* PLS/OPLS models in metabolomics: the impact of permutation of dataset rows on the K-fold cross-validation quality parameters. *Mol. BioSyst.* **11**, 13–19 (2015).
2. Chirico, N. & Gramatica, P. Real External Predictivity of QSAR Models: How To Evaluate It? Comparison of Different Validation Criteria and Proposal of Using the Concordance Correlation Coefficient. *J. Chem. Inf. Model.* **51**, 2320–2335 (2011).